EDL-M455

DA 36-039 SC-87499

Numerical Results for Low Frequency Scattering by Elliptic Cylinders and by Isolated Semi-Elliptic Protuberances

J. E. BURKE

E. J. CHRISTENSEN

S. B. LYTTLE

SYLVANIA ELECTRONIC SYSTEMS
Government Systems Management
for GENERAL TELEPHONE & ELECTRONICS

ELECTRONIC DEFENSE LABORATORIES
MOUNTAIN VIEW CALIFORNIA

PREPARED FOR THE UNITED STATES ARMY

ASTIA AVAILABILITY NOTICE

QUALIFIED REQUESTORS MAY OBTAIN COPIES OF
THIS REPORT FROM ASTIA.

U S ARMY ELECTRONICS RESEARCH UNIT
POST OFFICE BOX 205
MOUNTAIN VIEW, CALIFORNIA

DISTRIBUTION LIST FOR EDL PUBLICATION: M-455

COMMANDING OFFICER
US ARMY ELECTRONICS RESEARCH UNIT
POST OFFICE BOX 205
MOUNTAIN VIEW, CALIFORNIA 1E1

CHIEF OF RESEARCH & DEVELOPMENT
OCS, DEPARTMENT OF THE ARMY
WASHINGTON 25, D C 2E1

TECHNICAL LIBRARY, OASD R&D
ROOM 3E1065, THE PENTAGON
WASHINGTON 25, D C 3E1

COMMANDING OFFICER
HARRY DIAMOND LABORATORIES
ATTN - TECH REF SEC--ORDTL--06.33
WASHINGTON 25, D C 4E1

CHIEF, BUREAU OF WEAPONS, RAAV
DEPARTMENT OF THE NAVY
WASHINGTON 25, D C 5E1

CHIEF, BUREAU OF NAVAL WEAPONS
DEPARTMENT OF THE NAVY
ATTN - CODE R-12
WASHINGTON 25, D C 6E1

OFFICE OF NAVAL RESEARCH
DEPARTMENT OF THE NAVY
ATTN - CODE 427
WASHINGTON 25, D C 7E1

CENTRAL INTELLIGENCE AGENCY
ATTN - OCR MAIL ROOM
2430 E STREET, NW
WASHINGTON 25, D C 8E1

US ATOMIC ENERGY COMMISSION
DIVISION OF MILITARY APPLICATION
ATTN - CLASSIFIED TECH LIBRARY
1901 CONSTITUTION AVE, NW
WASHINGTON 25, D C 9E1

CHIEF OF STAFF, US AIR FORCE
DEPARTMENT OF THE AIR FORCE
ATTN - AFRSTB
WASHINGTON 25, D C 10E1

DEPUTY CHIEF OF STAFF FOR MIL OPNS
DEPARTMENT OF THE ARMY
ATTN - OPOR, R&D BRANCH
WASHINGTON 25, D C 11E1

DIRECTOR, US NAVAL RESEARCH LAB
COUNTERMEASURES BRANCH
ATTN - CODE 2027
WASHINGTON 25, D C 12E1

CHIEF OF STAFF, US AIR FORCE
DEPARTMENT OF THE AIR FORCE
ATTN - AFDRD-SC-3
WASHINGTON 25, D C 13E1

COMMANDER, AIR RESEARCH & DEVELOPMENT COMMAND
ATTN - RDSSTL--HQ TECH LIBRARY BRANCH
ANDREWS AIR FORCE BASE
WASHINGTON 25, D C 14E1

COMMANDING GENERAL
US ARMY MATERIEL COMMAND,
ATTN - AMCRD/DE-E-E
WASHINGTON 25, D C 15E1

MARINE CORPS LIAISON OFFICER
ATTN - SELRA-LNR
US ARMY ELECTRONICS R&D LABORATORY
FORT MONMOUTH, NEW JERSEY 16E1

COMMANDING OFFICER
US ARMY ELECTRONICS R&D LABORATORY
ATTN - SELRA-SE
FORT MONMOUTH, NEW JERSEY 17E1

COMMANDING OFFICER
US ARMY ELECTRONICS R&D LABORATORY
ATTN - SELRA-ADT
FORT MONMOUTH, NEW JERSEY 18E1

LIAISON OFFICER
US CONTINENTAL ARMY COMMAND
US ARMY ELECTRONICS R&D LABORATORY
FORT MONMOUTH, NEW JERSEY 19E3

CHIEF, US ARMY SECURITY AGENCY
ARLINGTON HALL STATION
ARLINGTON 12, VIRGINIA 20E1

DEPUTY PRESIDENT
US ARMY SECURITY AGENCY BOARD
ARLINGTON HALL STATION
ARLINGTON 12, VIRGINIA 21E1

COMMANDER
ARMED SERVICES TECHNICAL INFORMATION AGENCY
ATTN - TISIA
ARLINGTON HALL STATION
ARLINGTON 12, VIRGINIA 22E20

COMMANDING OFFICER
US ARMY FOREIGN SCIENCE & TECHNOLOGY CENTER
ATTN - AMXST-PP-CB
ARLINGTON HALL STATION
ARLINGTON 12, VIRGINIA 23E1

DIRECTOR OF COMMUNICATIONS & ELECTRONICS
HQ TACTICAL AIR COMMAND
LANGLEY AFB, VIRGINIA 24E1

(CONTINUED ON REVERSE SIDE)

(25JUN63)

US ARMY ELECTRONICS RESEARCH UNIT
POST OFFICE BOX 205
MOUNTAIN VIEW, CALIFORNIA

DISTRIBUTION LIST FOR EDL PUBLICATION: M-455 (CONTINUED FROM REVERSE SIDE)

REDSTONE SCIENTIFIC INFORMATION CENTER
US ARMY MISSILE COMMAND
REDSTONE ARSENAL, ALABAMA 25E5

COMMANDING GENERAL
US ARMY AIR DEFENSE CENTER
FORT BLISS, TEXAS 26E1

PRESIDENT
US ARMY AIR DEFENSE BOARD
FORT BLISS, TEXAS 27E1

COMMANDING OFFICER
US ARMY ELECTRONICS R&D ACTIVITY
ATTN - SELWS
WHITE SANDS MISSILE RANGE, N. M. 28E4

COMMANDING OFFICER
US ARMY R&D ACTIVITY, HUACHUCA
ATTN - SELHU-EE
FORT HUACHUCA, ARIZONA 29E1

COMMANDING OFFICER
US ARMY COMMUNICATIONS-ELECTRONICS
COMBAT DEFELOPMENT AGENCY
ATTN - CAGCE-AT
FORT HUACHUCA, ARIZONA 30E1

COMMANDER,
WRIGHT AIR DEVELOPMENT DIVISION
ATTN - ASRNCF1
WRIGHT-PATTERSON AFB, OHIO 31E1

A S D
ASAPRD — DIST
WRIGHT-PATTERSON AFB, OHIO 32E2

COMMANDER, AERONAUTICAL SYSTEMS DIVISION
AIR FORCE SYSTEMS COMMAND
ATTN - ASRNCC-1
WRIGHT-PATTERSON AFB, OHIO 33E1

DIRECTOR, NATIONAL SECURITY AGENCY
ATTN - C3/TDL
FORT GEORGE G MEADE, MARYLAND 34E2

COMMANDER, ROME AIR DEVELOPMENT CENTER
ATTN - RCYLD
GRIFFISS AIR FORCE BASE
ROME, NEW YORK 35E1

COMMANDER, FIELD COMMAND
DEFENSE ATOMIC SUPPORT AGENCY
ATTN - DEVELOPMENT DIVISION
SANDIA BASE
ALBUQUERQUE, NEW MEXICO 36E1

SANDIA CORPORATION LIBRARY
SANDIA BASE
ALBUQUERQUE, NEW MEXICO 37E1

THE RAND CORPORATION
ATTN - ELECTRONICS DEPARTMENT
1700 MAIN STREET
SANTA MONICA, CALIFORNIA 38E1

MIT LINCOLN LABORATORY
ATTN - LIBRARY
PO BOX 73
LEXINGTON 73, MASSACHUSETTS 39E1

DIRECTOR, COMMUNICATIONS & ELECTRONICS
AIR DEFENSE COMMAND
ENT AIR FORCE BASE
COLORADO SPRINGS, COLORADO 40E1

RESEARCH LABORATORY OF ELECTRONICS
MASSACHUSETTS INSTITUTE OF TECHNOLOGY
ATTN - LIBRARY
COMBRIDGE 39, MASSACHUSETTS 41EU1
UNCLASSIFIED ONLY

COMMANDER, AF CAMBRIDGE RESEARCH CENTER
ATTN - CRREL
HANSCOM FIELD
BEDFORD, MASSACHUSETTS 42E1

COMMANDING OFFICER & DIRECTOR
US NAVY ELECTRONICS LABORATORY
SAN DIEGO 52, CALIFORNIA 43E1

AIR FORCE MISSILE TEST CENTER
AFMTC-MTBAT
PATRICK AIR FORCE BASE, FLORIDA 44EC1
CLASSIFIED ONLY

AIR FORCE MISSILE TEST CENTER
AFMTC TECH LIBRARY — MU 135
PATRICK AIR FORCE BASE, FLORIDA 45EU1
UNCLASSIFIED ONLY

COMMANDER, AIR PROVING GROUND COMMAND
ATTN - APGC—PGAPI
EGLIN AIR FORCE BASE, FLORIDA 46E1

COMMANDING GENERAL
US ARMY ELECTRONICS COMMAND
ATTN - AMSEL-EW-A/FILIPPO
BUILDING 2525
FORT MONMOUTH, NEW JERSEY 47E1

ELECTRONIC DEFENSE LABORATORIES
P. O. Box 205
Mountain View, California

TECHNICAL MEMORANDUM

EDL-M455
August 1, 1962

NUMERICAL RESULTS FOR LOW FREQUENCY SCATTERING BY ELLIPTIC CYLINDERS AND BY ISOLATED SEMI-ELLIPTIC PROTUBERANCES

by

J. E. Burke, E. J. Christensen, and S. B. Lyttle

Prepared for the U. S. Army Electronics Research and Development Laboratory under Contract DA 36-039 SC-87499.

Approved for publication. . . . . V. Twersky
Head of Research

SYLVANIA ELECTRIC PRODUCTS INC.

NUMERICAL RESULTS FOR LOW FREQUENCY SCATTERING BY ELLIPTIC CYLINDERS AND BY ISOLATED SEMI-ELLIPTIC PROTUBERANCES

by

J. E. Burke, E. J. Christensen, and S. B. Lyttle

CONTENTS

NUMERICAL RESULTS FOR LOW FREQUENCY SCATTERING BY ELLIPTIC CYLINDERS AND BY ISOLATED SEMI-ELLIPTIC PROTUBERANCES

by

J. E. Burke, E. J. Christensen, and S. B. Lyttle

ABSTRACT

The low frequency approximations ("closed form" and series) derived previously for the fields scattered by elliptic cylinders, and by semi-elliptic protuberances, are applied numerically. For the two cases, $\underset{\sim}{E}$ or $\underset{\sim}{H}$ parallel to the generators, the results presented include total scattering cross sections, forward and back scattered intensity and phase curves, and far-field scattering patterns; for various angles of incidence, various eccentricities, and for various values of $ka \leq 1.1$ (where $k = 2\pi/\lambda$ and $2a$ is the major axis of the scatterers). Attention is restricted to the low frequency range not covered by published tables of Mathieu functions.

1. INTRODUCTION

The problem of scattering by a perfectly conducting elliptic cylinder is separable in elliptic coordinates and the solution can be represented as an infinite series of periodic and radial Mathieu functions[1, 2, 3]. However, since Sieger's[1] original derivation of this solution in 1908, the only detailed calculations based on it appear to be those of Morse and Rubenstein[4] for the strip (the elliptic cylinder with eccentricity equal to 1). In this report the exact series are used to obtain numerical values for the scattering amplitudes for a family of elliptic cylinders (ranging from strips to circles), and for the corresponding semi-elliptic protuberances on ground planes.

For limited values of $ka \geq 1.0$, where $k = 2\pi/\lambda$ and $2a$ is the major axis of the cylinder, tables and graphs[5, 6] of the Mathieu functions can be used to evaluate the exact series for the scattering amplitudes. In the present report we consider the essentially complementary range $ka \leq 1.1$ and evaluate the series in "closed form". The closed forms are obtained by

initially truncating the exact series and then using values for the Mathieu functions obtained from known low frequency approximations[7]. The validity of these forms is investigated by comparing them numerically with "exact" results based on tabulated functions. In addition to considering closed forms, we demonstrate the utility of elementary series approximations[7] (in powers of k) for the scattering coefficients and for the scattering amplitudes.

Although we work with relatively simple analytical expressions, their numerical application is complicated by the fact that four variables are involved; ka, the eccentricity, the angle of incidence, and the angle of observation. To make the computations tractable they were performed on a Burroughs 220 electronic computer. The extensive numerical results thus obtained are preserved in permanent tables and in punched cards; the latter provide data in a usable form for electronic computing programs on related multiple scattering problems[8, 9]. It is not possible to present the complete set of tables here and we merely illustrate their contents through a series of graphs. For cylinders, and for protuberances, these graphs include forward and back scattered intensity and phase curves, total scattering cross sections, and far-field scattering patterns; for various angles of incidence, various eccentricities, and for various values of $ka \leq 1.1$. A variety of results are given so as to demonstrate the overall dependence of the amplitudes on the four variables.

In the following, we begin with a brief review of the scattering problem and the derivation of the series solution by separating variables in elliptic coordinates. Then approximations for the Mathieu functions are introduced, and the accuracy of the resulting expressions (closed form and series) for the amplitudes is discussed. In the final section the tables that have been compiled are described and graphs of results taken from them are given.

2. REVIEW OF SCATTERING BY AN ELLIPTIC CYLINDER

In two dimensions the scattering of a plane wave by a cylinder parallel to the z axis is specified in the region external to the scatterer by a solution of

$$(\nabla^2 + k^2)\psi(\underline{r})e^{-i\omega t} = 0, \quad \nabla^2 = \partial_x^2 + \partial_y^2, \quad k = 2\pi/\lambda, \tag{1}$$

satisfying prescribed conditions at the surface of the cylinder. The solution has the form

$$\psi(\underline{r}) = \psi_0(\underline{r}) + u(\underline{r}), \tag{2}$$

where

$$\psi_0(\underline{r}) = e^{ikr\cos(\varphi - \varphi_0)} \tag{3}$$

represents the incident plane wave, and where the associated scattered wave fulfills

$$u(\underline{r}) \sim e^{ikr}\sqrt{2/(i\pi kr)}\, g(\varphi, \varphi_0), \quad r \to \infty. \tag{4}$$

The "scattering amplitude" $g(\varphi, \varphi_0)$ indicates the "far-field" response in the direction φ to plane wave excitation of direction φ_0.

For the elliptic cylinder the boundary conditions are applied on the surface

$$\frac{x^2}{a^2} + \frac{y^2}{b^2} = 1, \quad -\infty < z < \infty, \tag{5}$$

where $2a$ and $2b$ are the major and minor axes respectively; see Fig. 1. In particular, for an incident electromagnetic field specified by either $\underline{E}_o = \psi_0 \underline{z}/z = \psi_0 \hat{\underline{z}}$ or by $\underline{H}_o = \psi_0 \hat{\underline{z}}$ (the two principal polarizations), the z component of the corresponding total field on the surface of a perfect conductor satisfies either

$$\psi = 0, \quad \text{if } \underline{E}_o = \psi_0 \hat{\underline{z}} \tag{6}$$

or

$$\partial_n \psi = 0, \quad \text{if } \underline{H}_o = \psi_0 \hat{\underline{z}}. \tag{7}$$

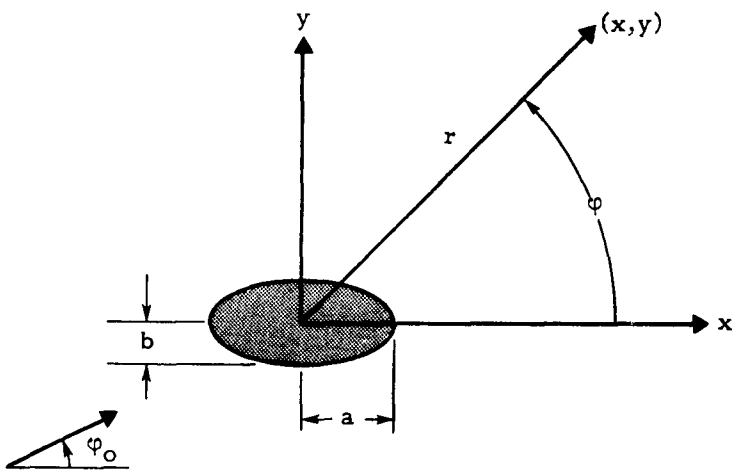

Fig. 1 Geometry for the scattering of a plane wave by an elliptic cylinder.

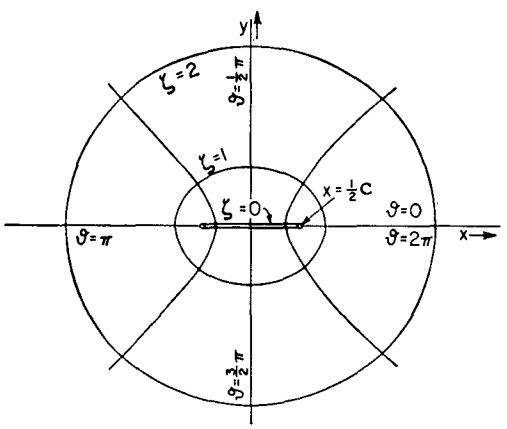

Fig. 2. Elliptic coordinates.

To solve the problem posed for the elliptic cylinder, one introduces elliptic coordinates (ζ,θ) defined by

$$x+iy = re^{i\varphi} = \frac{c}{2}\cosh(\zeta+i\theta); \tag{8}$$

as illustrated in Fig. 2, the coordinate curves ζ = constant and θ = constant are ellipses and hyperbolas respectively, and each curve has foci on the x axis at $\pm c/2$. Then Eq. (1) becomes

$$\left[\frac{\partial^2}{\partial\zeta^2} + \frac{\partial^2}{\partial\theta^2} + h^2(\cosh^2\zeta - \cos^2\theta)\right]\psi(\zeta,\theta) = 0, \quad h^2 = \frac{k^2c^2}{4} = k^2(a^2-b^2), \tag{9}$$

and the cylinder (5) is specified by the complete coordinate surface $\zeta = \zeta_o$ where

$$a = \frac{c}{2}\cosh\zeta_o, \quad b = \frac{c}{2}\sinh\zeta_o\ . \tag{10}$$

By separating variables, the solution of the boundary value problem can be written as a series of particular integrals of (9) of the form $S_n(\theta)R_n(\zeta)$; thus

$$\psi(\zeta,\theta) = \sum_{n=0}^{\infty} \alpha_n S_n(\theta)R_n(\zeta), \tag{11}$$

where the constants α_n are determined by applying the boundary conditions at $\zeta = \zeta_o$.

In (11) the S_n are the periodic Mathieu functions (even or odd, of period π or 2π) and the R_n are the radial Mathieu functions of the first and second kind (analogous to Bessel functions of the first and second kind). These functions are discussed in detail in the literature[2, 10, 11] and in the following we only state those forms and properties needed to make (11) explicit.

For a given value of h, the periodic Mathieu functions, which we denote by $S_{en}(\theta)$ (instead of by $S_{en}(h,\cos\theta)$ as in reference 11), form a complete set of orthogonal functions:

$$\int_0^{2\pi} S_{em}(\theta)S_{on}(\theta)d\theta = 0, \quad \int_0^{2\pi} S_{jm}(\theta)S_{jn}(\theta)d\theta = \begin{cases} 0 & m \neq 0 \\ 2\pi M_{jm} & m = n \end{cases}, \tag{12}$$

$j = e, o$.

where the present M's equal those of reference 11 divided by 2π. Their Fourier expansions are of the form

$$S_{em}(\theta) = \sum_{n=0}^{\infty *} B_n^m(h)\cos n\theta, \qquad S_{om}(\theta) = \sum_{n=0}^{\infty *} A_n^m(h)\sin n\theta, \tag{13}$$

where $\sum^*$ means that m and n have the same parity and where the values of the coefficients depend on the normalization of the $S_{\frac{e}{o}m}(\theta)$; as in reference 11 we use

$$\begin{aligned} &S_{em}(\theta) \to \cos m\theta, \qquad S_{om}(\theta) \to \frac{\sin m\theta}{m}, \quad \text{for } h \to 0, \\ &S_{em}(0) = \sum_{n=0}^{\infty *} B_n^m(h) = 1, \quad \frac{d}{d\theta} S_{om}(\theta)\Big|_{\theta=0} \sum_n^* A_n^m(h) = 1. \end{aligned} \tag{14}$$

The present functions are related to the ce_n and se_n of references 2 and 10 through

$$S_{en} = ce_n(2M_{e0})^{1/2}, \qquad S_{om} = se_n(2M_{on})^{1/2}. \tag{15}$$

The radial functions of the first kind $J_{\frac{e}{o}m}(\zeta)$, may be written as series of Bessel functions:

$$\begin{aligned} J_{em}(\zeta) &= \sum_{n=0}^{\infty *} (-1)^{(n-m)/2} B_n^m(h) J_n(h\cosh\zeta), \\ J_{om}(\zeta) &= \tanh\zeta \sum_{n=1}^{\infty *} (-1)^{(n-m)/2} A_n^m(h) J_n(h\cosh\zeta). \end{aligned} \tag{16}$$

The functions of the second kind, $N_{\frac{e}{o}m}$, follow from (16) by replacing the Bessel functions by the corresponding Neumann functions. However, for small values of h, the expansions involving products of Bessel and Neumann functions are more convenient:

$$N_{e2m}(\zeta) = \frac{1}{B_0^{2m}(h)} \sum_{n=0}^{\infty} (-1)^{n-m} B_{2n}^{2m}(h) N_n\left(\frac{he^{\zeta}}{2}\right) J_n\left(\frac{he^{-\zeta}}{2}\right), \tag{17}$$

For large values of ζ, the $J_{\frac{e}{o}m}$ and $N_{\frac{e}{o}m}$ behave asymptotically like their Bessel function counterparts, i.e., $J_{\frac{e}{o}m}(\zeta) \sim J_m(kr)$, $N_{\frac{e}{o}m}(\zeta) \sim N_m(kr)$. In particular, the linear combinations

$$H_{\frac{e}{o}m}(\zeta) = J_{\frac{e}{o}m}(\zeta) + iN_{\frac{e}{o}m}(\zeta), \tag{18}$$

are analogous to the Hankel functions and correspond to outgoing cylindrical waves as $\zeta \to \infty$:

$$H_{em}(\zeta) \sim i^{-m}\sqrt{2/(i\pi h\cosh\zeta)}\, e^{ih\cosh\zeta} \sim i^{-m}\sqrt{2/(i\pi kr)}\, e^{ikr}, \quad \zeta \to \infty. \tag{19}$$

In order to express the formal representation (11) for ψ in terms of the above functions, it is convenient to consider the wave functions ψ_o and u separately. Thus, employing the contracted notation $\sum_{j,n} F_{j_n} = \sum_{n=0}^{\infty} F_{e_n} + \sum_{n=0}^{\infty} F_{o_n}$, the usual expansion[2, 11] of the plane wave may be written as

$$\psi_o(\zeta,\theta) = e^{ikr\cos(\varphi-\varphi_o)} = \sum_{j,n} i^n S_{j_n}(\varphi_o) S_{j_n}(\theta) J_{j_n}(\zeta) M_{j_n}^{-1}. \tag{20}$$

Similarly, for both polarizations, the representation of u in terms of outgoing radial functions is of the form

$$u(\zeta,\theta) = \sum_{j,n} i^n a_{j_n} S_{j_n}(\varphi_o) S_{j_n}(\theta) H_{j_n}(\zeta) M_{j_n}^{-1} \tag{21}$$

The scattering coefficients a_{j_n}, determined by applying the boundary condition (6) or (7) are given by

$$a_{j_n} = -\frac{J_{j_n}(\zeta_o)}{H_{j_n}(\zeta_o)} \equiv a_{j_n}^{-}, \qquad (\text{for } \underset{\sim}{E} = \psi \hat{\underset{\sim}{z}}), \tag{22}$$

and

$$a_{j_n} = \frac{-J'_{j_n}(\zeta_o)}{H'_{j_n}(\zeta_o)} \equiv a_{j_n}^{+}, \quad J'_{j_n} = \left.\frac{\partial J_{j_n}}{\partial \zeta}\right|_{\zeta_o}, \text{ etc.} \quad (\text{for } \underset{\sim}{H} = \psi \hat{\underset{\sim}{z}}). \tag{23}$$

The Mathieu function series representation for the scattering amplitude follows by letting ζ or kr become infinite in u of (21). Thus, using the asymptotic form of H_{em} of (19), we obtain

$$u \sim e^{ih\cosh\zeta}\sqrt{2/(i\pi h\cosh\zeta)}\, g_{\pm}(\theta,\varphi_o) \sim e^{ikr}\sqrt{2/(i\pi kr)}\, g_{\pm}(\varphi,\varphi_o) \tag{24}$$

where

$$g_{\pm}(\varphi,\varphi_o) = g_{\pm}(\varphi_o,\varphi) = \sum_{j,n} a_{j_n}^{\pm} S_{j_n}(\varphi_o) S_{j_n}(\varphi) M_{j_n}^{-1}. \tag{25}$$

The amplitudes for the elliptic cylinders can be used to obtain the analogous ones for semi-elliptic protuberances on ground planes; see Fig. 3. These follow by taking twice the symmetric or anti-symmetric components of the cylinder results with respect to reflection of one angle in the plane of one axis; a procedure equivalent to that used originally by Rayleigh[12] to

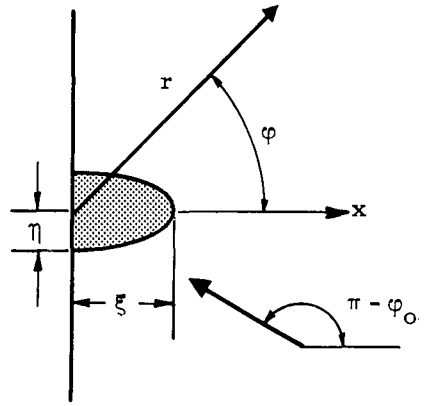

(a)

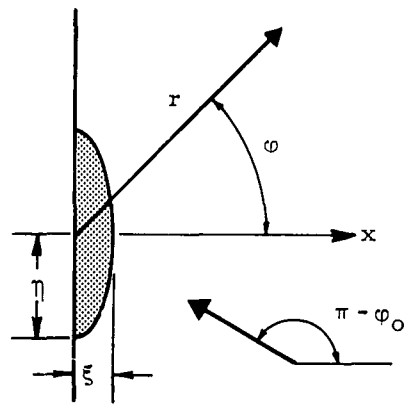

(b)

Fig. 3. Geometry for scattering by a semi-elliptic protuberance on a ground plane. Case (a) shows the major axis perpendicular to the ground plane ($\delta = \eta/\xi = b/a \equiv \rho \leq 1$) and case (b) shows the minor axis perpendicular ($\delta = \eta/\xi = a/b \equiv \rho^{-1} \geq 1$); $\delta = 0$ corresponds to perpendicular strips, $\delta = 1$ to semi-circles, and $\delta = \infty$ to flat strips.

treat the semi-circular protuberance. Thus, if the minor axis is in the ground plane $x = 0$ (see Fig. 3a), if $\pi - \varphi_0 (0 \le \varphi_0 \le \frac{\pi}{2})$ is the direction of incidence, and if $\underset{\sim}{H}$ is parallel to the generators, we obtain

$$f_+(\varphi, \pi - \varphi_0) = g_+(\varphi, \varphi_0) + g_+(\varphi, \pi - \varphi_0). \tag{26}$$

Similarly for $\underset{\sim}{E}$ parallel

$$f_-(\varphi, \pi - \varphi_0) = g_-(\varphi, \varphi_0) - g_-(\varphi, \pi - \varphi_0). \tag{27}$$

The corresponding results for the major axis in the ground plane (see Fig. 3b) follow from (26) and (27) by replacing $g_\pm(\nu, \mu)$ by $g_\pm(\frac{\pi}{2} + \nu, \frac{\pi}{2} + \mu)$, or, equivalently, by interchanging a and b.

The real part of the scattering amplitude for the special value $\varphi = \varphi_0$ is proportional to the total scattering cross section Q. Thus, for cylinders

$$Q_\pm = \frac{4}{k} \operatorname{Re} g_\pm(\varphi_0, \varphi_0) = \frac{2}{\pi k} \int_0^{2\pi} |g_\pm(\tau, \varphi_0)|^2 d\tau, \tag{28}$$

and for protuberances

$$Q_\pm = -\frac{4}{k} \operatorname{Re} f_\pm(\varphi_0, \pi - \varphi_0) = \frac{2}{\pi k} \int_{-\pi/2}^{\pi/2} |f_\pm(\tau, \varphi_0)|^2 d\tau. \tag{29}$$

For limited values of $ka > 1$ numerical values for the scattering amplitudes (25) to (27) can be obtained by using tables and graphs[5, 6] of the Mathieu functions. If ka is large enough, one can use asymptotic methods to obtain high frequency approximations[13, 14]. On the other hand, for $k < 1.0$ the required values of the Mathieu functions are not readily available. They could be calculated by employing tables[15, 16] of the Fourier coefficients A_m^n, B_m^n. However, these are given for values of $h = (ka)(1 - \rho^2)^{1/2}$ and consequently ka and the ratio $\rho = b/a$ cannot be varied independently. In addition, this coupling complicates the calculation of the radial functions; in general, for the given h the values of the Bessel and Neumann functions needed in (16), (17), etc., are not given in published tables.

In the following sections we restrict attention to computations in the low frequency range not covered by published tables. The coupling described above is avoided by using truncated series approximations for

the Mathieu functions. Thus, in terms of $\rho = b/a$, $\chi = (ka)/2$, and $L = \ln \frac{4\gamma\chi(1+\rho)}{e}$ (where $\ln \gamma = 0.577215\ldots$ is Euler's constant), for the radial functions we use[7]

$$J_{e_0} = 1 - \chi^2 \frac{1+\rho^2}{2} + \frac{\chi^4}{32}(7 - 6\rho^2 + 7\rho^4) - \frac{\chi^6}{576}(23 - 15\rho^2 - 15\rho^4 + 23\rho^6),$$

$$J_{e_1} = \chi\left[1 - \chi^2 \frac{3+\rho^2}{8} + \frac{\chi^4}{192}(13 - 2\rho^2 + 5\rho^4)\right] = J_{o_1}(a \leftrightarrow b), \quad J_{e_2} = \frac{\chi^2}{4}\left[1 + \rho^2 + \frac{\chi^2}{6}(1 - 6\rho^2 + \rho^4)\right],$$

(30)
$$J_{e_3} = \frac{\chi^3}{24}(3\rho^2 + 1) = J_{o_3}(a \leftrightarrow b), \quad J_{o_2} = \frac{\rho\chi^2}{2}\left(1 - \chi^2 \frac{1+\rho^2}{6}\right), \quad J_{e_m} = \frac{\chi^m}{(m-1)!} \sum_{\nu=0}^{[m/2]} C_{m\nu} \left(\frac{1-\rho^2}{4}\right)^\nu,$$

$$J_{o_m} = \frac{\rho\chi^m}{m!} \sum_{\nu=0}^{[m/2]} (m-2\nu) C_{m\nu} \left(\frac{1-\rho^2}{4}\right)^\nu, \quad C_{m\nu} = \frac{(-1)^\nu (m-\nu-1)!}{\nu!(m-2\nu)!}, \quad [m/2] = \text{integral part of } m/2,$$

and

$$N_{e_0} = \frac{2}{\pi}\left[J_{e_0} L + \chi^2\rho - \frac{\chi^4}{16}(2 + 3\rho - 4\rho^2 + 3\rho^3 + 2\rho^4) + \frac{\chi^6}{16}\left(1 - \frac{2}{9}\rho - \rho^2 + \frac{34}{27}\rho^3 - \rho^4 - \frac{2}{9}\rho^5 + \rho^6\right)\right],$$

$$N_{e_1} = \frac{-2}{\chi\pi(1+\rho)}\left[1 + \frac{\chi^2}{8}(1 + 6\rho + \rho^2 - 8(1+\rho)L) + \frac{\chi^4 L}{8}(3 + 3\rho + \rho^2 + \rho^3)\right.$$

(31)
$$\left. - \frac{\chi^4}{96}(19 + 62\rho + 36\rho^2 + 2\rho^3 + \rho^4)\right] = N_{o_1}(a \leftrightarrow b),$$

$$N_{e_2} = \frac{-4}{\chi^2\pi(1+\rho)^2}\left[1 + \frac{\chi^2}{6}(1 + 4\rho + \rho^2)\right] = N_{o_2}, \quad N_{e_3} = \frac{-16}{\chi^3\pi(1+\rho)^3} = N_{o_3}, \quad N_{e_m} = -\frac{1}{\pi}\left(\frac{1}{\chi}\right)^m \left(\frac{2}{1+\rho}\right)^m (m-1)!,$$

where $a \leftrightarrow b$ indicates the interchange of a and b.

Similarly, for the derivatives with respect to ζ_0 we use[7]

$$J'_{e_0} = -\chi^2\rho\left[1 - \frac{\chi^2}{4}(1+\rho^2) + \frac{\chi^4}{96}(9 - 10\rho^2 + 9\rho^4)\right], \quad J'_{e_1} = \chi\rho\left[1 - \frac{\chi^2}{8}(11 + \rho^2) + \frac{\chi^4}{192}(61 + 14\rho^2 + 5\rho^4)\right] = J'_{o_1}(a \leftrightarrow b),$$

(32)
$$J'_{e_2} = \chi^2\rho\left[1 - \frac{\chi^2}{3}(1+\rho^2)\right], \quad J'_{e_3} = \frac{\chi^3\rho}{8}(3+\rho^2) = J'_{o_3}(a \leftrightarrow b), \quad J'_{o_2} = \frac{\chi^2}{2}\left[1 + \rho^2 - \frac{\chi^2}{6}(1 + 6\rho^2 + \rho^4)\right],$$

$$J'_{e_m} = \frac{\rho\chi^m}{(m-1)!} \sum_{\nu=0}^{[m/2]} (m-2\nu) C_{m\nu} \left(\frac{1-\rho^2}{4}\right)^\nu, \quad J'_{o_m} = \frac{\chi^m}{m!} \sum_{\nu=0}^{[m/2]} (m-2\nu) C_{m\nu}\left[1 + (m-2\nu-1)\rho^2\right]\left(\frac{1-\rho^2}{4}\right)^\nu,$$

$$N'_{e_0} = \frac{2}{\pi}\left\{1 + \frac{\chi^2}{2}(1 + \rho^2 - 4\rho L) + \frac{\chi^4}{32}\left[-42\rho^2 + \rho^4 + 16\rho(1+\rho^2)L\right]\right\},$$

(33)
$$N'_{e_1} = \frac{2}{\chi\pi(1+\rho)}\left\{1 + \frac{\chi^2}{8}\left[3 + 10\rho - 5\rho^2 + 8\rho(1+\rho)L\right] - \frac{\chi^4 L}{8}(11\rho + 11\rho^2 + \rho^3 + \rho^4)\right.$$
$$\left. + \frac{\chi^4}{96}(7 + 50\rho + 144\rho^2 + 62\rho^3 + \rho^4)\right\} = N'_{o_1}(a \leftrightarrow b),$$

$$N'_{e_2} = \frac{8}{\chi^2\pi(1+\rho)^2}\left[1 - \frac{\chi^2}{6}(1 - 2\rho + \rho^2)\right] = N'_{o_2}, \quad N'_{e_3} = \frac{32}{\pi\chi^3}\left(\frac{2}{1+\rho}\right)^3 = N'_{o_3}, \quad N'_{e_m} = \frac{1}{\pi}\left(\frac{1}{\chi}\right)^m \left(\frac{2}{1+\rho}\right)^m \frac{m!}{2}.$$

Many truncated series approximations for the periodic Mathieu functions appear in the literature[2, 10, 11]. For present purposes it is convenient to use those given in reference 10:

$$
\begin{aligned}
S_{e_0}(M_{e_0})^{-\frac{1}{2}} &\approx 1-\tfrac{1}{2}\left(\tfrac{h}{2}\right)^2\cos 2\varphi+\left(\tfrac{h}{2}\right)^4\left\{\frac{\cos 4\varphi}{32}-\frac{1}{16}\right\}-\left(\tfrac{h}{2}\right)^6\left\{\frac{\cos 6\varphi}{1152}-\frac{11}{18}\cos 2\varphi\right\},\\
S_{e_1}(2M_{e_1})^{-\frac{1}{2}} &\approx \cos\varphi-\left(\tfrac{h}{2}\right)^2\frac{\cos 3\varphi}{8}+\left(\tfrac{h}{2}\right)^4\left\{\frac{\cos 5\varphi}{192}-\frac{\cos 3\varphi}{64}-\frac{\cos\varphi}{128}\right\}\\
&\quad-\left(\tfrac{h}{2}\right)^6\left\{\frac{\cos 7\varphi}{9\cdot 2^{10}}-\frac{\cos 5\varphi}{9\cdot 2^7}-\frac{\cos 3\varphi}{3\cdot 2^{10}}+\frac{\cos\varphi}{2^9}\right\},\\
S_{e_2}(2M_{e_2})^{-\frac{1}{2}} &\approx \cos 2\varphi-\left(\tfrac{h}{2}\right)^2\left\{\frac{\cos 4\varphi}{12}-\frac{1}{4}\right\}+\left(\tfrac{h}{2}\right)^4\left\{\frac{\cos 6\varphi}{384}-\frac{19}{288}\cos 2\varphi\right\},\\
S_{e_3}(2M_{o_3})^{-\frac{1}{2}} &\approx \cos 3\varphi-\left(\tfrac{h}{2}\right)^2\left\{\frac{\cos 5\varphi}{16}-\frac{\cos\varphi}{8}\right\}+\left(\tfrac{h}{2}\right)^4\left\{\frac{\cos 7\varphi}{640}-\frac{5}{512}\cos 3\varphi+\frac{\cos\varphi}{64}\right\},\\
S_{o_1}(2M_{o_1})^{-\frac{1}{2}} &\approx \sin\varphi-\tfrac{1}{8}\left(\tfrac{h}{2}\right)^2\sin 3\varphi+\left(\tfrac{h}{2}\right)^4\left\{\frac{\sin 5\varphi}{192}+\frac{\sin 3\varphi}{64}-\frac{\sin\varphi}{128}\right\}\\
&\quad-\left(\tfrac{h}{2}\right)^6\left\{\frac{\sin 7\varphi}{9\cdot 2^{10}}+\frac{\sin 5\varphi}{9\cdot 2^7}-\frac{\sin 3\varphi}{3\cdot 2^{10}}-\frac{\sin\varphi}{2^9}\right\},\\
S_{o_2}(2M_{o_2})^{-\frac{1}{2}} &\approx \sin 2\varphi-\left(\tfrac{h}{2}\right)^2\frac{\sin 4\varphi}{12}+\left(\tfrac{h}{2}\right)^4\left\{\frac{\sin 6\varphi}{384}-\frac{\sin 2\varphi}{288}\right\},\\
S_{o_3}(2M_{o_3})^{-\frac{1}{2}} &\approx \sin 3\varphi-\left(\tfrac{h}{2}\right)^2\left\{\frac{\sin 5\varphi}{16}-\frac{\sin\varphi}{8}\right\}+\left(\tfrac{h}{2}\right)^4\left\{\frac{\sin 7\varphi}{640}-\frac{5}{512}\sin 3\varphi-\frac{\sin\varphi}{64}\right\}.
\end{aligned}
\tag{34}
$$

These give most directly the angular factors $S_n(\varphi)S_n(\varphi_0)M_n^{-1}$ which appear in (25). Using Eqs. (30) to (34) the exact series for the amplitudes can be evaluated in closed form.

Explicit series approximations for the scattering amplitudes have been obtained[7] by inserting (30) to (34) into (25) and expanding in powers of k (treating L as a constant). The amplitudes correct to order k^6 thus obtained are given in reference 7 and they will not be repeated here. However, for future reference we note some leading approximations. Thus for cylinders with H parallel the real and imaginary parts to order k^4 are

$$
\begin{aligned}
\mathrm{Re}\,g_+(\varphi,\varphi_0) &= -\pi^2\left(\frac{ka}{2}\right)^4\left[\rho^2+\frac{(1+\rho)^2}{2}(\rho^2\cos\varphi\cos\varphi_0+\sin\varphi\sin\varphi_0)\right],\\
\mathrm{Im}\,g_+(\varphi,\varphi_0) &= -\pi\left(\frac{ka}{2}\right)^2\left[\rho-(1+\rho)(\rho\cos\varphi\cos\varphi_0+\sin\varphi\sin\varphi_0)\right]+\pi\left(\frac{ka}{2}\right)^4\left\{\frac{\rho}{4}(3+3\rho^2-8\rho L)\right.\\
&\quad+\frac{\rho(1-\rho^2)}{2}(\cos 2\varphi+\cos 2\varphi_0)-\frac{(1+\rho)(1-\rho^2)}{8}\left[\rho(\cos\varphi\cos 3\varphi_0+\cos\varphi_0\cos 3\varphi)\right.\\
&\quad\left.+\sin\varphi\sin 3\varphi_0+\sin\varphi_0\sin 3\varphi\right]-\frac{\rho(1+\rho)^2}{4}(7-2\rho+4\rho L)\cos\varphi\cos\varphi_0\\
&\quad-\frac{(1+\rho)^2}{4}(7\rho-2+4L)\sin\varphi\sin\varphi_0+\frac{(1+\rho)^2}{8}\left[2\rho\cos 2\varphi\cos 2\varphi_0+(1+\rho^2)\sin 2\varphi\sin 2\varphi_0\right]\Big\}
\end{aligned}
\tag{35}
$$

Similarly, letting $D = \pi^2(\pi^2 + 4L^2)^{-1}$, the amplitude for $\underset{\sim}{E}$ parallel is specified to order k^2 by

$$\mathrm{Re}\, g_{-}(\varphi,\varphi_0) = -D + \frac{D}{2}\left(\frac{ka}{2}\right)^2\left[\frac{4\rho}{L}(1-D) + (1-\rho^2)(\cos 2\varphi_0 + \cos 2\varphi)\right],$$

$$\mathrm{Im}\, g_{-}(\varphi,\varphi_0) = \frac{2LD}{\pi} - \left(\frac{ka}{2}\right)^2\left[\frac{2\rho D(1-2D)}{\pi} + \frac{LD}{\pi}(1-\rho^2)(\cos 2\varphi + \cos 2\varphi_0) + \pi(1+\rho)(\cos\varphi\cos\varphi_0 + \rho\sin\varphi\sin\varphi_0)\right]. \tag{36}$$

3. ACCURACY OF THE APPROXIMATIONS

In this section we investigate the numerical validity of the closed forms and series approximations for treating elliptic cylinders with arbitrary eccentricity and $ka < 1.0$. The scattering coefficients are considered first (for $ka \le 1.2$) and then the scattering amplitudes (for $ka \le 1.1$). In each case the range of ka includes some values in common with the tables of references 5 and 6.

Consider initially the closed form approximations $\mathrm{Im}\, a_{jm}^{+} = (32)(33)\left[(32)^2 + (33)^2\right]^{-1}$, etc., for the coefficients $a_{jn}^{\pm}$ for $n = 0$ and 1 (the leading coefficients). For the limiting cases of strips $(\rho = 0)$ and circles $(\rho = 1)$, the accuracy of these formulas follows by comparing them numerically with "exact" results; results obtained by using tabulated values[18] for the Bessel functions, and for the Fourier coefficients[14, 15], in the series representations for the radial functions (e.g., in Eq. (16)). Thus, as illustrated in Table I, for $\rho = 0$ or 1 and $ka \le 1.2$, it is found that the closed forms for the leading coefficients practically equal exact values. Similarly, for intermediate values of ρ (i.e., $0 < \rho < 1$), and $1 < ka < 1.2$, the closed forms agree with calculations based on references 5 and 6. Such numerical comparisons indicate that for $ka \le 1.2$, the closed forms for the scattering coefficients are uniformly accurate for all ρ and that the approximation for $a_{e_1}^{+}$ when $\rho = 1$ is the least accurate.

Numerical results for a_{jn} with $n \ge 2$, show that for the range $ka < 1$ of primary interest, and for the larger range $ka \le 1.1$, all but a_{j2} and $\mathrm{Im}\, a_{j3}$ are negligible compared to the leading coefficients. These higher order terms are most significant for the circle, while for the strip only $\mathrm{Im}\, a_{j2}$

Im $a^{-}_{e_o}$

	ρ = 1		ρ = 0	
ka	E	C	E	C
1.0	0.114	0.114	-0.409	-0.409
1.1	0.214	0.214	---	---
1.2	0.305	0.305	-0.350	-0.350

Im $a^{-}_{e_1}$

	ρ = 0	
ka	E	C
1.0	-0.273	-0.273
1.1	---	---
1.2	-0.348	-0.349

Im $a^{+}_{e_o}$

	ρ = 1	
ka	E	C
1.0	-0.428	-0.428
1.1	-0.464	-0.465
1.2	-0.488	-0.489

Im $a^{+}_{o_1}$

	ρ = 1		ρ = 0	
ka	E	C	E	C
1.0	0.328	0.325	0.437	0.437
1.1	0.323	0.318	---	---
1.2	0.307	0.301	0.500	0.500

Table I. Comparison of "exact" (E) and closed form (C) values for the imaginary parts of the leading non-zero scattering coefficients for strips ($\rho = 0$) and for circles ($\rho = 1$); note that $a^{+}_{e_n} = a^{-}_{o_n} \equiv 0$ for $\rho = 0$ and $a^{\pm}_{e_n} = a^{\pm}_{o_n}$ for $\rho = 1.0$. The exact values are based on tabulated functions and the closed forms on the formulas Im $a^{-}_{j_n} = (30)(31)\left[(30)^2 + (31)^2\right]^{-1}$ and Im $a^{+}_{j_n} = (32)(33)\left[(32)^2 + (33)^2\right]^{-1}$.

needs to be retained. For the circle, the sum of the absolute errors introduced by the closed forms for $n \geq 2$ is less than 2 percent of the corresponding component of a leading coefficient.

As shown in Fig. 4, for certain ranges of the parameters, the closed forms for the coefficients may be replaced by truncated series. In general, the smaller the value of ρ the larger the range of ka for which the series apply; this is illustrated in Fig. 4a by the series for the imaginary part of $a_{e_1}^{+}$. In particular, the agreement of the different approximations in Fig. 4a, when $\rho \sim 0$, is typical of the results for the real and imaginary parts of $a_{e_n}^{+}$ and $a_{o_n}^{-}$; in general, the results for the other coefficients are not as good. The maximum range of ka for all ρ follows by comparing the series with exact results for the circular cylinder. Thus, Fig. 4b and the $\rho = 1$ curves of Fig. 4a determine the maximum ranges of the series for the real and imaginary parts of the leading coefficients ($a_{e_0}^{-}$ excepted). (The series for $a_{e_0}^{-}$ are more accurate than those considered, e.g., the k^4 series is valid for all ρ if $ka \leq 1.1$.)

The accuracy of (34) for calculating the angular factors $S_n(\varphi)S_n(\varphi_0)M_n^{-1}$ follows by comparing them numerically with results based on the tabulated Fourier coefficients. Thus, for $h \leq 1.1$ (i.e., for $0 \leq ka \leq 1.1$ and $0 \leq \rho \leq 1$) it is found that the two results differ by less than 1 percent. These approximations are least accurate for the strip $(\rho = 0)$ for which case $h = ka/2$; for the circle $(\rho = 1)$, $h = 0$ and (34) reduces to simple trigonometric functions (independent of k).

Combining (34) with the closed forms for the scattering coefficients leads to relatively accurate expressions for the leading terms of the series (25). Of course, because of the angular dependence, the errors in the individual terms can cancel or add up to give more or less accurate values for the amplitudes. As an illustration of the overall accuracy of the final forms, Fig. 5 compares closed form and exact results for the circular cylinder for $\underset{\sim}{H}$ parallel; thus, for example, the closed forms for $|g_+|^2$ are seen to be accurate to within 3.5 percent for all angles of observation. Better

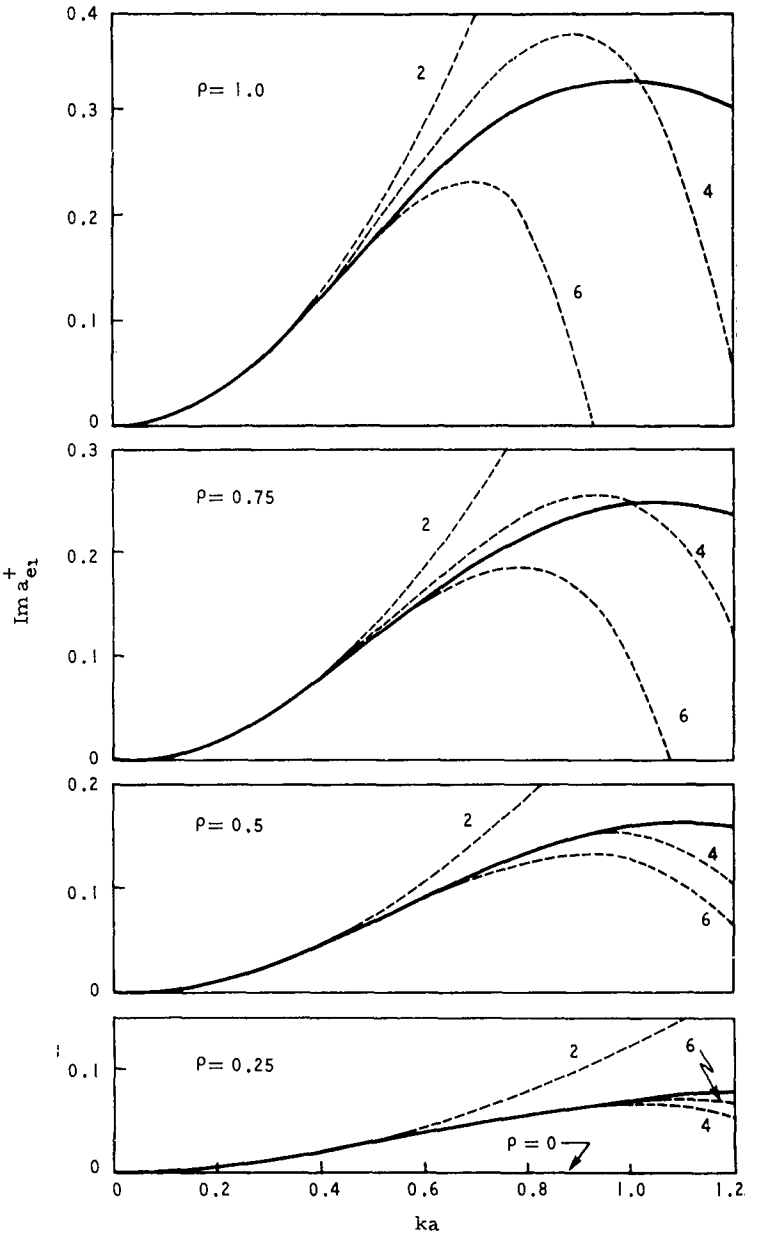

Fig. 4(a).

Fig. 4. Closed form and series approximations versus $ka \leq 1.2$ for (a) Im $a^{+}_{e_1}$ (for different values of $\rho = b/a$), and for (b) the real and imaginary parts of leading scattering coefficients for circular cylinders ($\rho = 1$). The solid curves are closed forms and the dashed ones are series approximations; the numbers give the highest power of k retained in the series.

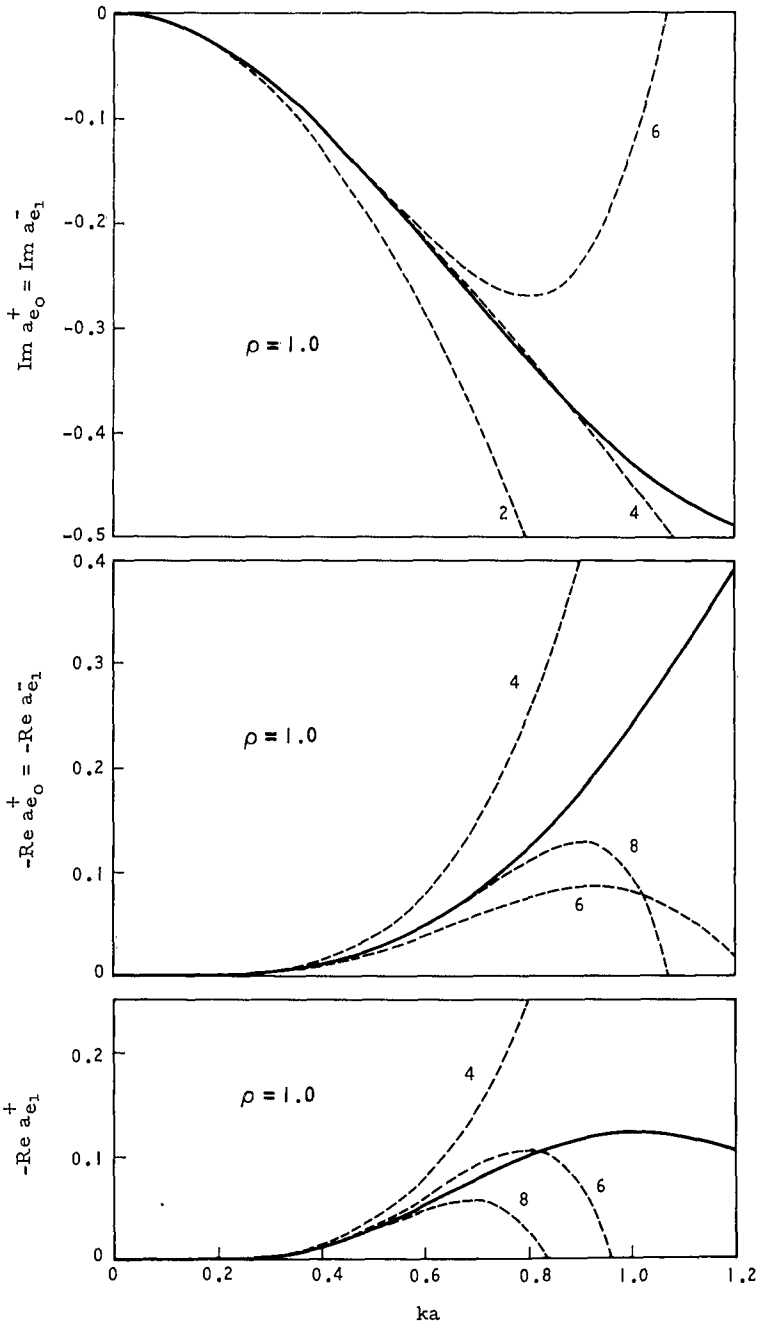
Im $a^{+}_{e_o}$ = Im $a^{-}_{e_1}$
ρ = 1.0
2
4
6
-Re $a^{+}_{e_o}$ = -Re $a^{-}_{e_1}$
ρ = 1.0
4
6
8
-Re $a^{+}_{e_1}$
ρ = 1.0
4
6
8
0
-0.1
-0.2
-0.3
-0.4
-0.5
0.4
0.3
0.2
0.1
0
0.2
0.4
0.6
0.8
1.0
1.2
ka

Fig. 4(b).

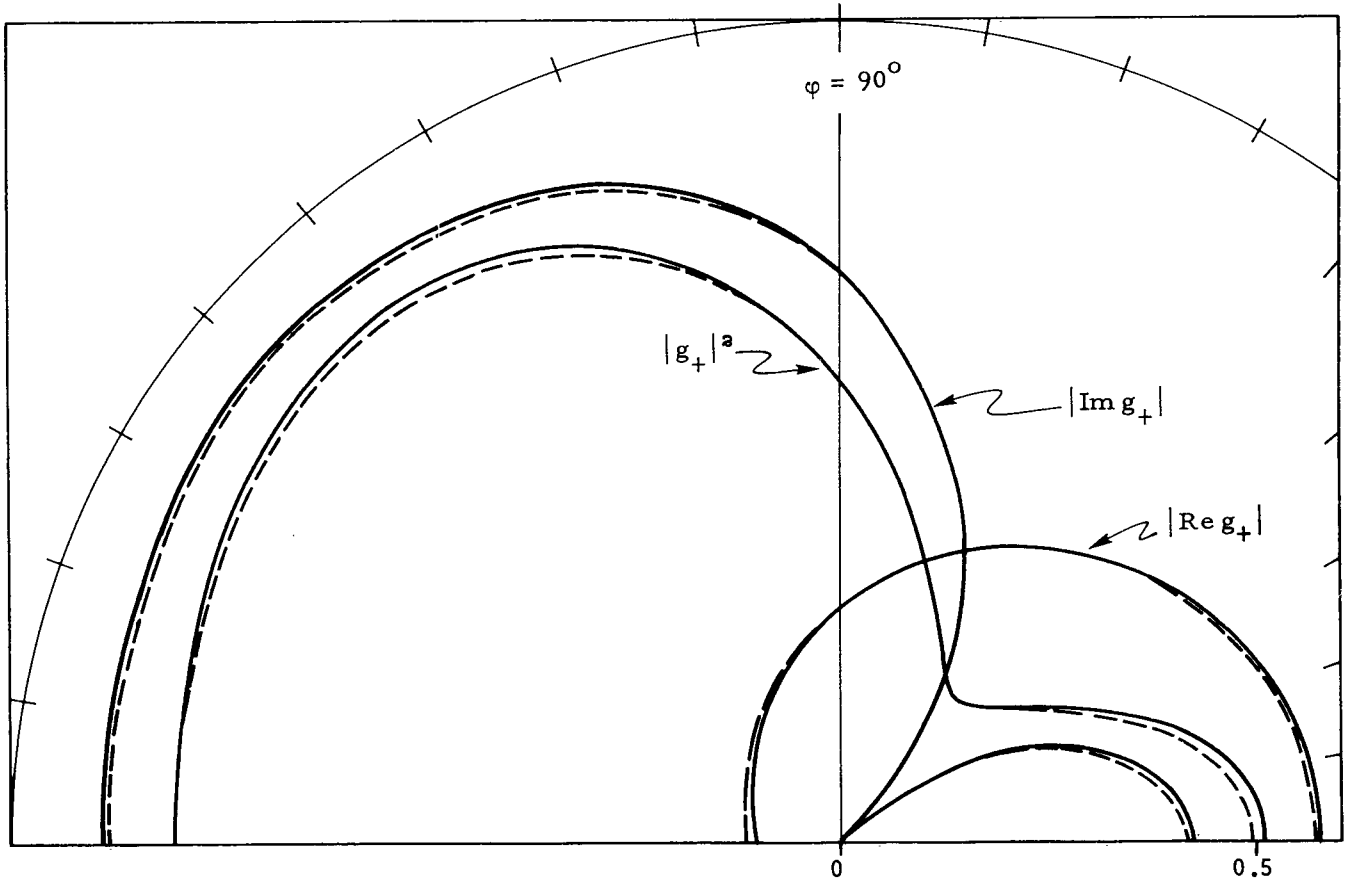

Fig. 5. Comparison of exact and closed form values for $|g_+(\varphi, 0)|^a$, $|\mathrm{Re}\, g_+(\varphi, 0)|$, and $|\mathrm{Im}\, g_+(\varphi, 0)|$, for the circular cylinder with ka = 1.1 and $\underset{\sim}{H}$ parallel; the solid curves are exact and the dashed ones are closed forms.

overall agreement is obtained for smaller ka, the circular cylinder with $\underset{\sim}{E}$ parallel, and for strips for both polarizations; e.g., for the case of Fig. 5, the closed forms and exact values are practically identical for $ka \leq 0.8$.

For special ranges of the parameters, the closed forms can be replaced by elementary series approximations; e.g., (35) and (36). This is illustrated in Figs. 6 and 7 which compare closed form and series results for cylinders. Thus, for example, Fig. 6 shows that for $\underset{\sim}{H}$ parallel, the k^4 approximation (35) applies (more or less) for $ka \leq 0.5$ when $\rho \leq 0.5$. Similarly, for $\underset{\sim}{E}$ parallel, Fig. 7 demonstrates that the k^2 series (36) can be used for $ka \leq 0.7$ when $\rho \leq 0.5$ The full range of ρ can be covered by suitably restricting ka and/or the angles; e.g., the k^2 series for $\underset{\sim}{E}$ parallel can be used for all ρ if $ka \leq 0.7$ and the direction of observation is not near the back direction (see Fig. 7b).

4. TABLES AND GRAPHS

The low frequency approximations described in the previous sections have been applied numerically in detail. Most of the calculations were performed on a Burroughs 220 electronic computer and the results are preserved in permanent tables. For cylinders and for protuberances, for $\underset{\sim}{E}$ and $\underset{\sim}{H}$ parallel, these tables include closed forms for the real and imaginary parts of the scattering amplitudes, and for the corresponding intensities, for the ranges

$$
\begin{aligned}
&0.1 \leq ka \leq 1.1, \quad \Delta(ka) = 0.2, \\
&0 \leq \rho = b/a \leq 1.0, \quad \Delta\rho = 0.25 \\
&\varphi_0 = 0, 10^\circ, 45^\circ, 80^\circ, 90^\circ, \\
&0 \leq \varphi \leq 350^\circ, \quad \Delta\varphi = 10^\circ.
\end{aligned}
\tag{39}
$$

In addition, tables of forward and back scattered intensities and phases, $Re\, g_\pm(\varphi_0, \varphi_0)$, $Re\, f_\pm(\varphi_0, \pi - \varphi_0)$, and of $Im\, f_\pm(\varphi_0, \pi - \varphi_0)$ have been compiled for $0 \leq \varphi_0 \leq 90^\circ (2.5^\circ \leq \Delta\varphi_0 \leq 10^\circ)$ and the values of ρ and ka of (37); the

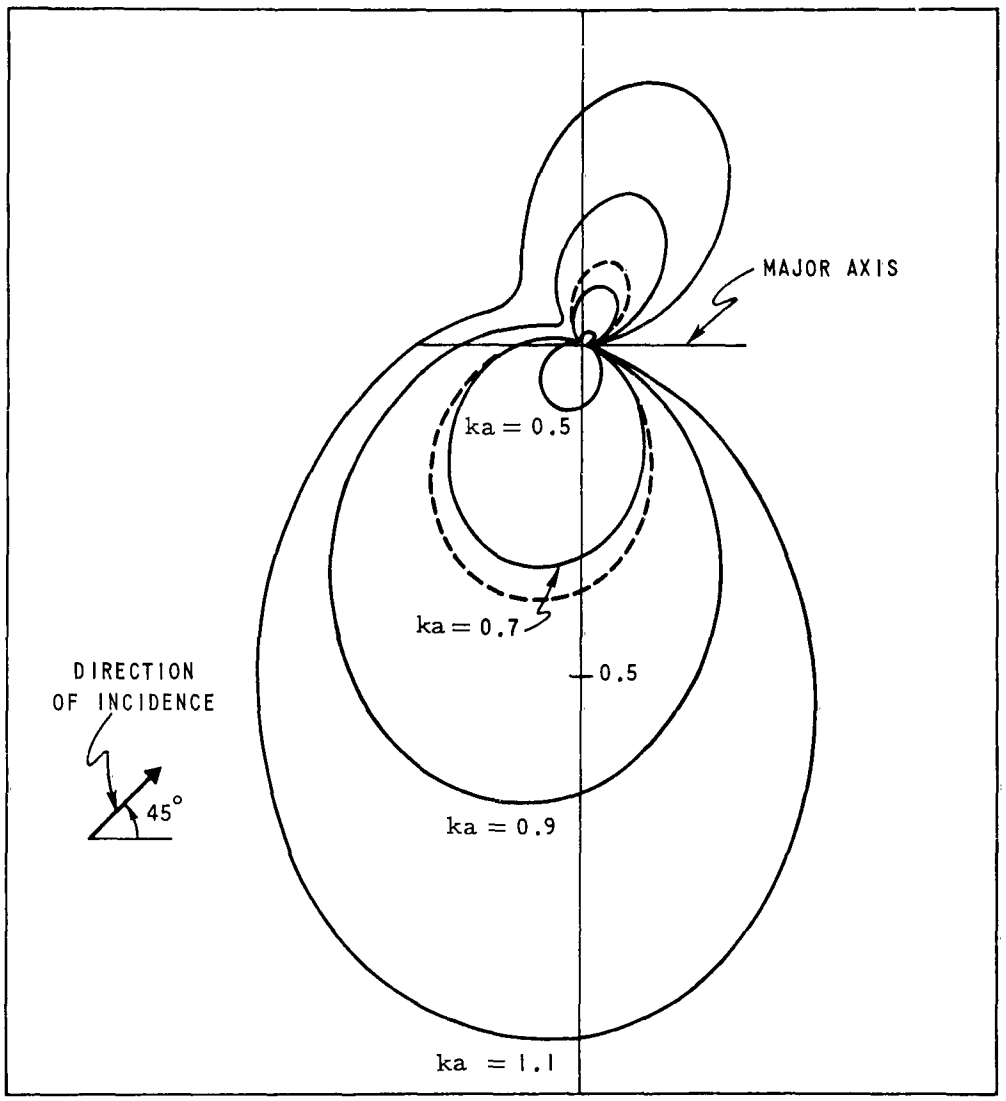

Fig. 6(a).

Fig. 6. Plots of $|g_+(\varphi, 45^\circ)|^2$ versus φ for (a) fixed $\rho = b/a = 0.5$ (and different values of ka), and for (b) fixed ka = 0.5 (and different values of ρ); the dashed curves are based on the k^4 series (35).

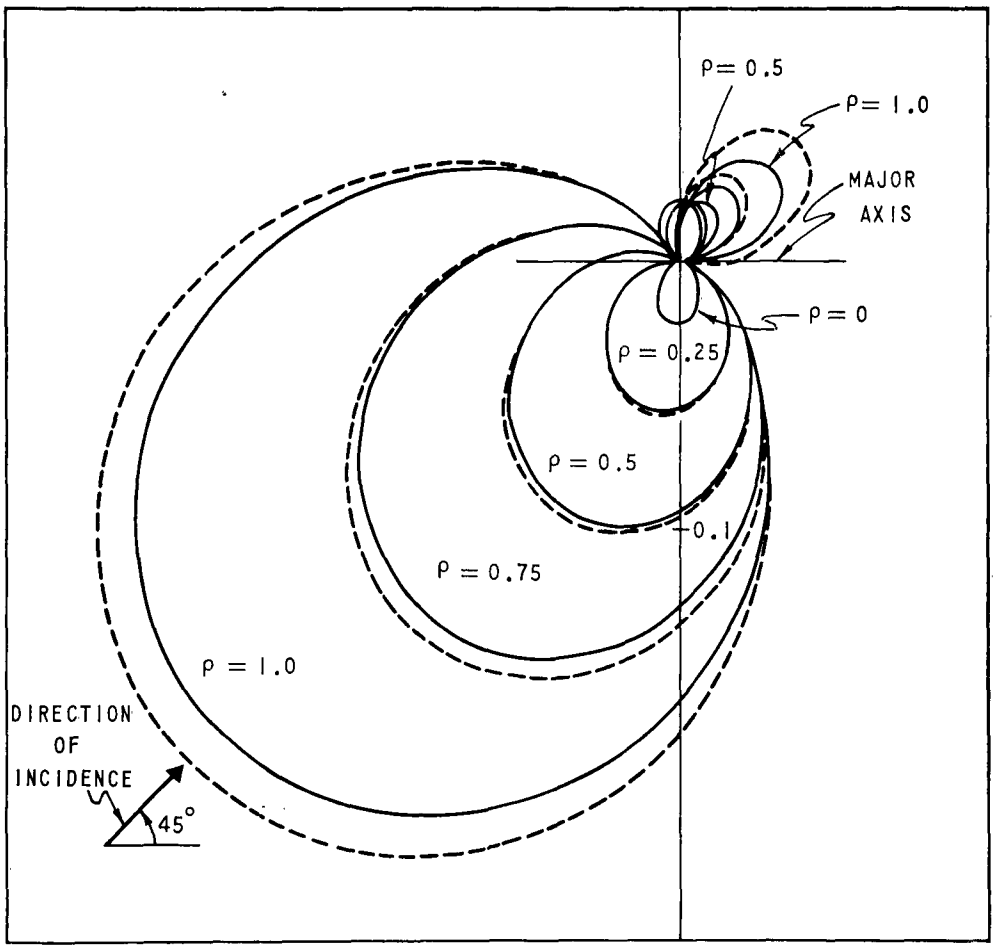
ρ= 0.5
ρ= 1.0
MAJOR
AXIS
ρ = 0
ρ = 0.25
ρ = 0.5
0.1
ρ = 0.75
ρ = 1.0
DIRECTION
OF
INCIDENCE
45°

Fig. 6(b).

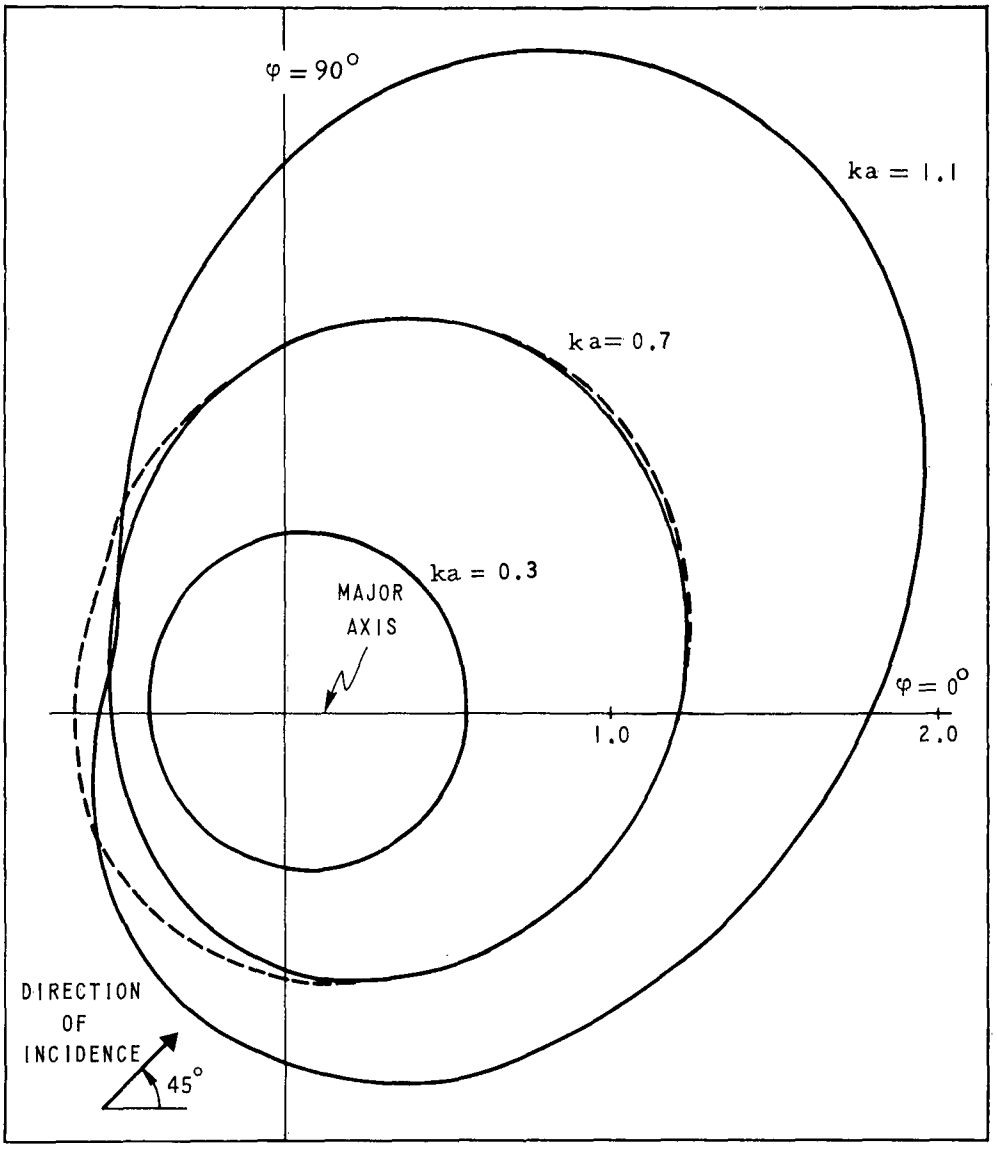

Fig. 7(a).

Fig. 7. Plots of $|g_{-}(\varphi, 45^{\circ})|^2$ versus φ for (a) fixed $\rho = 0.5$ (and different values of ka) and for (b) fixed ka = 0.7 (and different values of ρ); the dashed curves are based on the k^2 series (36). For case (a) the series equals the closed form when $ka \leq 0.3$.

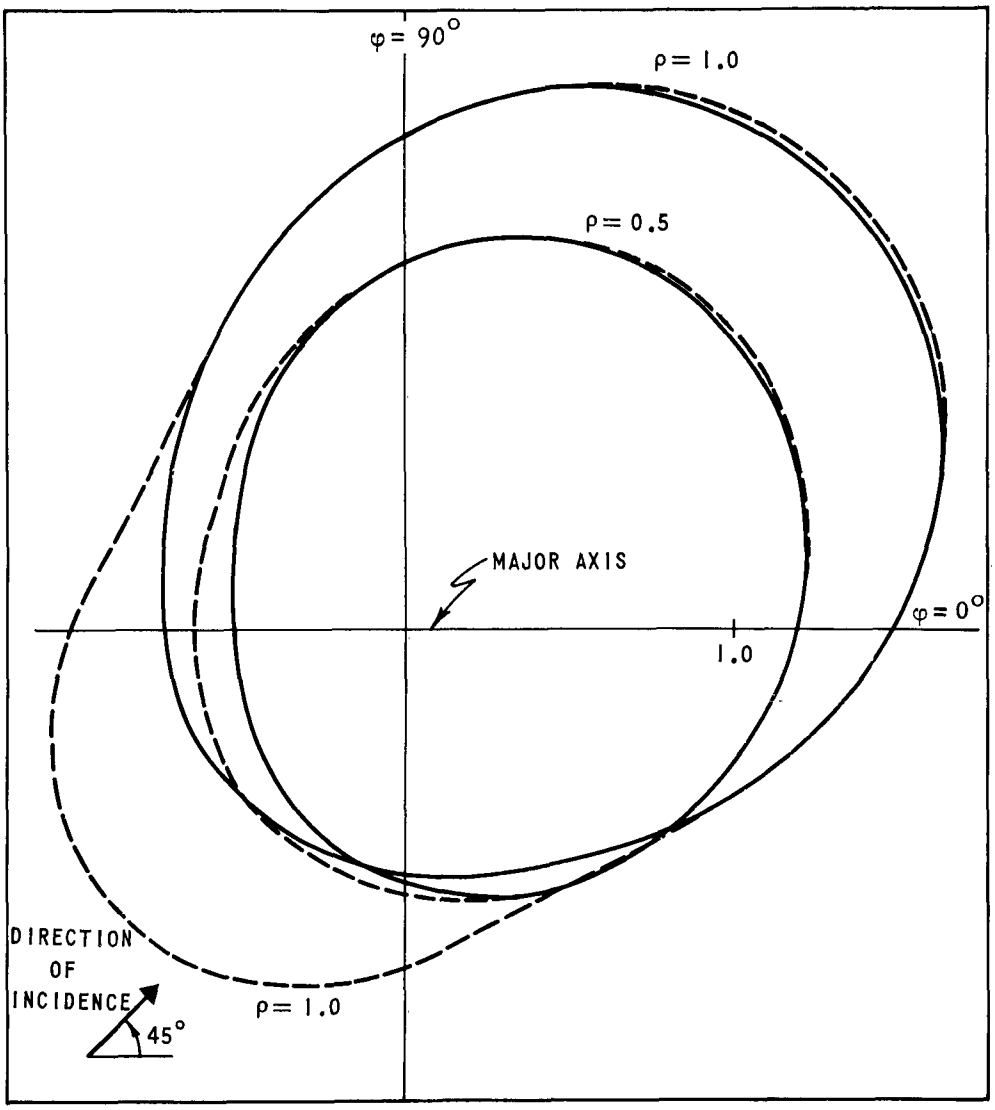

Fig. 7(b).

smaller increments of φ_o were used for protuberances for near-grazing incidence (with respect to the ground plane) to facilitate obtaining the analogous results for elliptically striated surfaces[9].

It is not possible to present the complete set of tables here, and in the following we merely illustrate their contents through a series of graphs. These are given in four sets corresponding to cylinders with $\underset{\sim}{E}$ perpendicular or parallel (Set I and Set II), and to protuberances with $\underset{\sim}{E}$ perpendicular or parallel (Set III and Set IV). The individual graphs are labeled Graph I-1, Graph I-2, etc., where the integer always refers to the same quantity. Thus, without regard to a specific set, the graphs are described in general by the following:

Graph 1: k/4 times the total scattering cross section (i.e., the negative of the real part of the scattering amplitude in the forward direction) versus the angle of incidence (φ_o), for different values of ρ = b/a and ka.

Graph 2: Forward scattered intensity versus the angle of incidence, for different values of ρ and ka.

Graph 3: Forward scattered intensity versus the angle of incidence, for different values of ρ and φ_o.

Graph 4: Back scattered intensity versus the angle of incidence, for different values of ρ and ka.

Graph 5: Back scattered intensity and phase curves versus ka, for different values of ρ and φ_o.

Graph 6 and higher:
Far-field scattering patterns versus the angle of observation (φ), for different values of ρ, ka, and φ_o.

More detailed descriptions of the individual graphs (e.g., the explicit values of the parameters considered) are listed at the beginning of each set.

. . . . .

The authors wish to thank Miss Mary Brockett who drew the graphs.

SET I: Graphical Results for Elliptic Cylinders and $\underline{H}$ Parallel.

Graph I-1: $-\mathrm{Re}\, g_+(\varphi_o, \varphi_o)$ versus φ_o for ka = 0.5, 0.7, 0.9, and 1.1, and different values of ρ.*

Graph I-2: $|g_+(\varphi_o, \varphi_o)|^2$ versus φ_o for ka = 0.5, 0.7, 0.9, and 1.1 and different values of ρ.*

Graph I-3: $|g_+(\varphi_o, \varphi_o)|^2$ and the phase of $g_+(\varphi_o, \varphi_o)$ versus ka $\leq$ 1.1, for φ = 0°(a), 45°(b), and 90°(c), and different values of ρ.*

Graph I-4: $|g_+(\pi+\varphi_o, \varphi_o)|^2$ versus φ_o for ka = 0.5, 0.7, 0.9, and 1.1, and different values of ρ.*

Graph I-5: $|g_+(\pi+\varphi_o, \varphi_o)|^2$ and the phase of $g_+(\pi+\varphi_o, \varphi_o)$ versus ka $\leq$ 1.1, for φ_o = 0°(a), 45°(b), and 90°(c), and different values of ρ.*

Graph I-6: $|g_+(\varphi, \varphi_o)|^2$ versus φ for φ_o = 0(a), 45°(b), and 90°(c), ka = 0.3, and different values of ρ.*

Graph I-7: $|g_+(\varphi, \varphi_o)|^2$ versus φ for φ_o = 0(a), 45°(b), and 90°(c), ka = 0.5, and different values of ρ.*

Graph I-8: $|g_+(\varphi, \varphi_o)|^2$ versus φ for φ_o = 0(a), 45°(b), and 90°(c), ka = 0.7, and different values of ρ.*

Graph I-9: $|g_+(\varphi, \varphi_o)|^2$ versus φ for φ_o = 0(a), 45°(b), and 90°(c), ka = 0.9, and different values of ρ.*

Graph I-10: $|g_+(\varphi, \varphi_o)|^2$ versus φ for φ_o = 0(a), 45°(b), and 90°(c) ka = 1.1, and different values of ρ.*

*The number next to a curve gives the value of ρ = b/a = (minor axis/major axis).

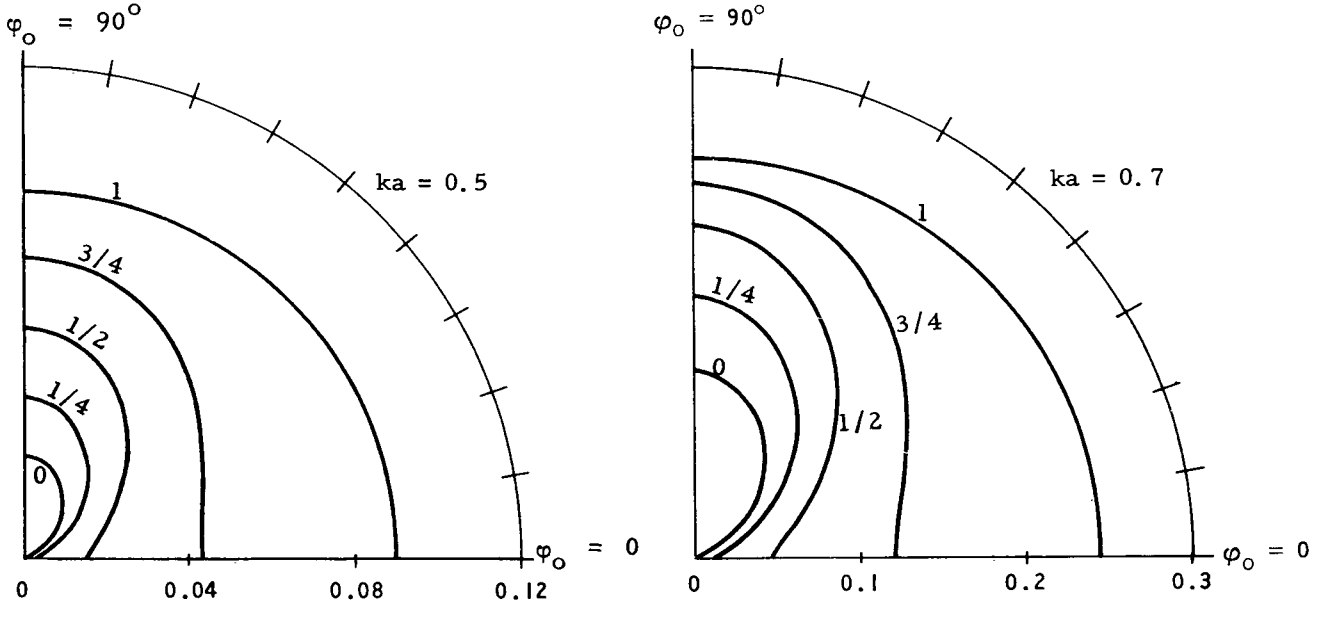

Graph I-1: -Re $g_+(\varphi_o, \varphi_o)$.

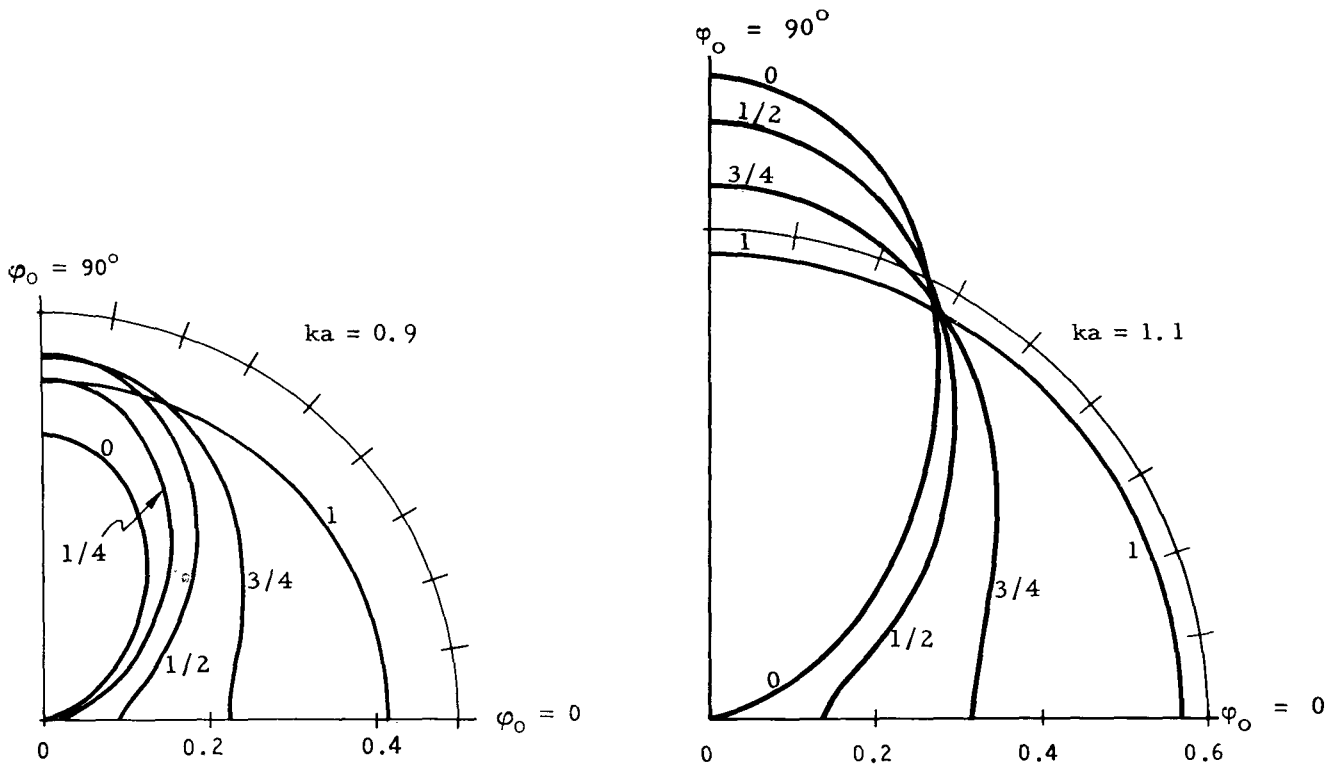

Graph I-1 (Con't): -Re $g_+(\varphi_o,\varphi_o)$.

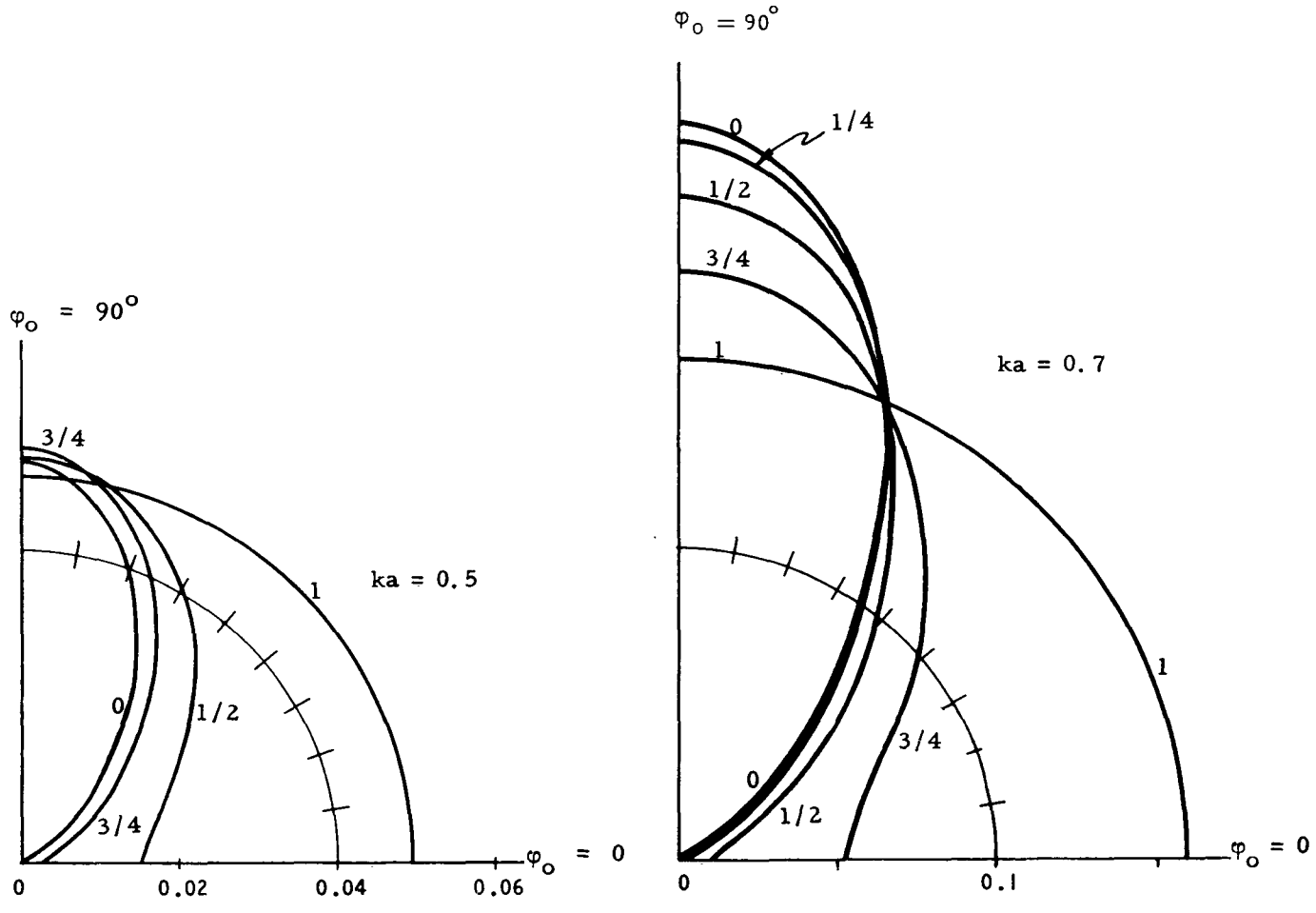

Graph I-2: $|g_+(\varphi_o, \varphi_o)|^2$.

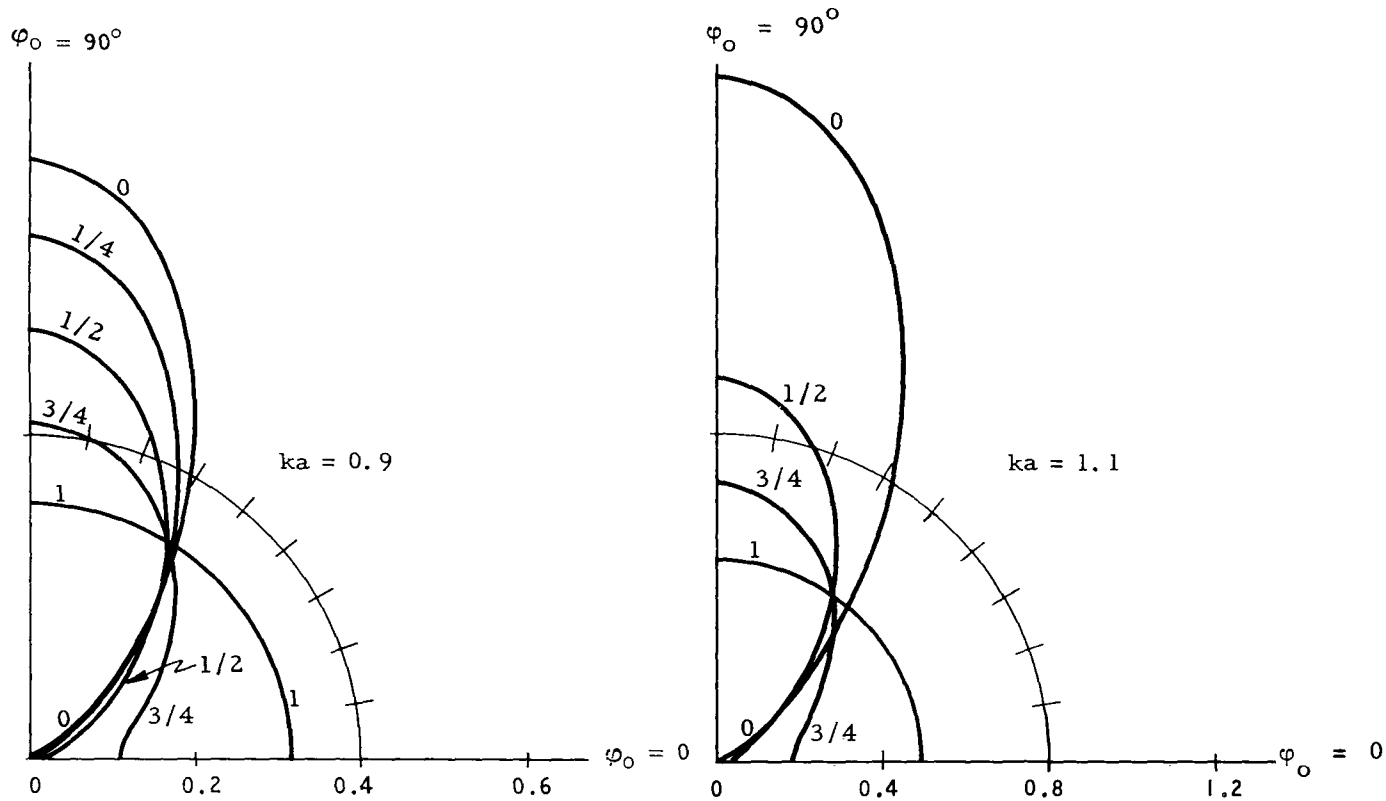

Graph I-2 (Con't): $|g_+(\varphi_o, \varphi_o)|^2$.

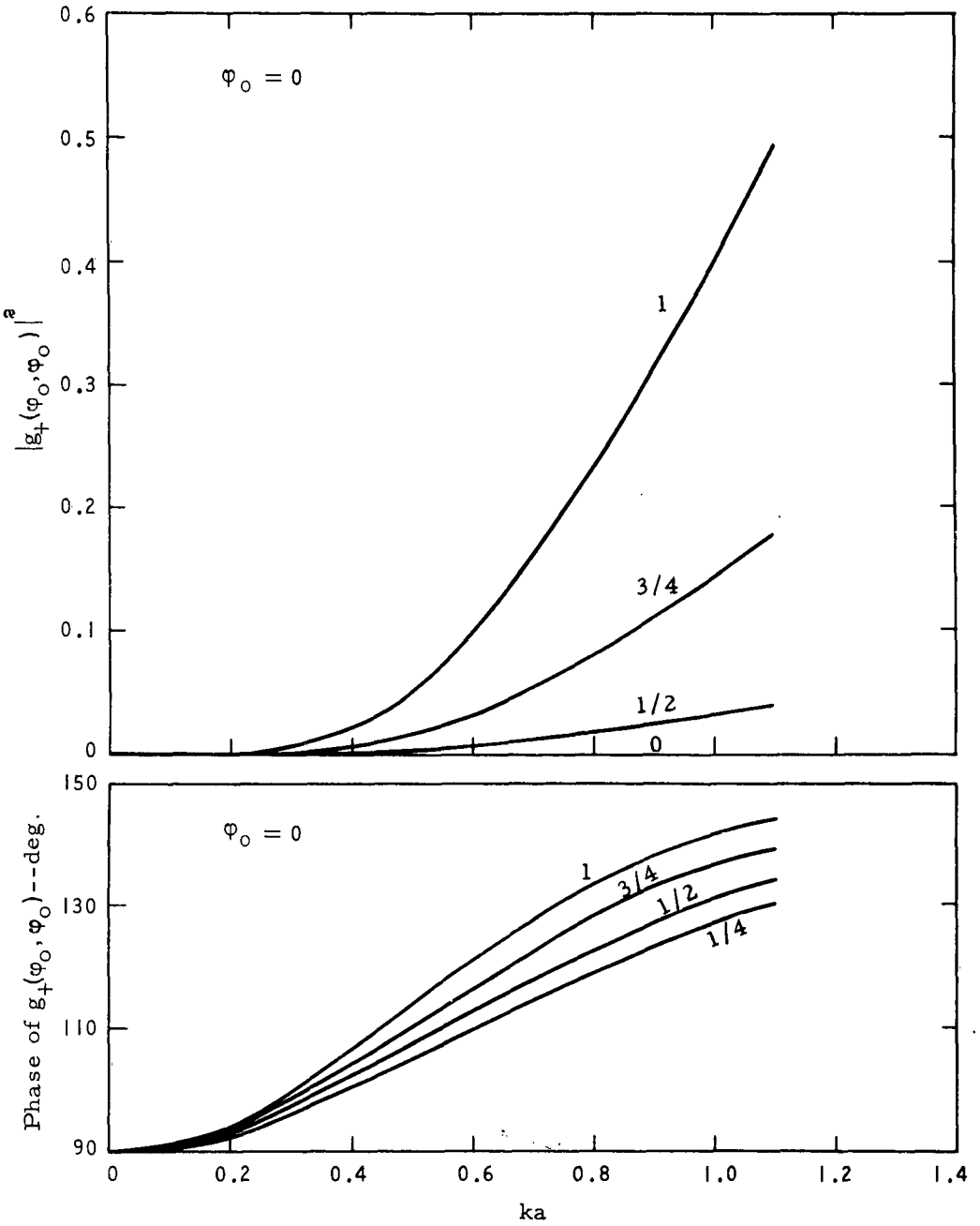
$\varphi_o = 0$
$|g_+(\varphi_o, \varphi_o)|^2$
1
3/4
1/2
0
$\varphi_o = 0$
Phase of $g_+(\varphi_o, \varphi_o)$--deg.
1
3/4
1/2
1/4
ka

Graph I-3(a).

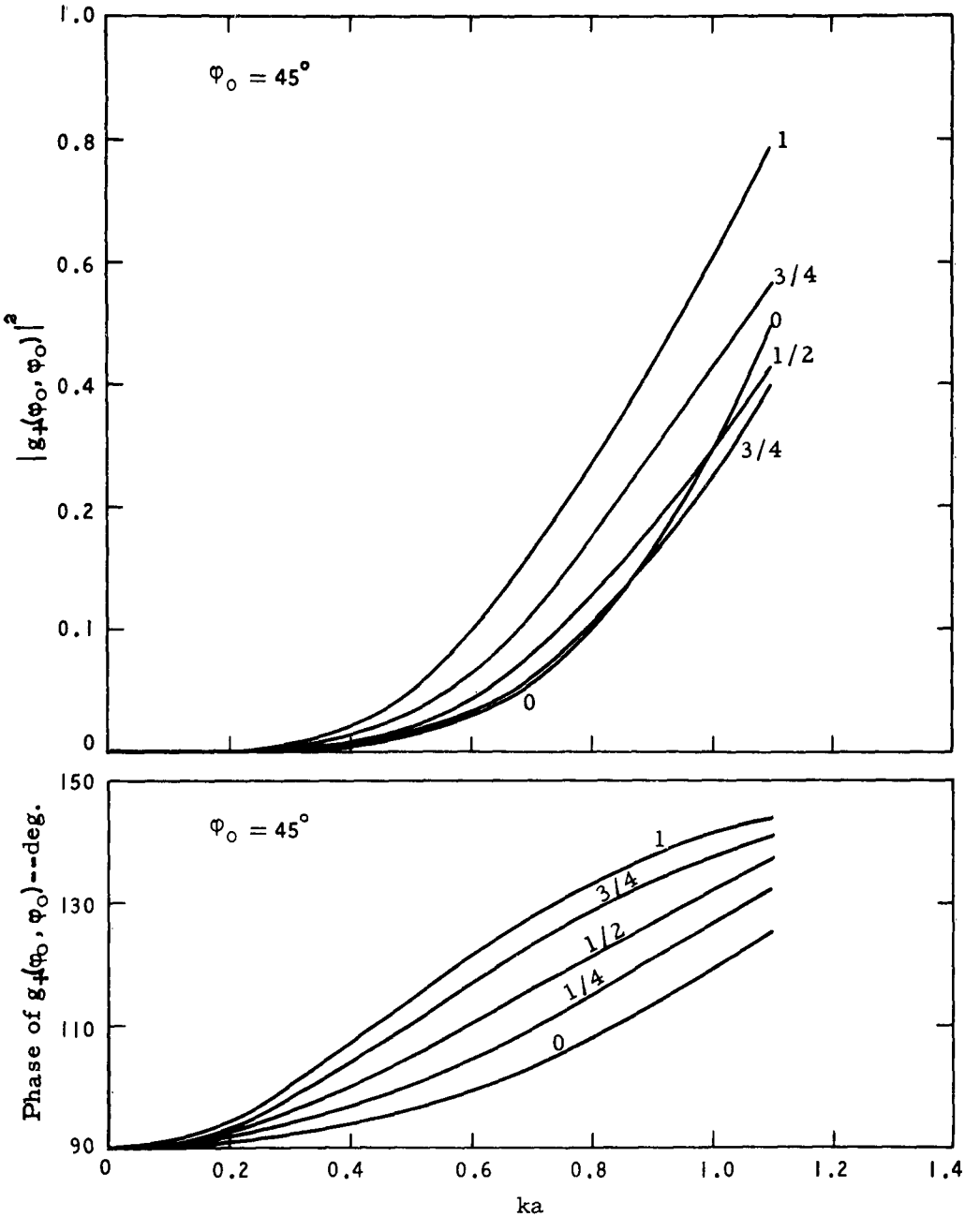
1.0
0.8
0.6
0.4
0.2
0.1
0
$\varphi_o = 45°$
1
3/4
0
1/2
3/4
0
$|g_+(\varphi_o, \varphi_o)|^2$
150
130
110
90
$\varphi_o = 45°$
1
3/4
1/2
1/4
0
Phase of $g_+(\varphi_o, \varphi_o)$--deg.
0
0.2
0.4
0.6
0.8
1.0
1.2
1.4
ka

Graph I-3(b).

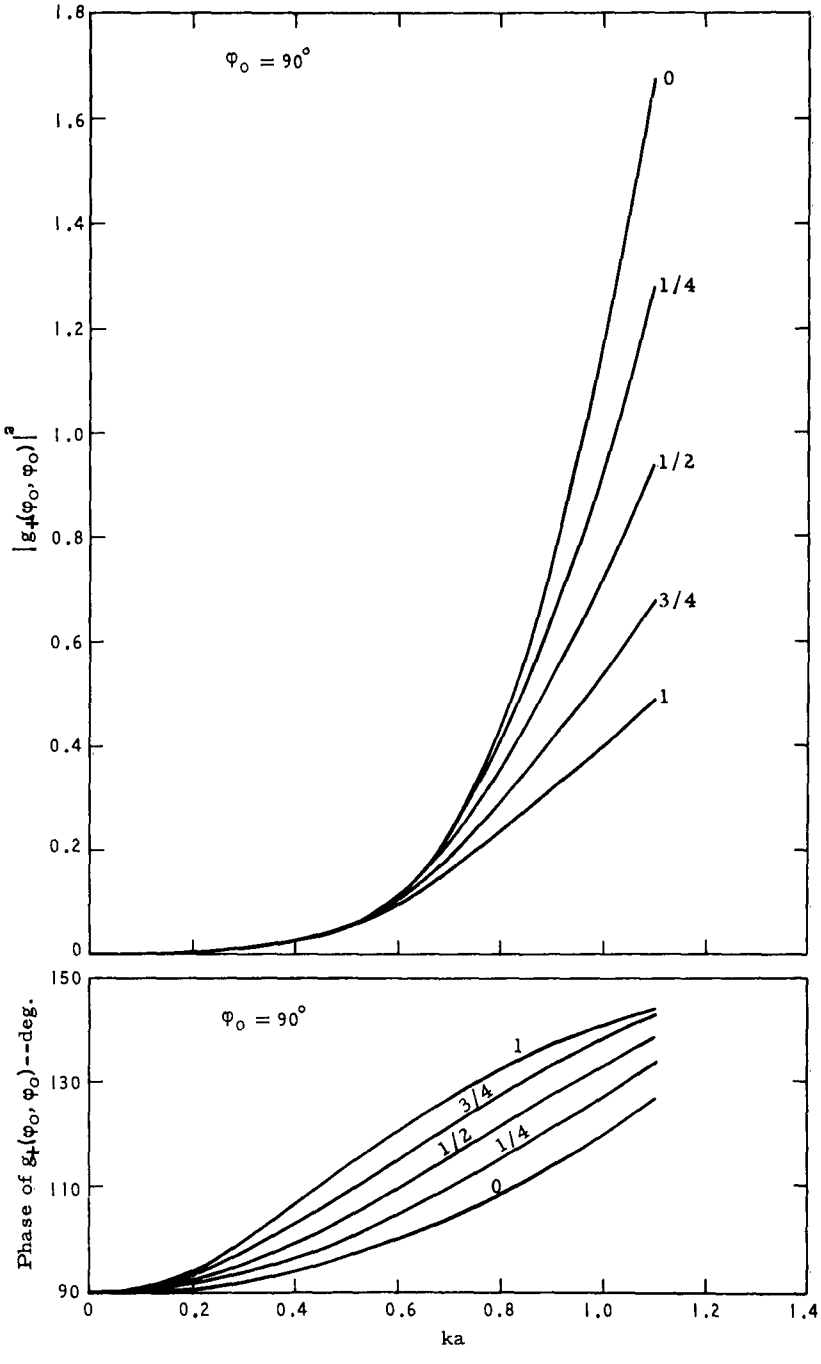
$\varphi_o = 90°$
0
1/4
1/2
3/4
1
$|g_4(\varphi_o, \varphi_o)|^2$
Phase of $g_4(\varphi_o, \varphi_o)$--deg.
ka

Graph I-3(c)

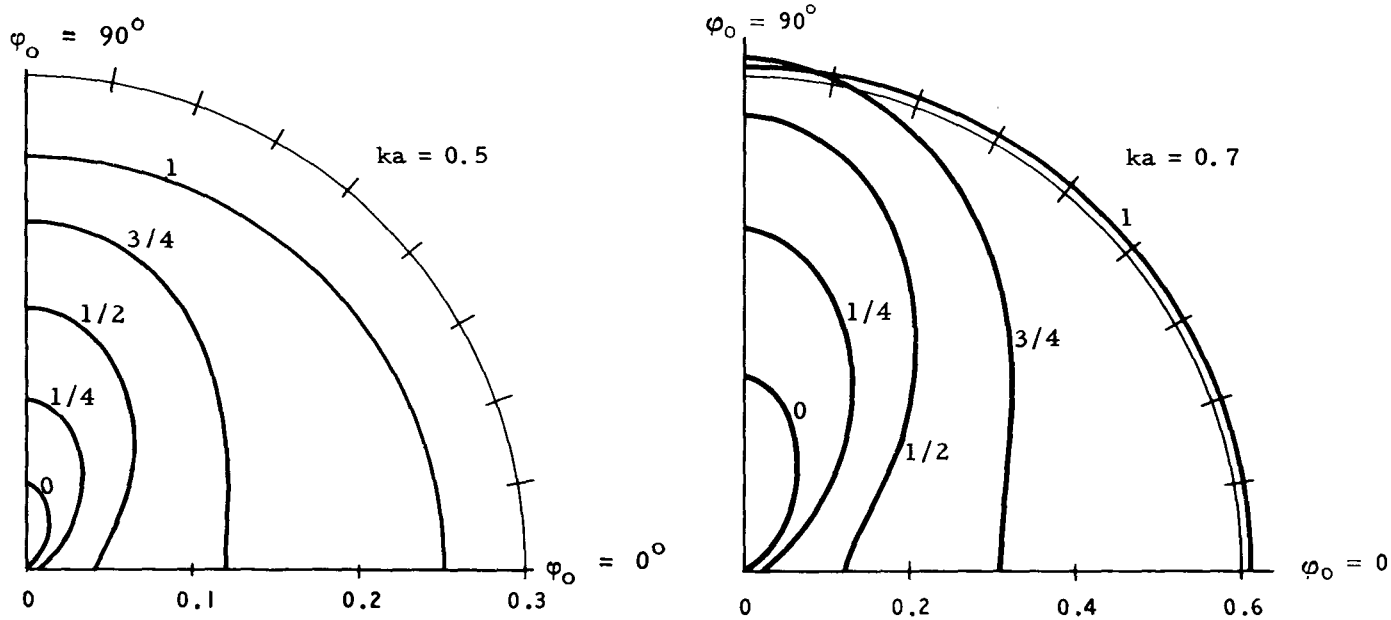

Graph I-4: $|g_+(\pi+\varphi_o, \varphi_o)|^2$.

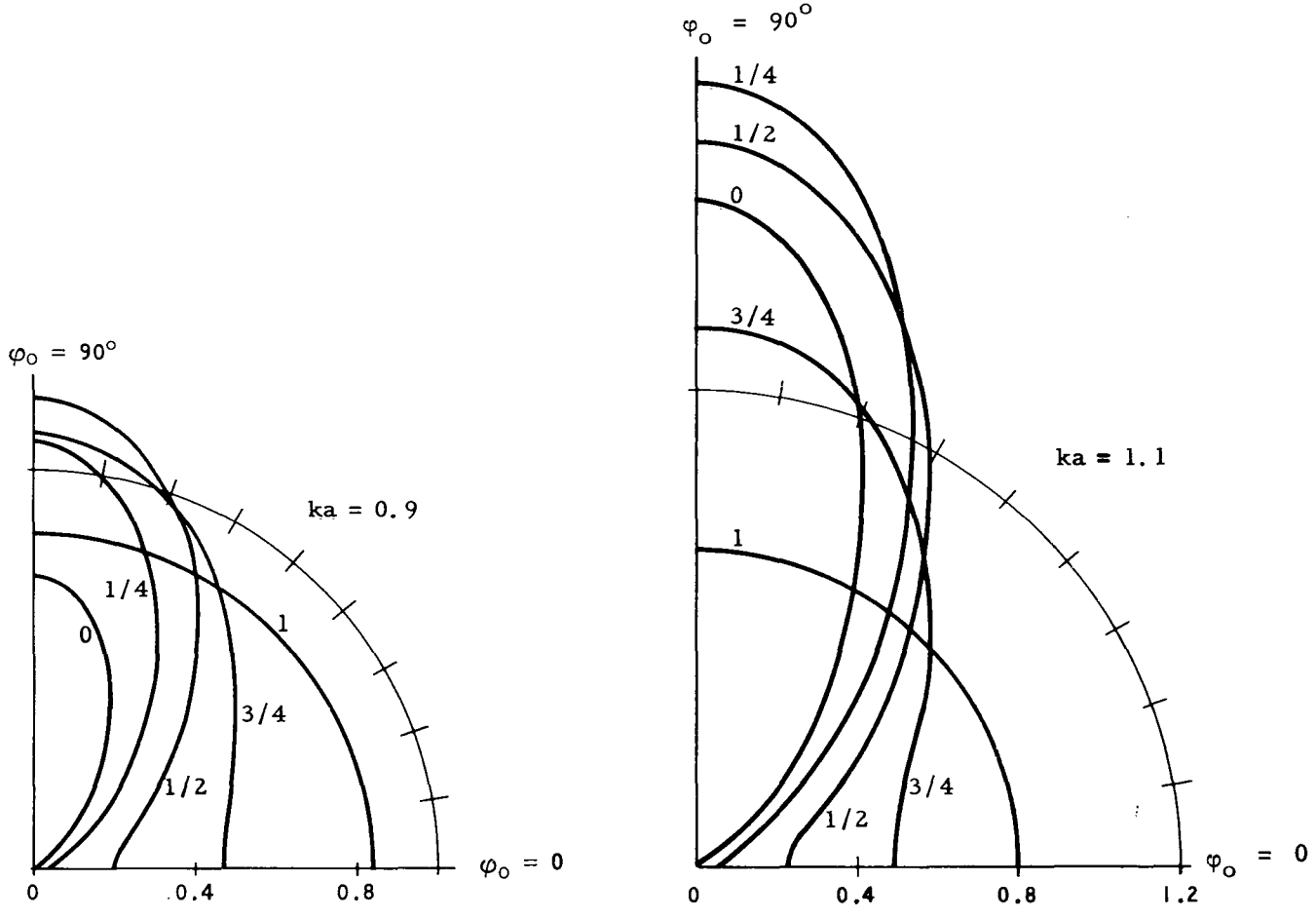

Graph I-4 (Con't): $|g_+(\pi+\varphi_o, \varphi_o)|^2$.

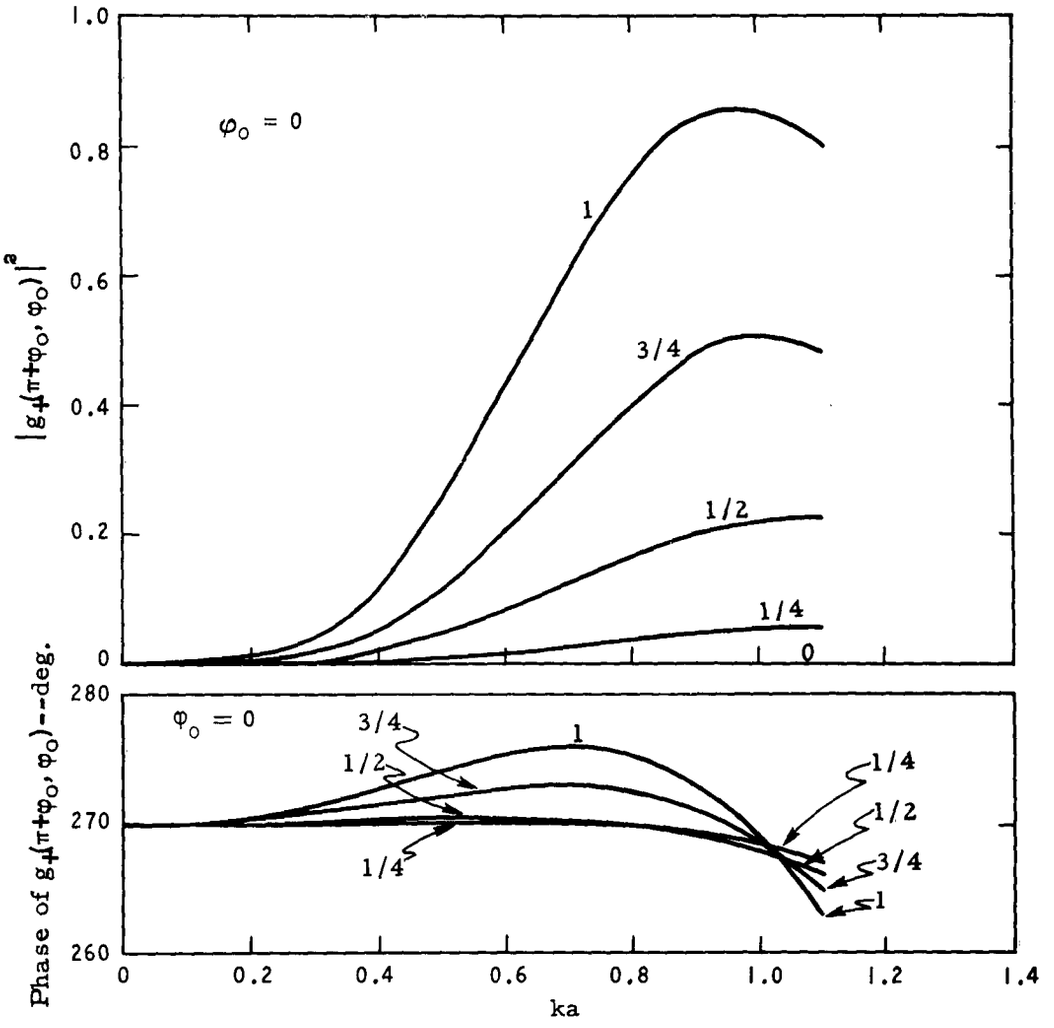
1.0
0.8
0.6
0.4
0.2
0
$\varphi_o = 0$
1
3/4
1/2
1/4
0
$|g_\perp(\pi+\varphi_o, \varphi_o)|^2$
280
270
260
$\varphi_o = 0$
3/4
1/2
1
1/4
1/2
3/4
1
1/4
Phase of $g_\perp(\pi+\varphi_o, \varphi_o)$--deg.
0
0.2
0.4
0.6
0.8
1.0
1.2
1.4
ka

Graph I-5(a).

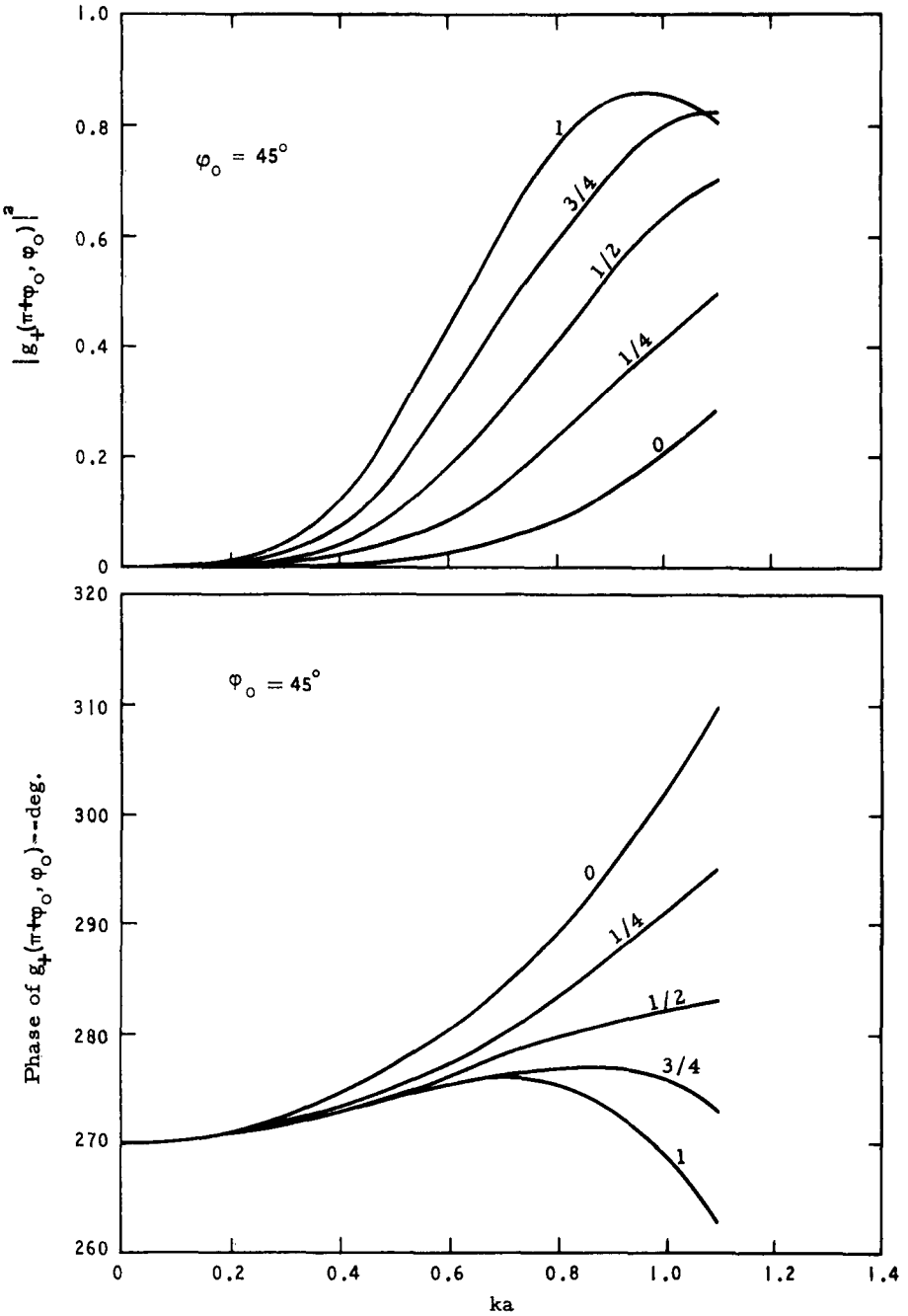
1.0
0.8
0.6
0.4
0.2
0
$|g_+(\pi+\varphi_0, \varphi_0)|^2$
$\varphi_0 = 45°$
1
3/4
1/2
1/4
0
320
310
300
290
280
270
260
Phase of $g_+(\pi+\varphi_0, \varphi_0)$--deg.
$\varphi_0 = 45°$
0
1/4
1/2
3/4
1
0
0.2
0.4
0.6
0.8
1.0
1.2
1.4
ka

Graph I-5(b).

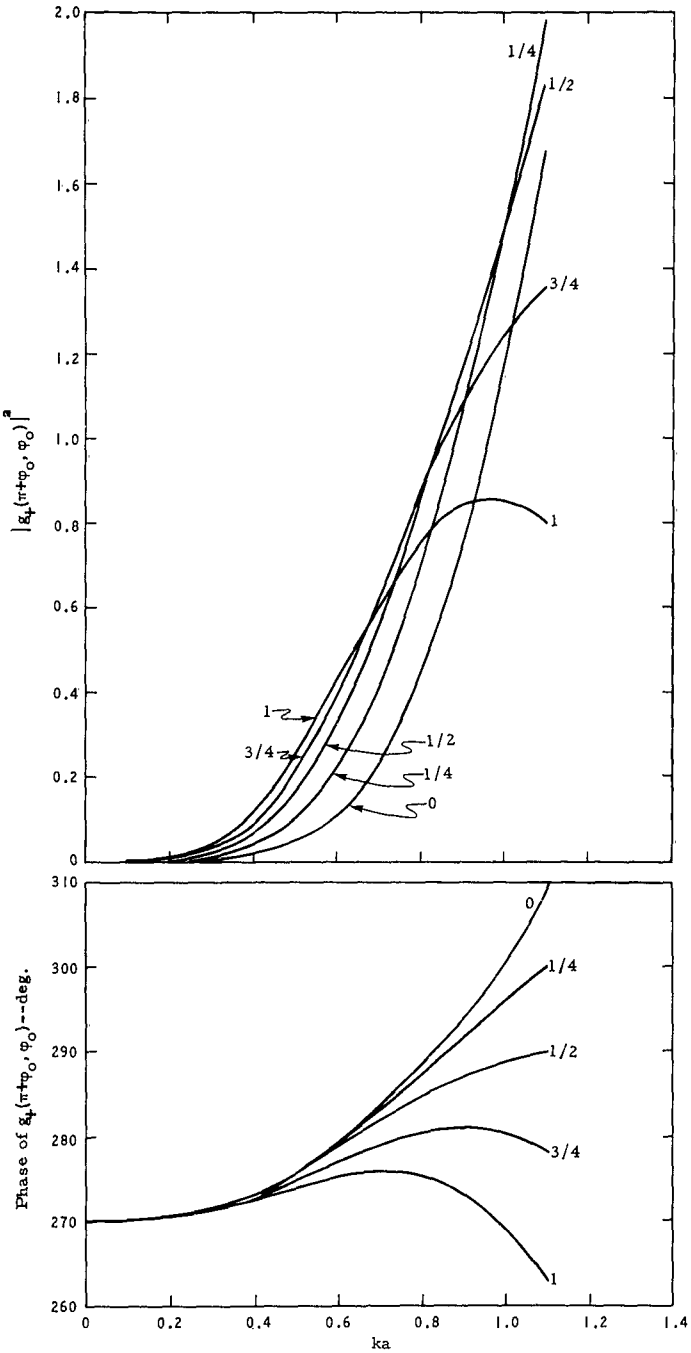
2.0
1.8
1.6
1.4
1.2
1.0
0.8
0.6
0.4
0.2
0
$|g_+(\pi+\varphi_o, \varphi_o)|^2$
1/4
1/2
3/4
1
1
3/4
1/2
1/4
0
310
300
290
280
270
260
Phase of $g_+(\pi+\varphi_o, \varphi_o)$--deg.
0
1/4
1/2
3/4
1
0
0.2
0.4
0.6
0.8
1.0
1.2
1.4
ka

Graph I-5(c)

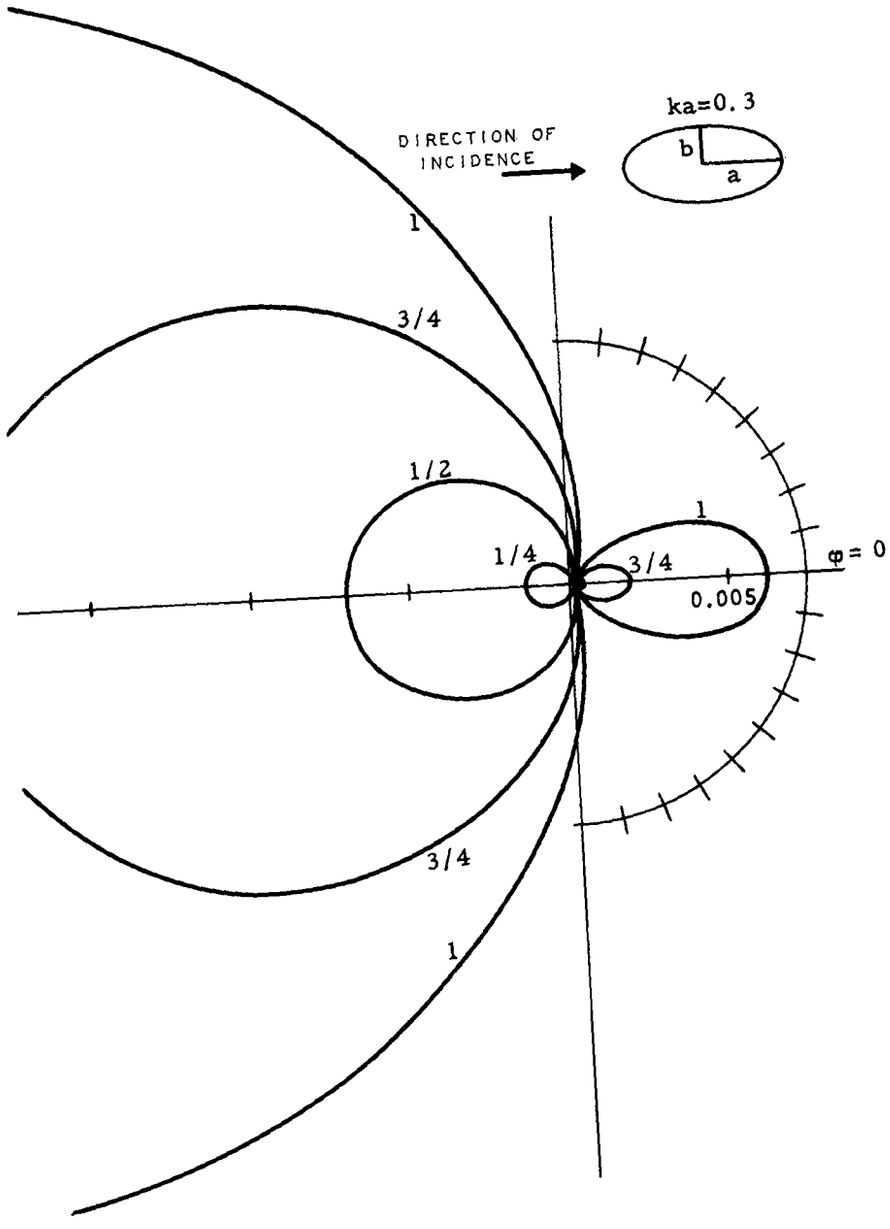

Graph I-6(a): $|g_+(\varphi, 0)|^2$.

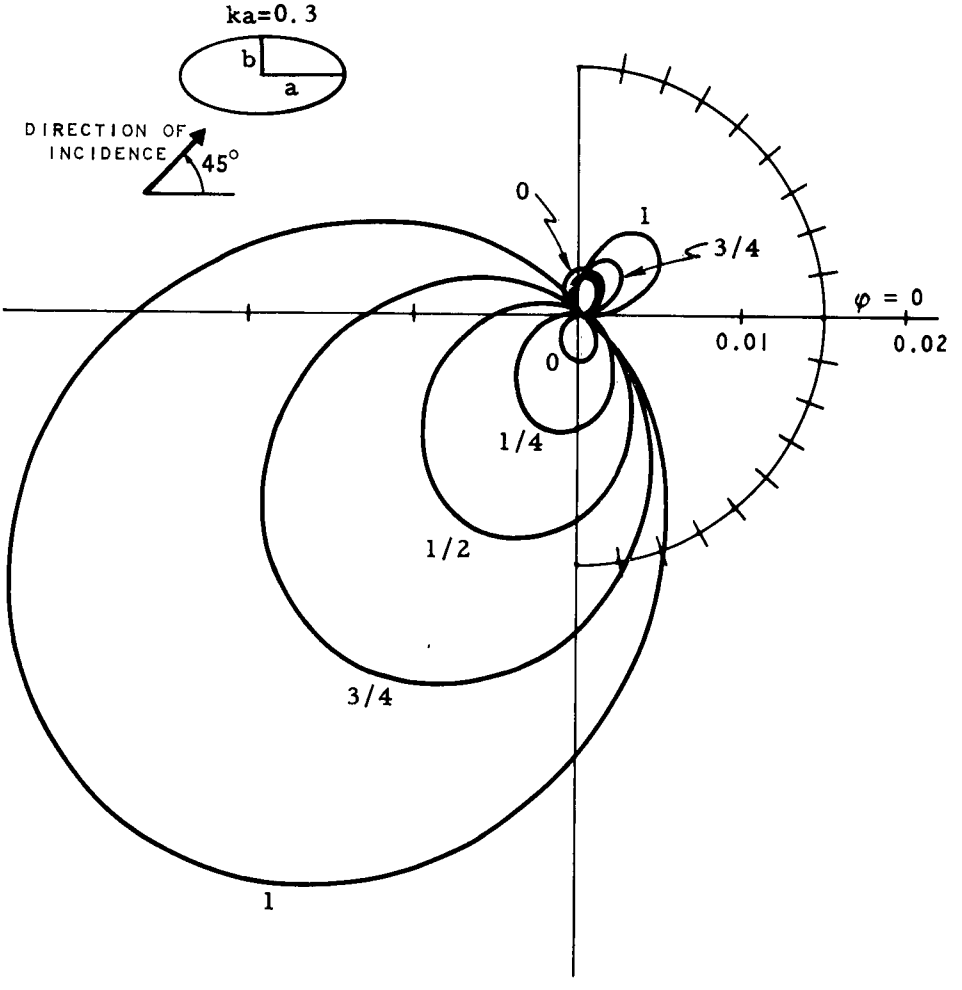

Graph I-6(b): $|g_+(\varphi, 45^\circ)|^2$.

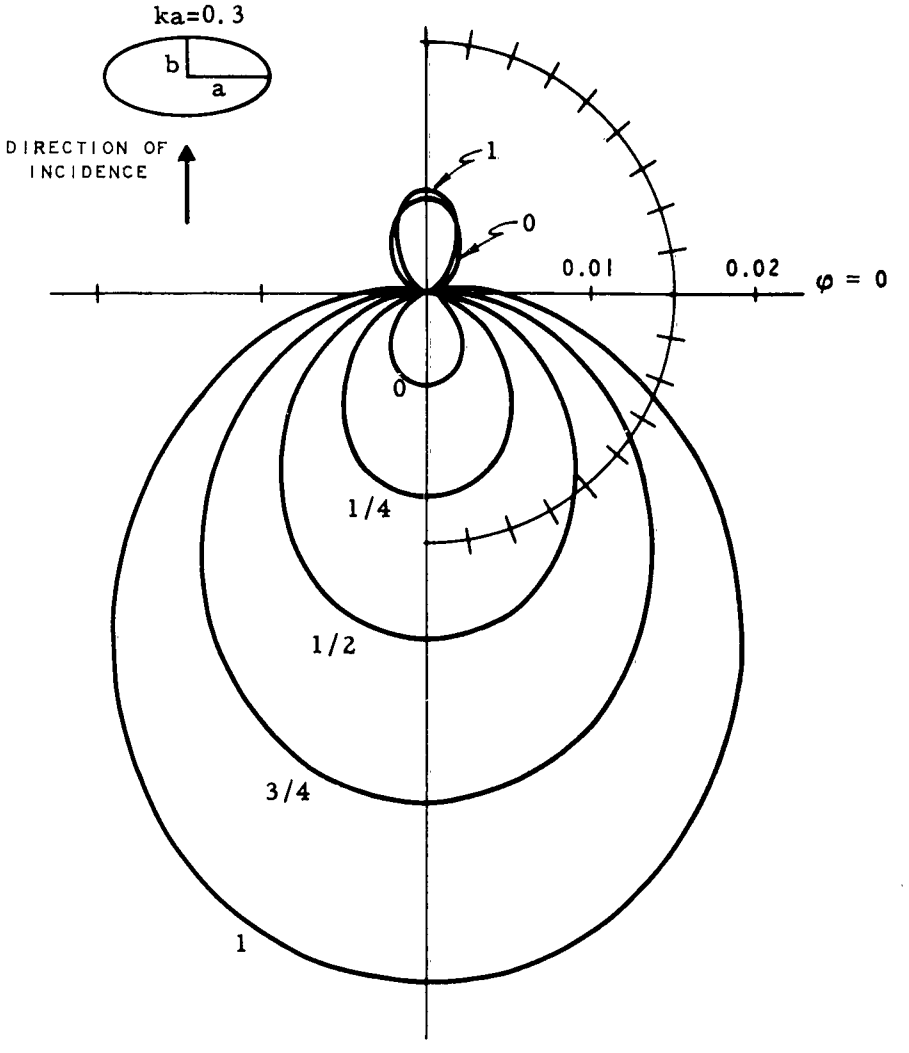

Graph I-6(c): $|g_+(\varphi, 90^\circ)|^2$.

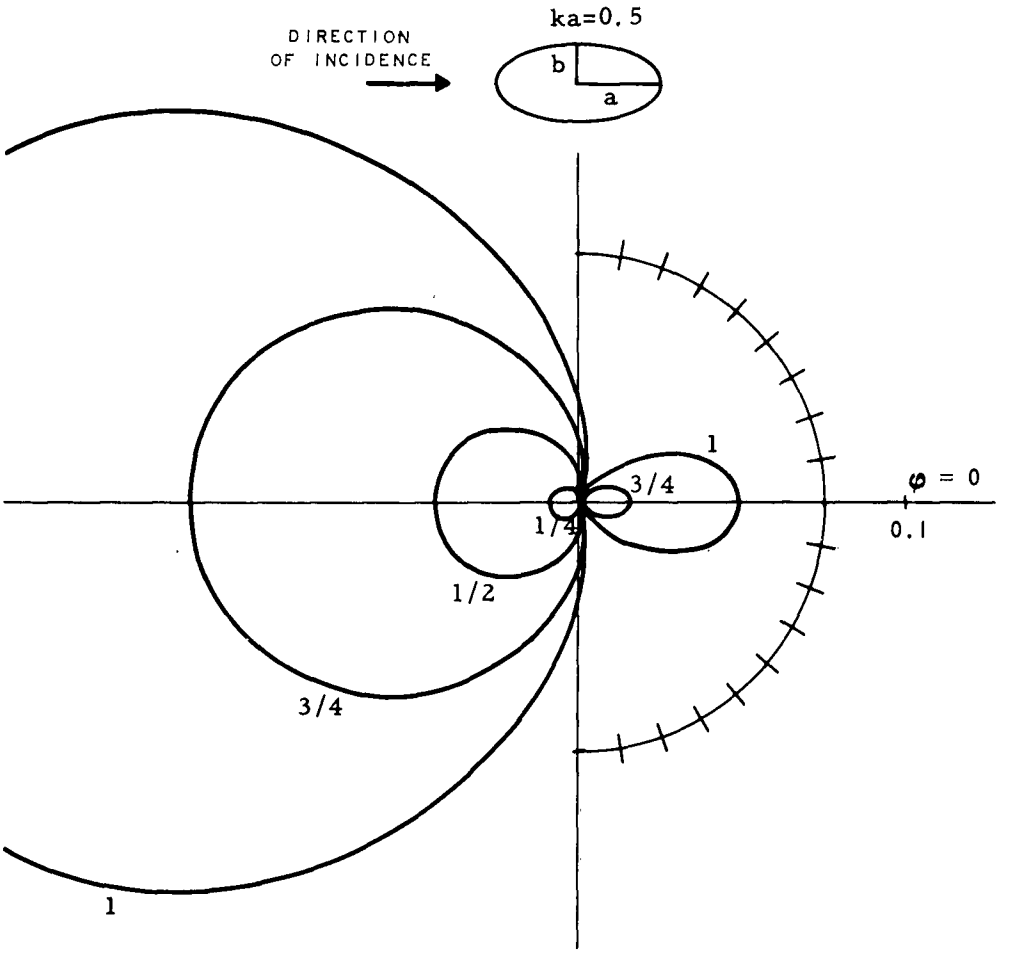

Graph I-7(a): $|g_+(\varphi, 0)|^2$.

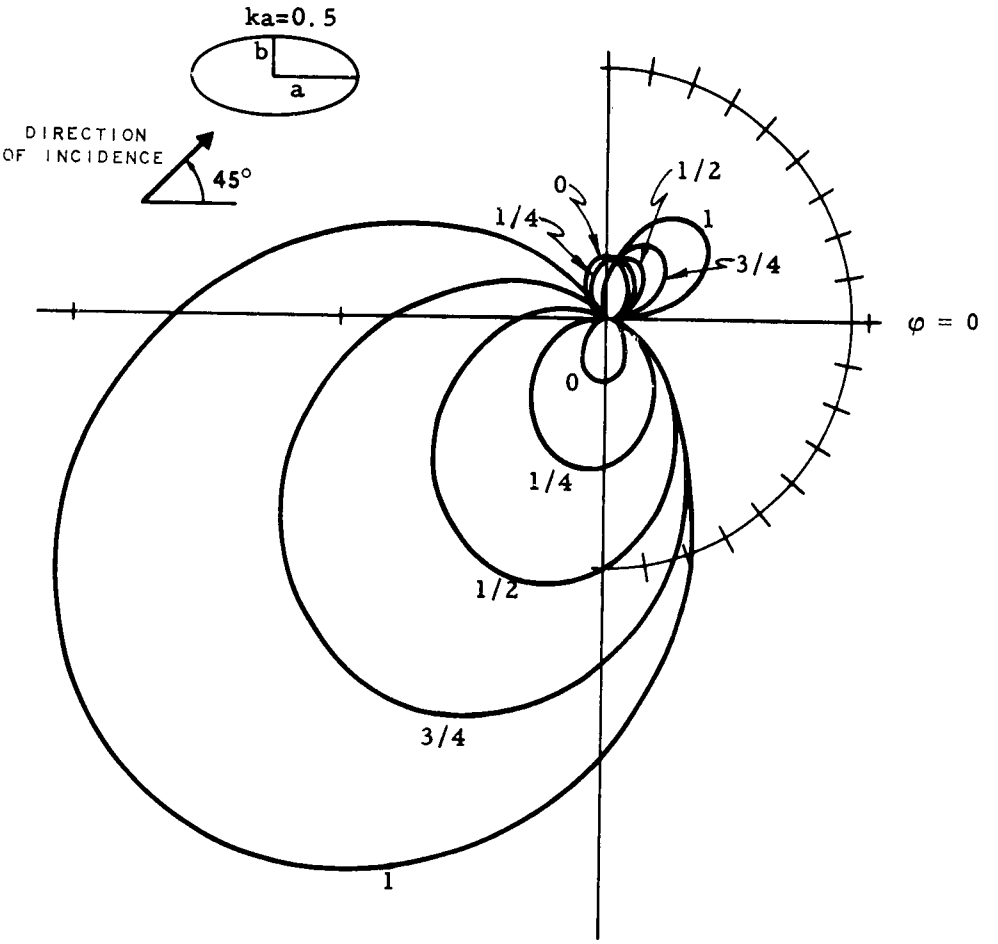

Graph I-7(b): $|g_+(\varphi, 45^\circ)|^2$.

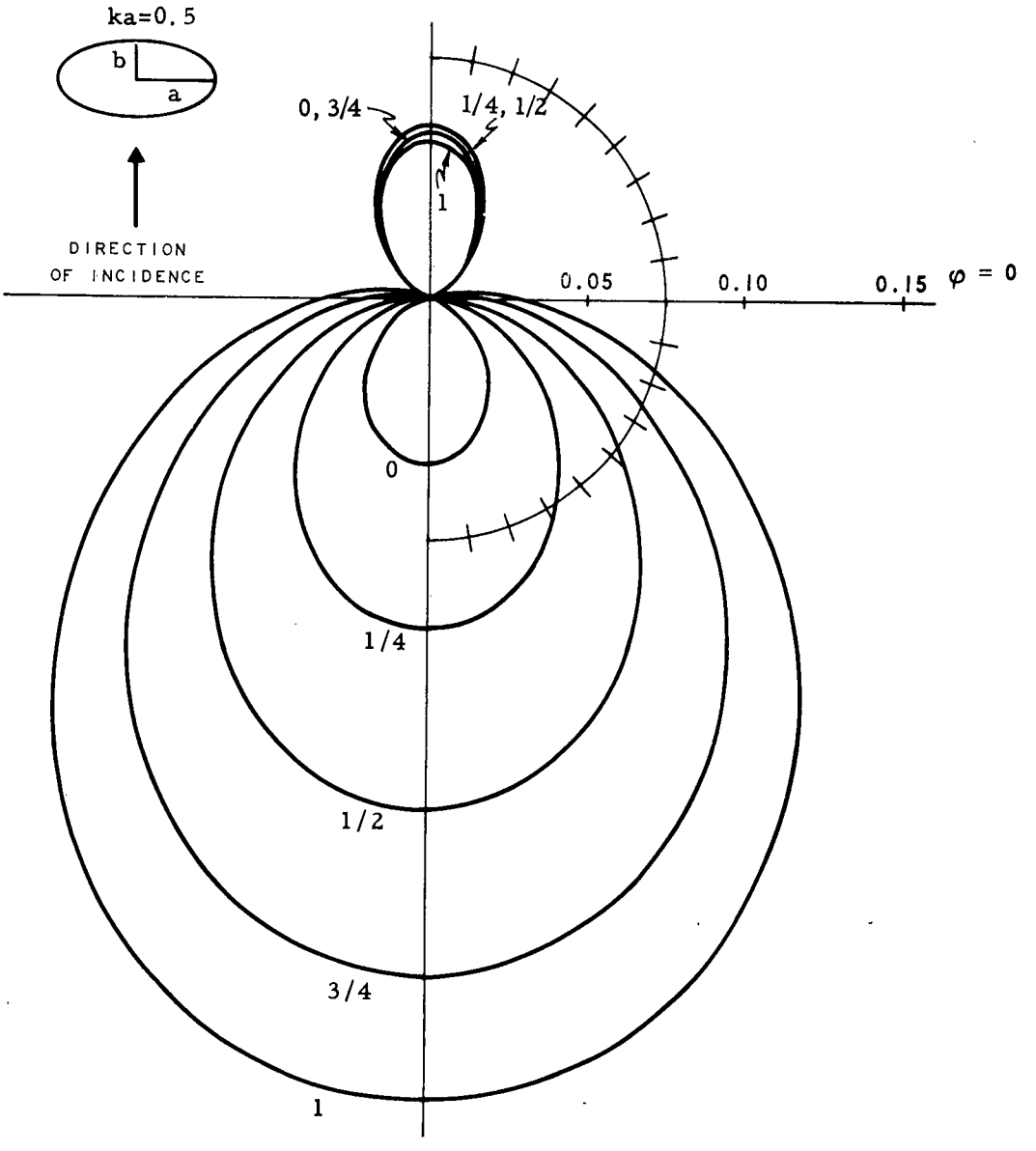

Graph I-7(c): $|g_+(\varphi, 90^\circ)|^2$.

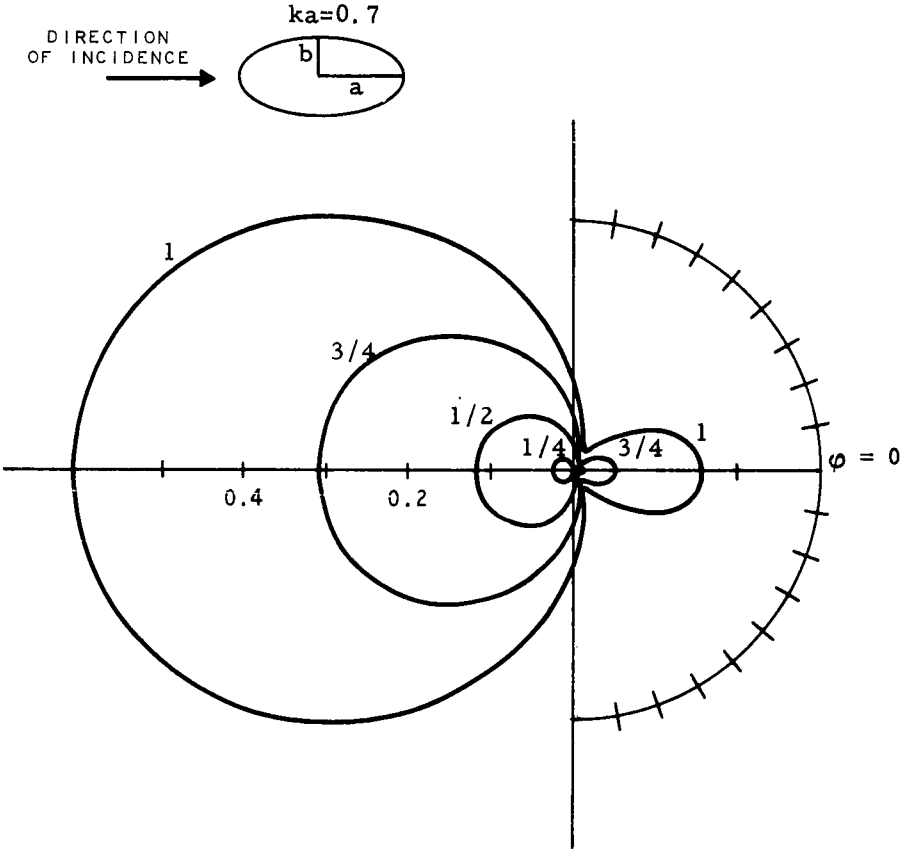

Graph I-8(a): $|g_+(\varphi, 0)|^2$.

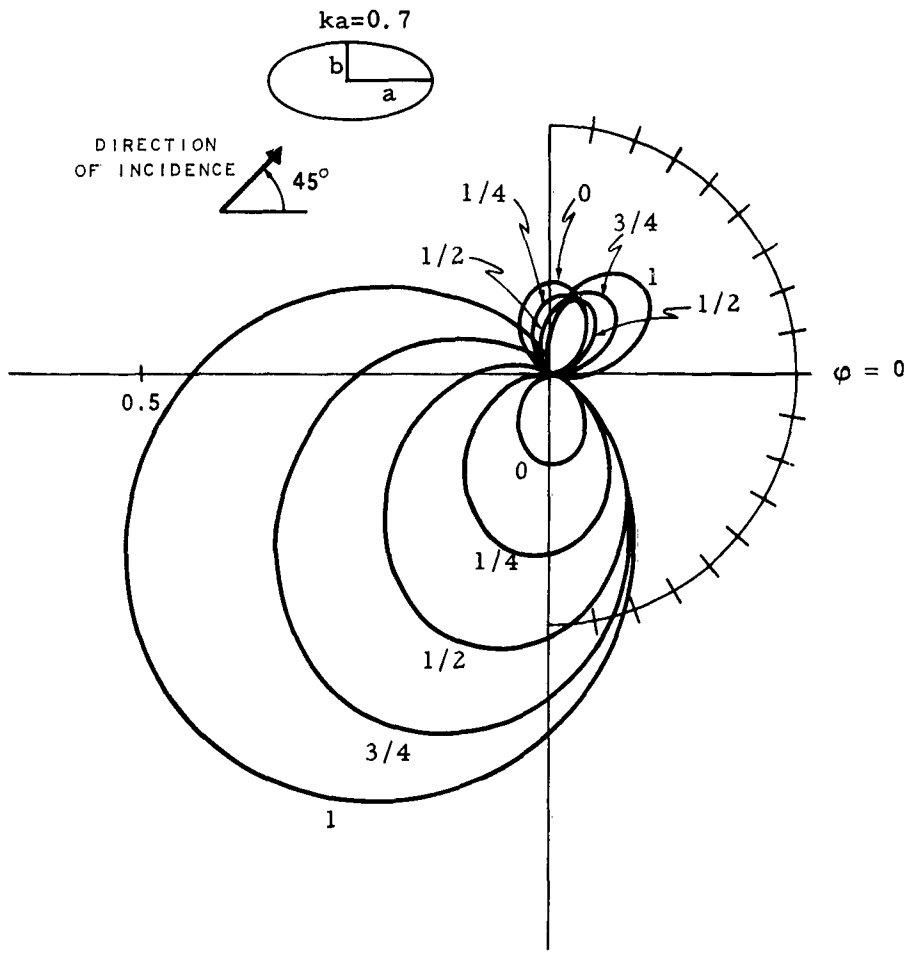

Graph I-8(b): $|g_+(\varphi, 45^\circ)|^2$.

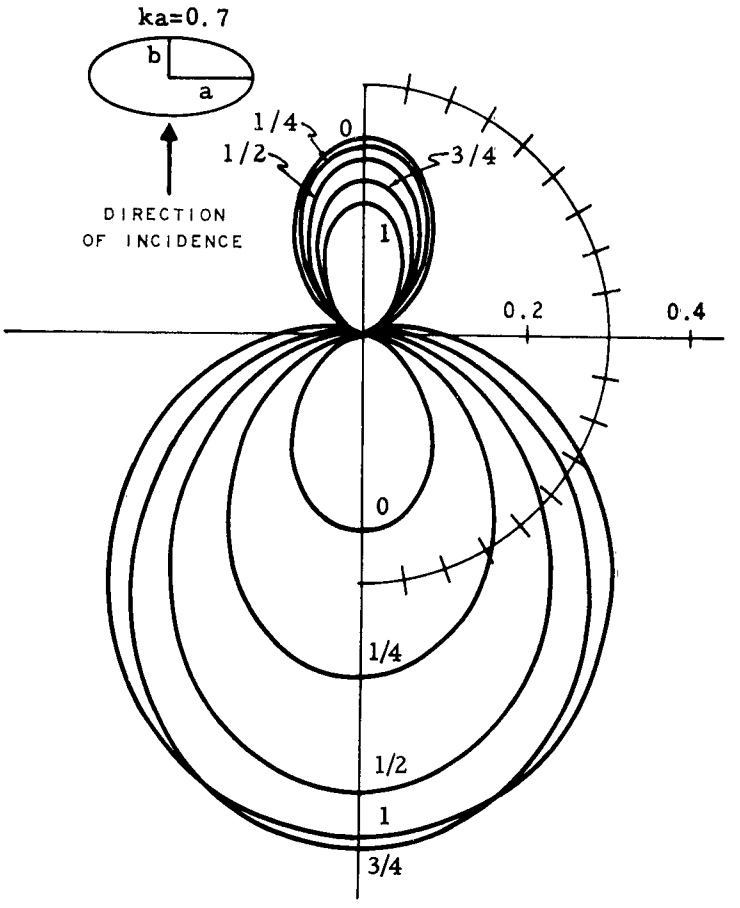

Graph I-8(c): $|g_+(\varphi, 90^\circ)|^2$.

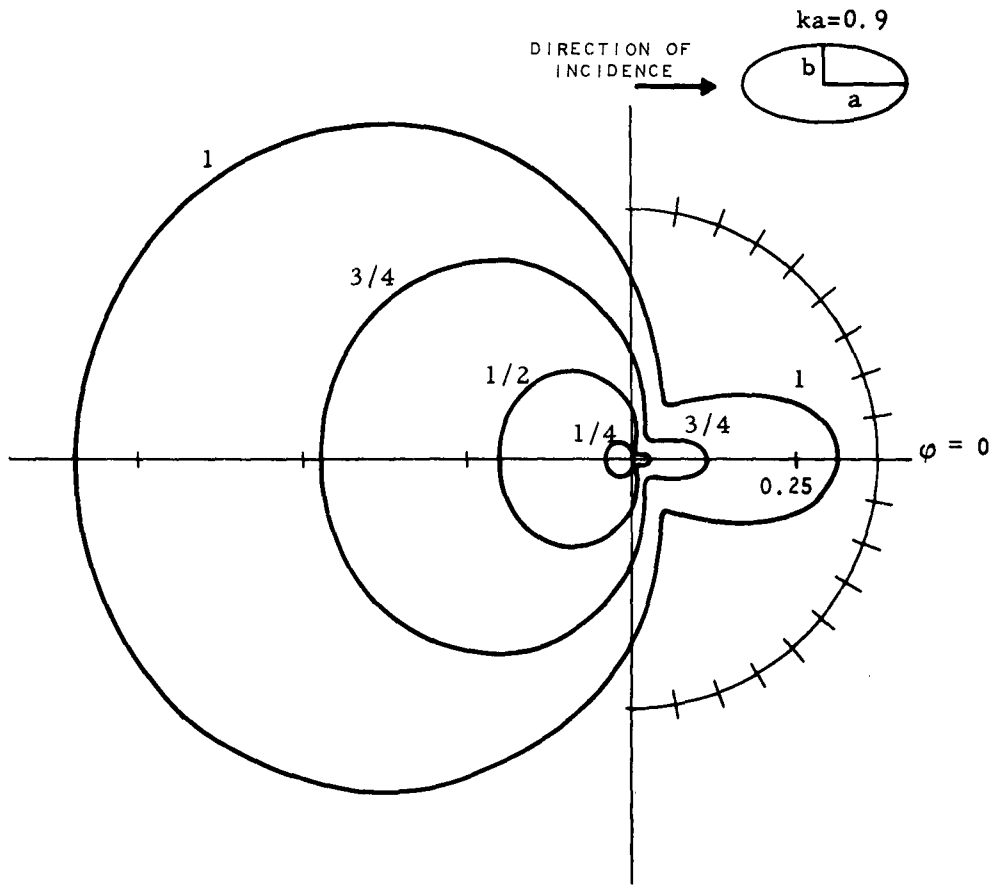

Graph I-9(a): $|g_+(\varphi, 0)|^2$.

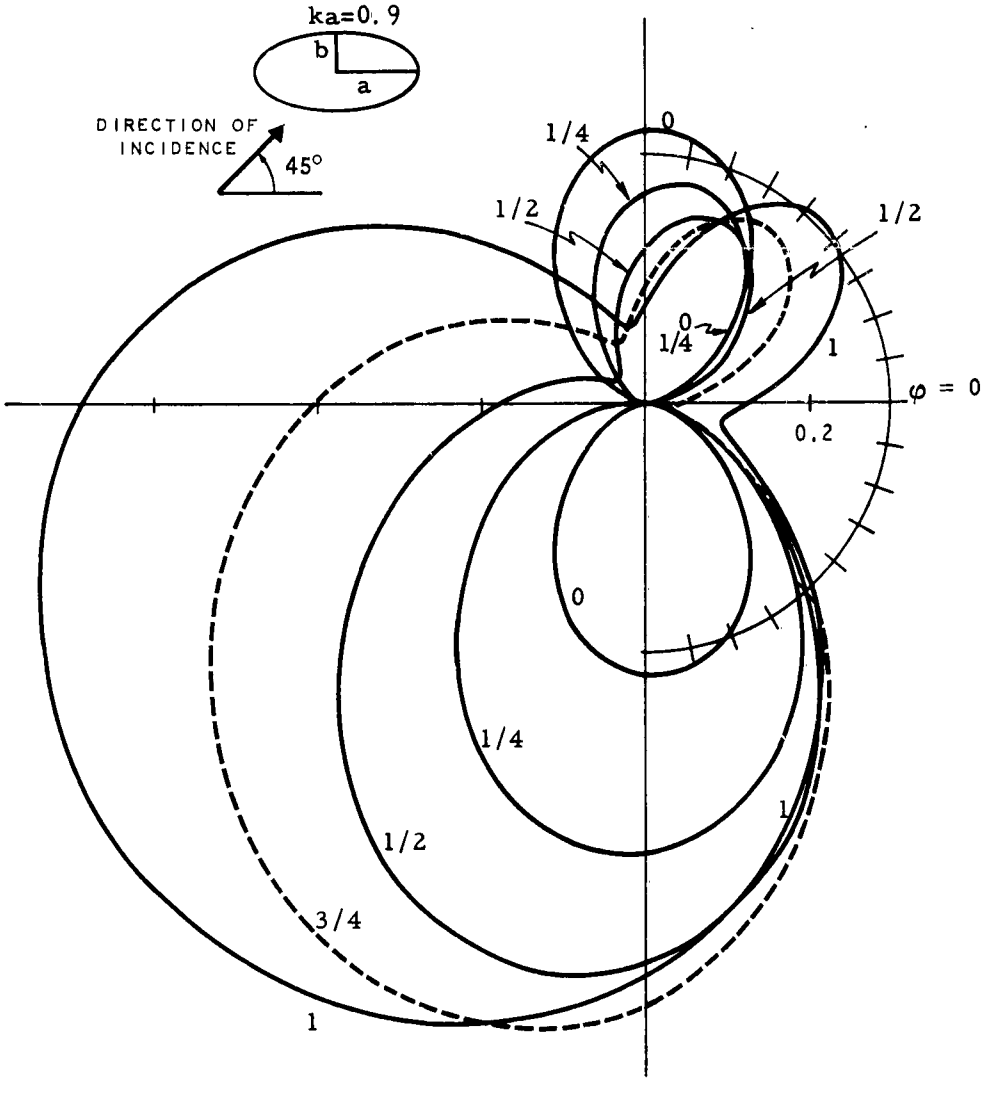

Graph I-9(b): $|g_+(\varphi, 45^\circ)|^2$.

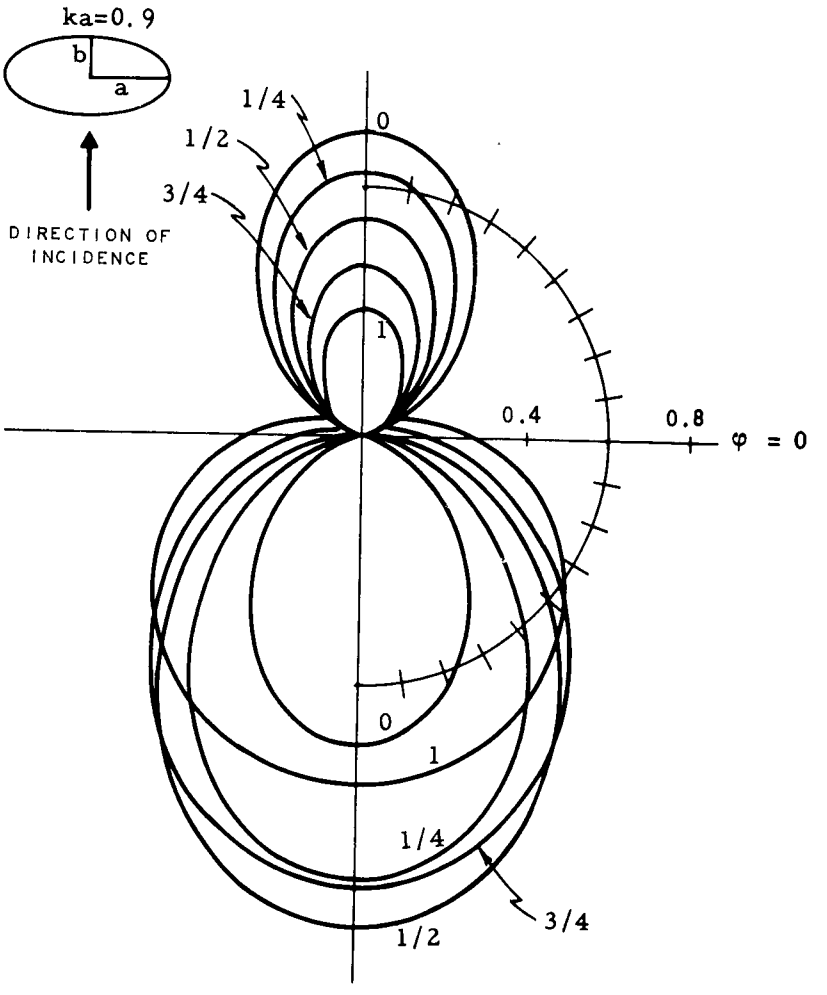

Graph I-9(c): $|g_+(\varphi, 90^o)|^2$.

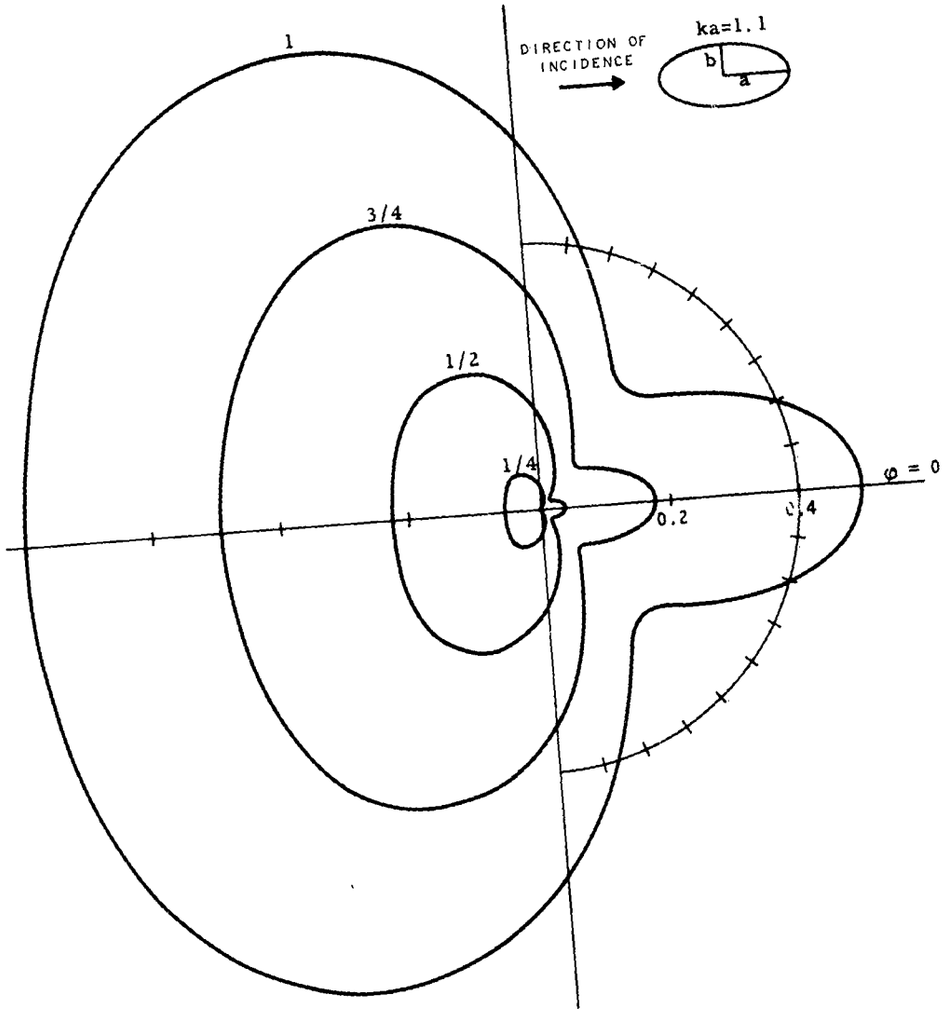

Graph I-10(a): $|g_+(\varphi, 0)|^2$.

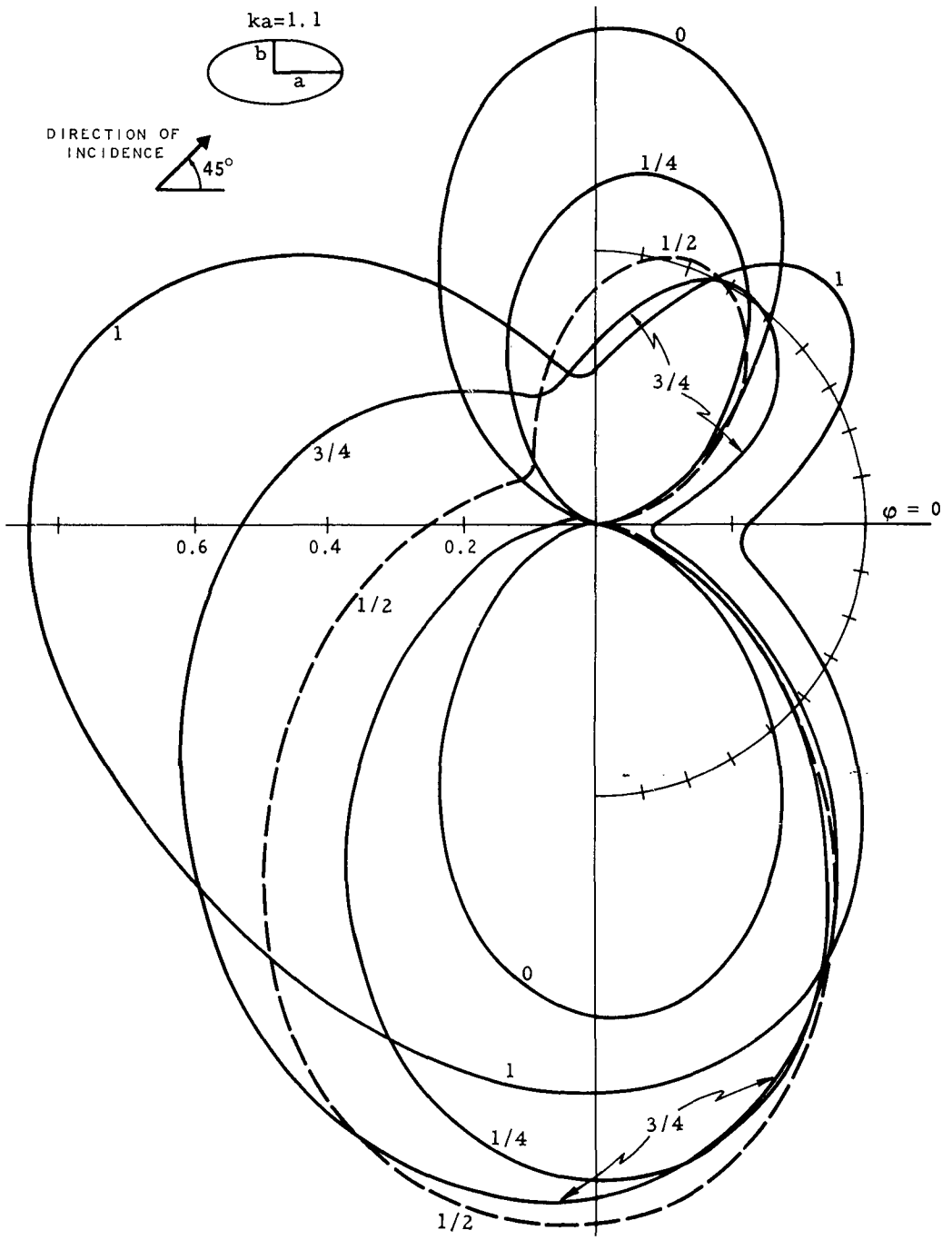

Graph I-10(b): $|g_+(\varphi, 45^\circ)|^2$.

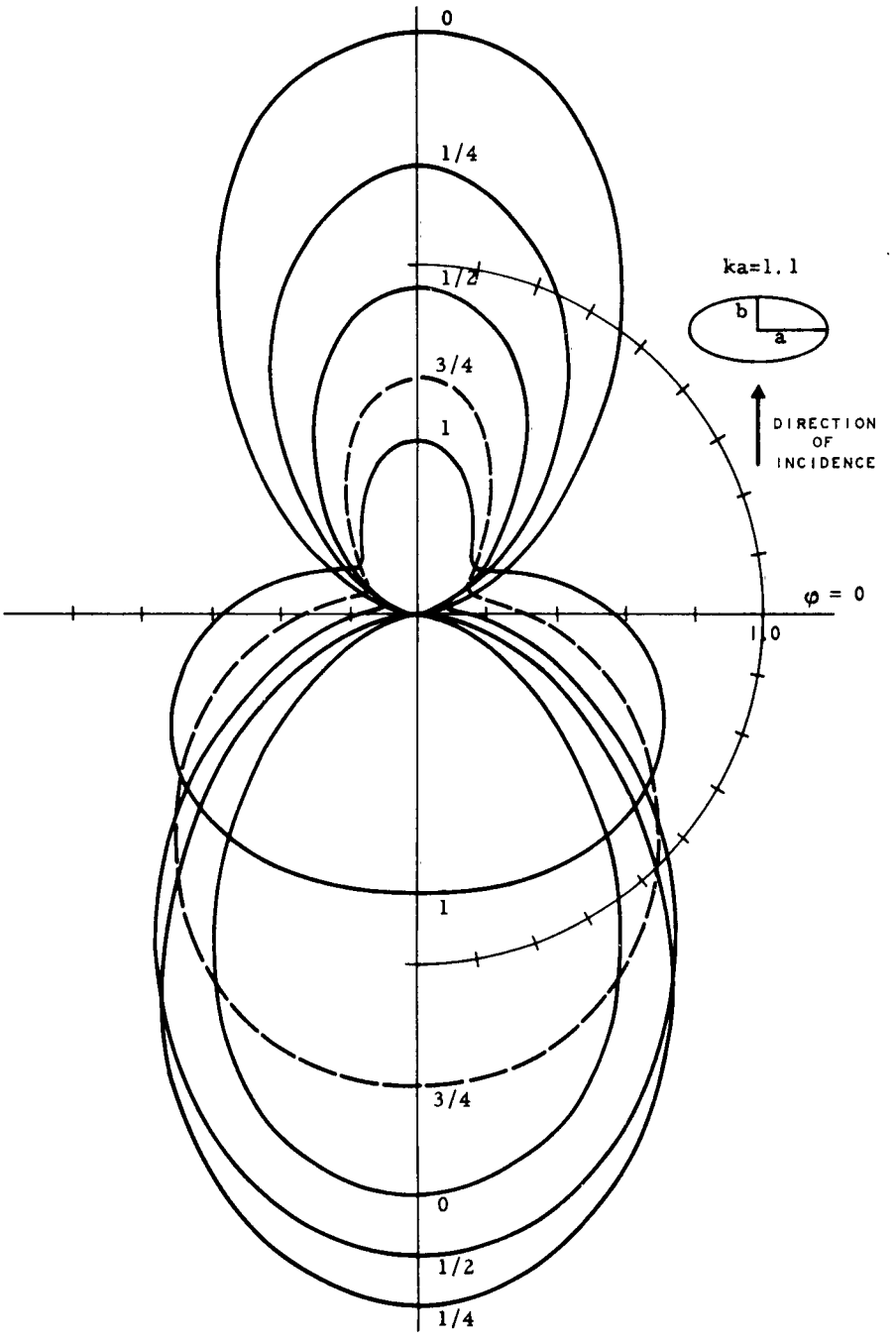

Graph I-10(c): $|g_+(\varphi, 90^\circ)|^2$.

SET II: Graphical Results for Elliptic Cylinders and $\underset{\sim}{E}$ Parallel.

Graph II-1: $-\mathrm{Re}\, g_-(\varphi_o, \varphi_o)$ versus φ_o for ka = 0.5, 0.7, 0.9, and 1.1, and different values of ρ.*

Graph II-2: $|g_-(\varphi_o, \varphi_o)|^2$ versus φ_o for ka = 0.5, 0.7, 0.9, and 1.1 and different values of ρ.*

Graph II-3: $|g_-(\varphi_o, \varphi_o)|^2$ and the phase of $g_-(\varphi_o, \varphi_o)$ versus $ka \leq 1.1$, for $\varphi_o = 0^o$(a), 45^o(b), and 90^o(c), and different values of ρ.*

Graph II-4: $|g_-(\pi+\varphi_o, \varphi_o)|^2$ versus φ_o for ka = 0.5, 0.7, 0.9, and 1.1 and different values of ρ.*

Graph II-5: $|g_-(\pi+\varphi_o, \varphi_o)|^2$ and the phase of $g_-(\pi+\varphi_o, \varphi_o)$ versus $ka \leq 1.1$, for $\varphi_o = 0^o$(a), 45^o(b), and 90^o(c), and different values of ρ.*

Graph II-6: $|g_-(\varphi, \varphi_o)|^2$ versus φ for $\varphi_o = 0$(a), 45^o(b), and 90^o(c), ka = 0.3, and different values of ρ.*

Graph II-7: $|g_-(\varphi, \varphi_o)|^2$ versus φ for $\varphi_o = 0$(a), 45^o(b), and 90^o(c), ka = 0.5, and different values of ρ.*

Graph II-8: $|g_-(\varphi, \varphi_o)|^2$ versus φ for $\varphi_o = 0$(a), 45^o(b), and 90^o(c), ka = 0.7, and different values of ρ.*

Graph II-9: $|g_-(\varphi, \varphi_o)|^2$ versus φ for $\varphi_o = 0$(a), 45^o(b), and 90^o(c), ka = 0.9, and different values of ρ.*

Graph II-10 $|g_-(\varphi, \varphi_o)|^2$ versus φ for $\varphi_o = 0$(a), 45^o(b), and 90^o(c), ka = 1.1, and different values of ρ.*

*The number next to a curve gives the value of ρ = b/a = (minor axis/major axis).

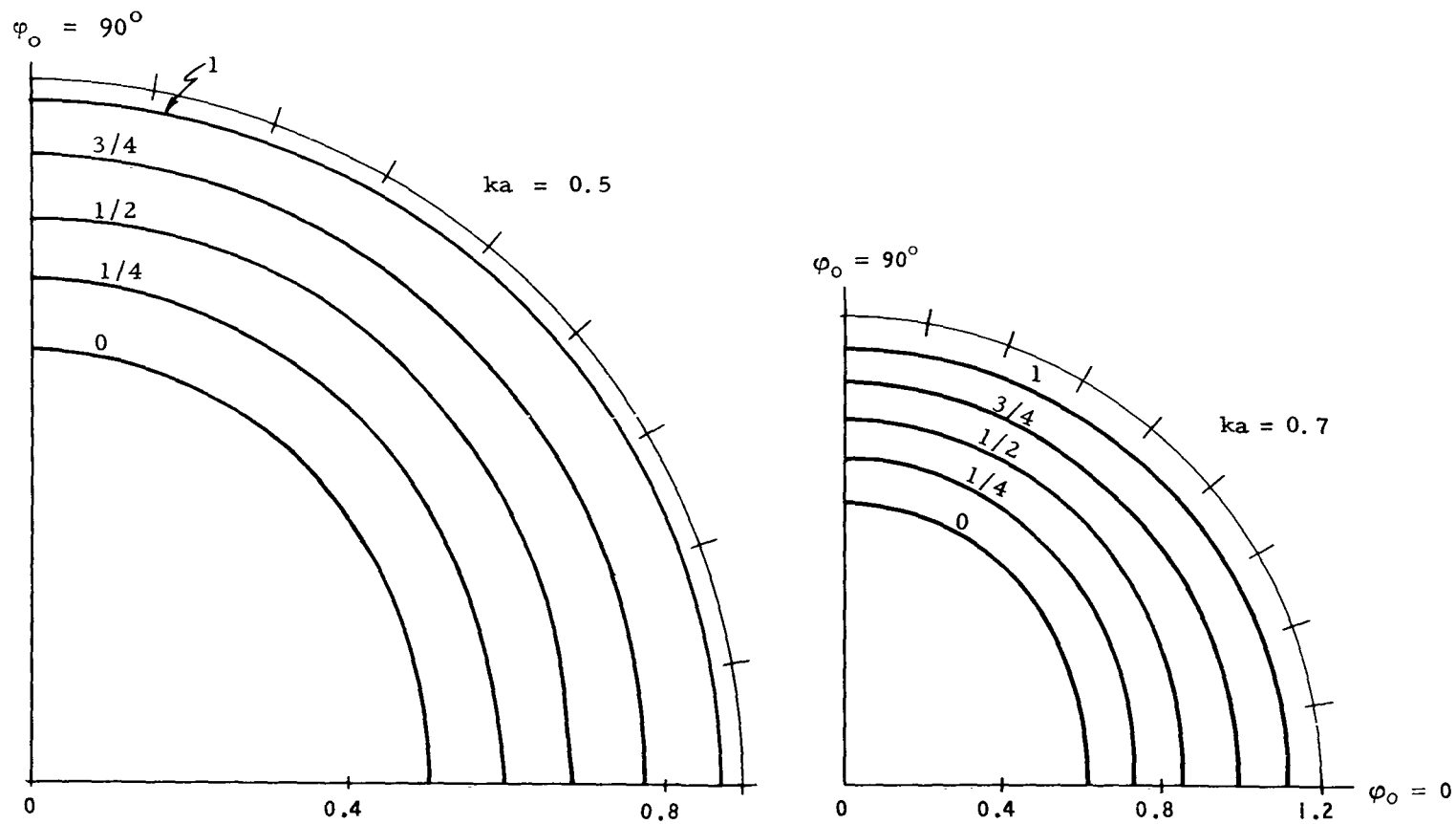

Graph II-1: -Re $g_-(\varphi_o, \varphi_o)$.

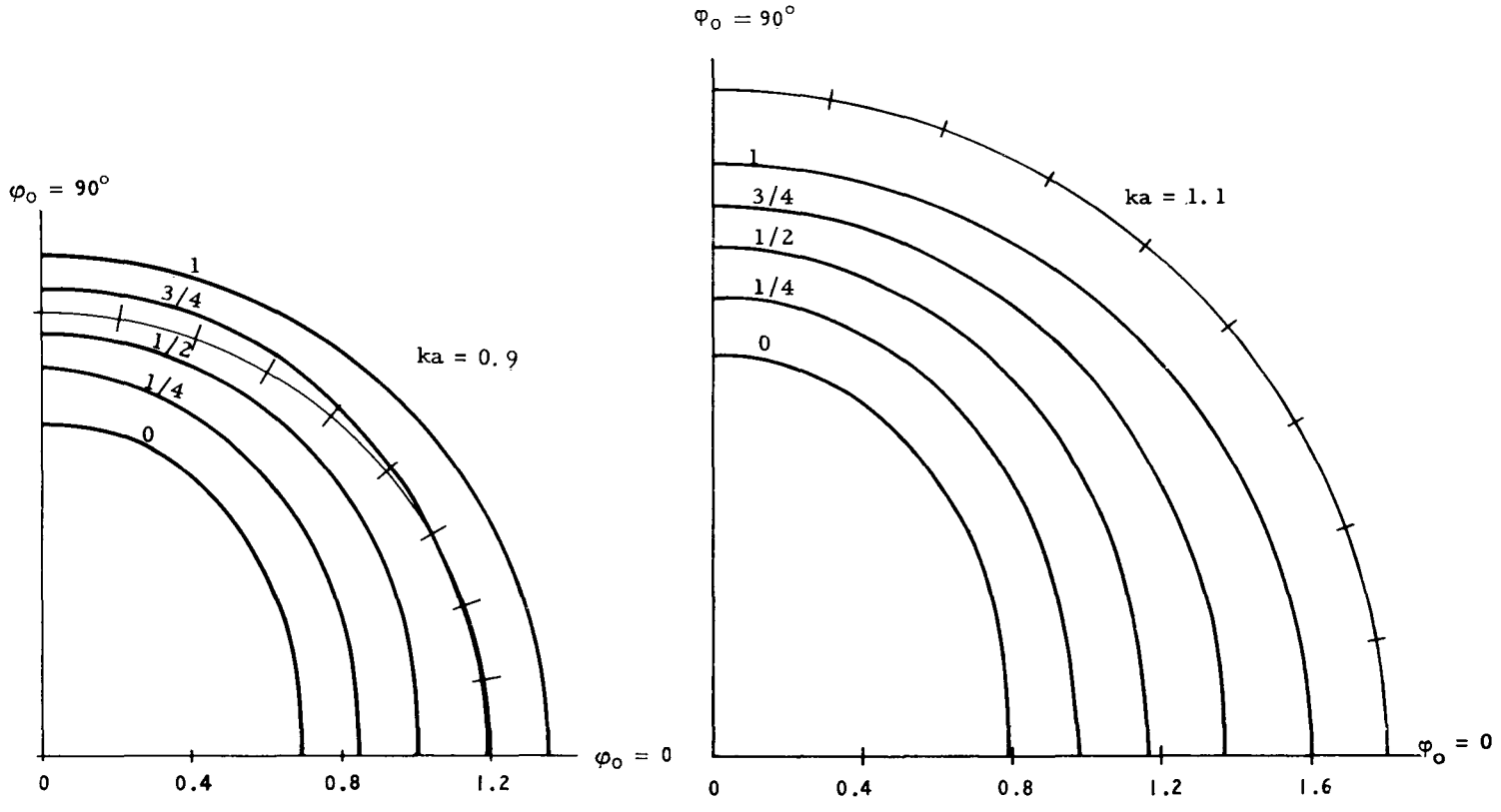

Graph II-1 (Con't): -Re $g_-(\varphi_o, \varphi_o)$.

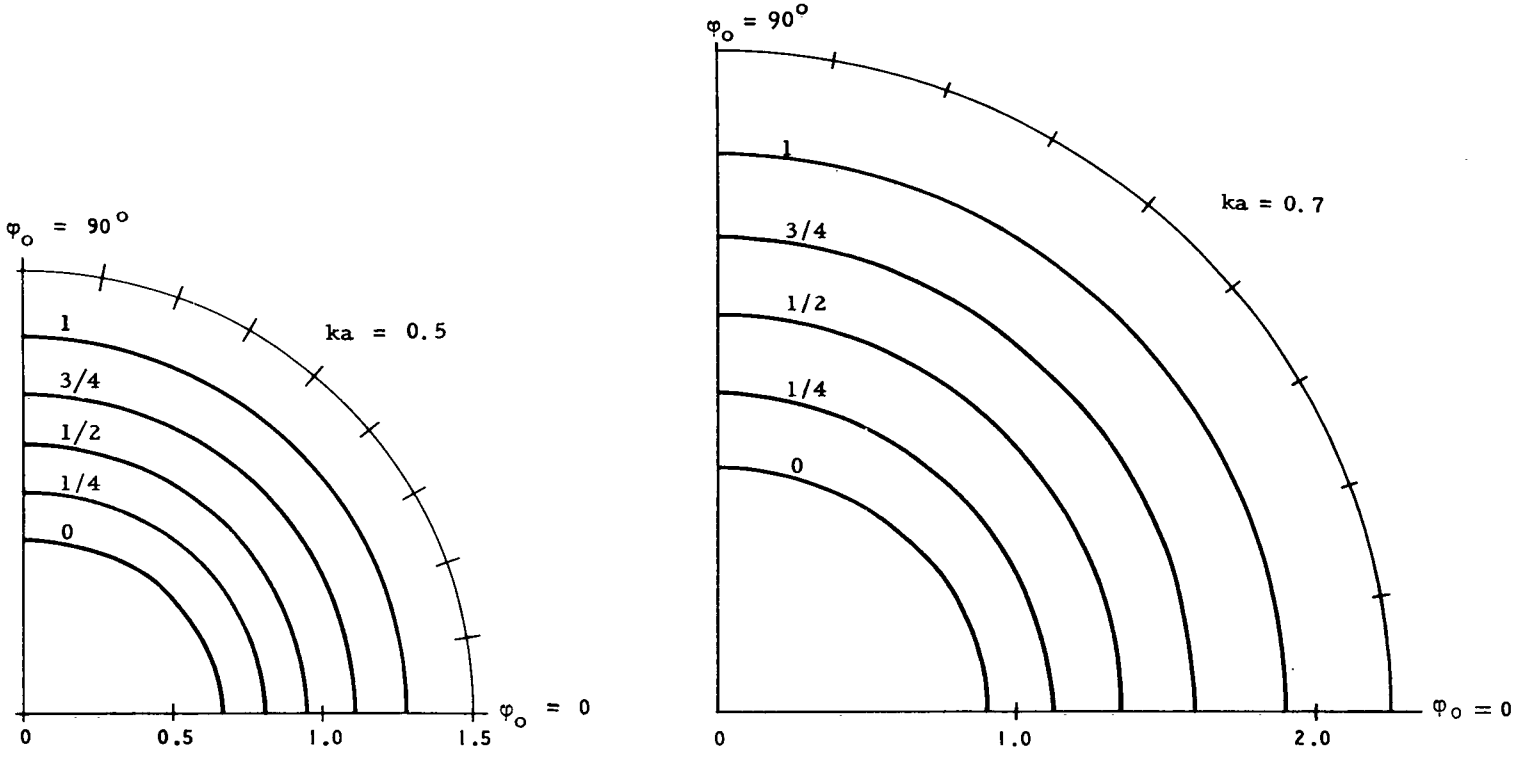

Graph II-2: $|g_-(\varphi_o, \varphi_o)|^2$.

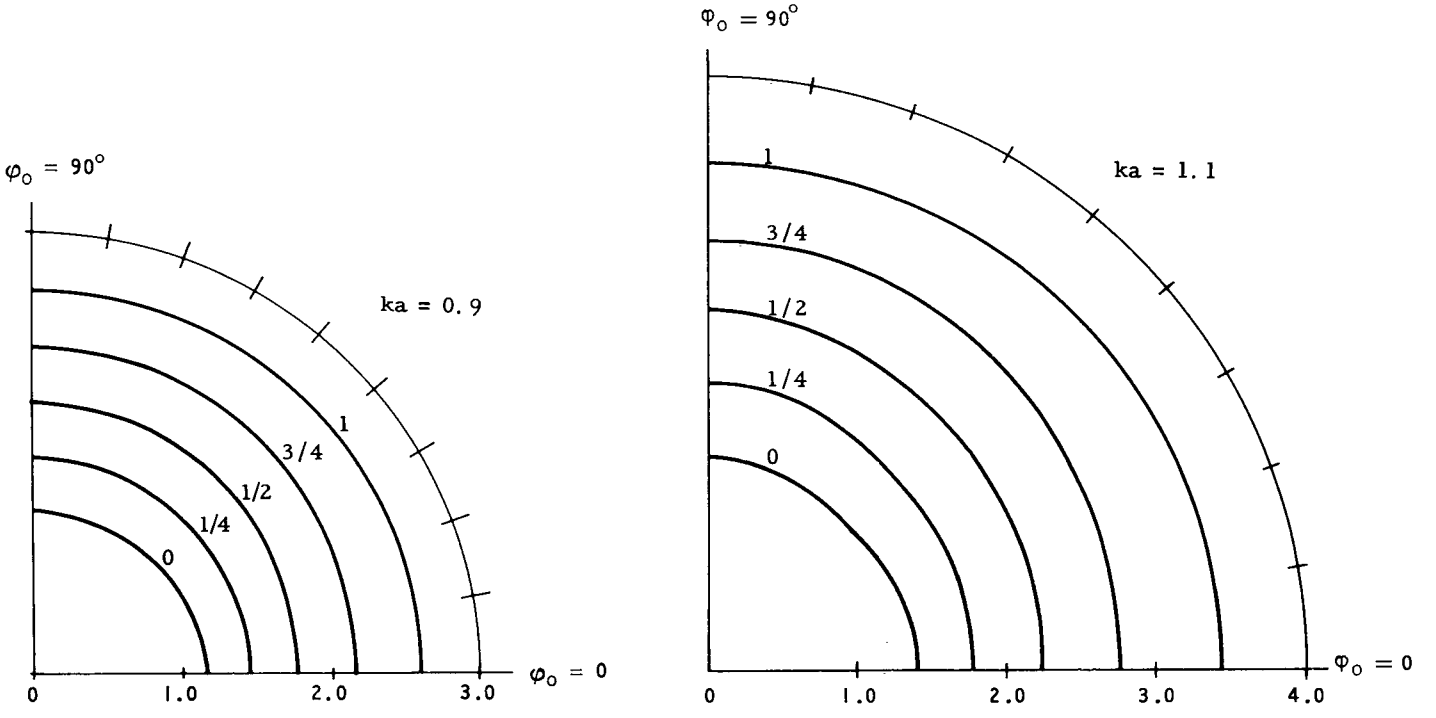

Graph II-2 (Con't): $|g_-(\varphi_o, \varphi_o)|^2$.

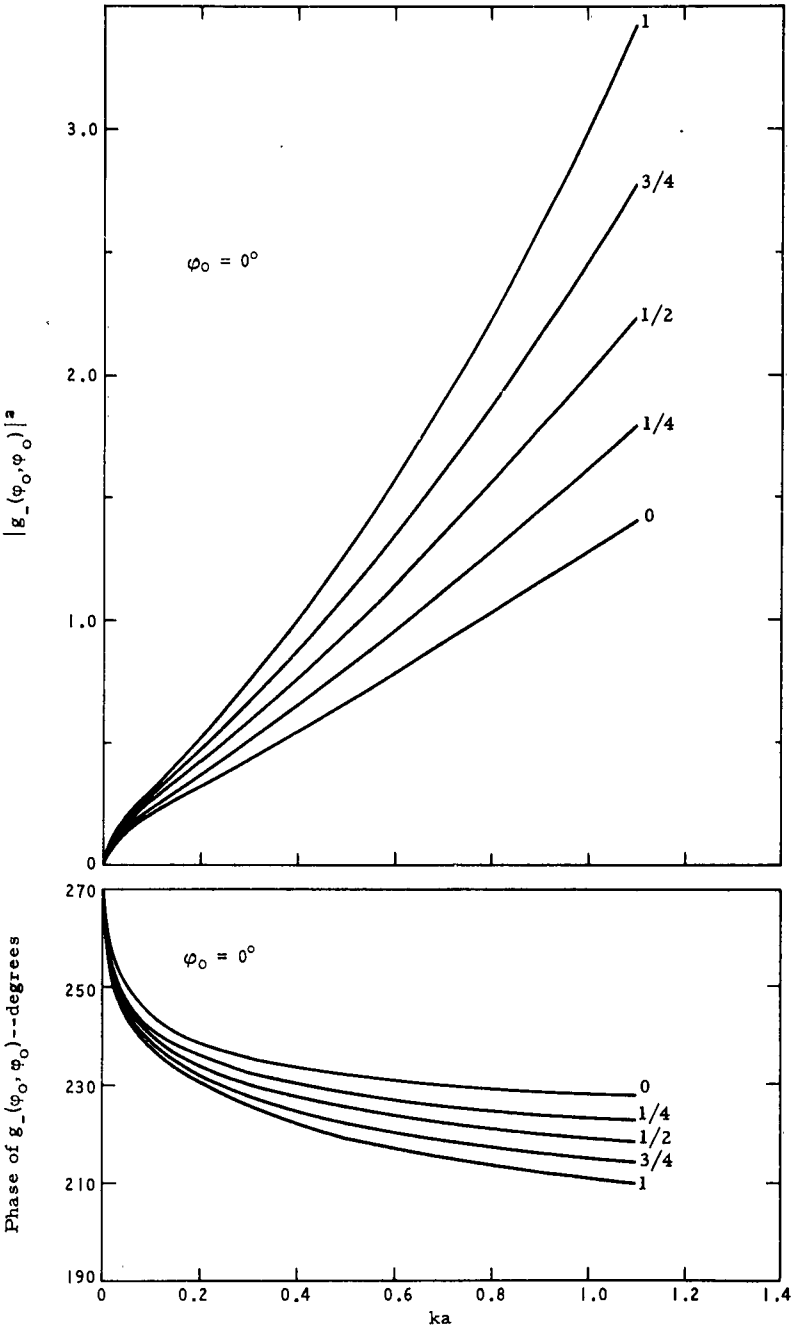
3.0
2.0
1.0
0
$|g_-(\varphi_o,\varphi_o)|^2$
$\varphi_o = 0°$
1
3/4
1/2
1/4
0
270
250
230
210
190
Phase of $g_-(\varphi_o,\varphi_o)$--degrees
$\varphi_o = 0°$
0
1/4
1/2
3/4
1
0
0.2
0.4
0.6
0.8
1.0
1.2
1.4
ka

Graph II-3(a)

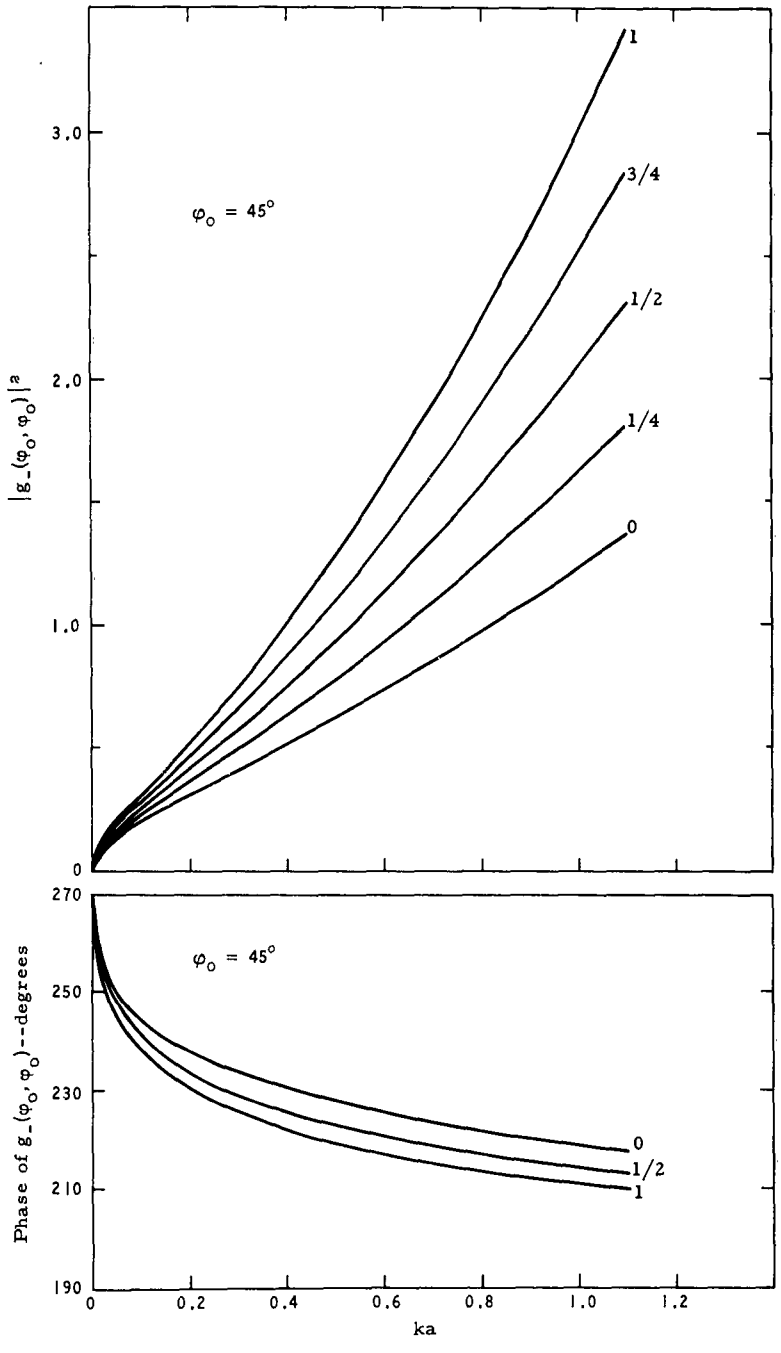
1
3/4
1/2
1/4
0
φ_o = 45°
$|g_-(\varphi_o, \varphi_o)|^2$
3.0
2.0
1.0
0
270
250
230
210
190
φ_o = 45°
Phase of $g_-(\varphi_o, \varphi_o)$--degrees
0
1/2
1
0
0.2
0.4
0.6
0.8
1.0
1.2
ka

Graph II-3(b)

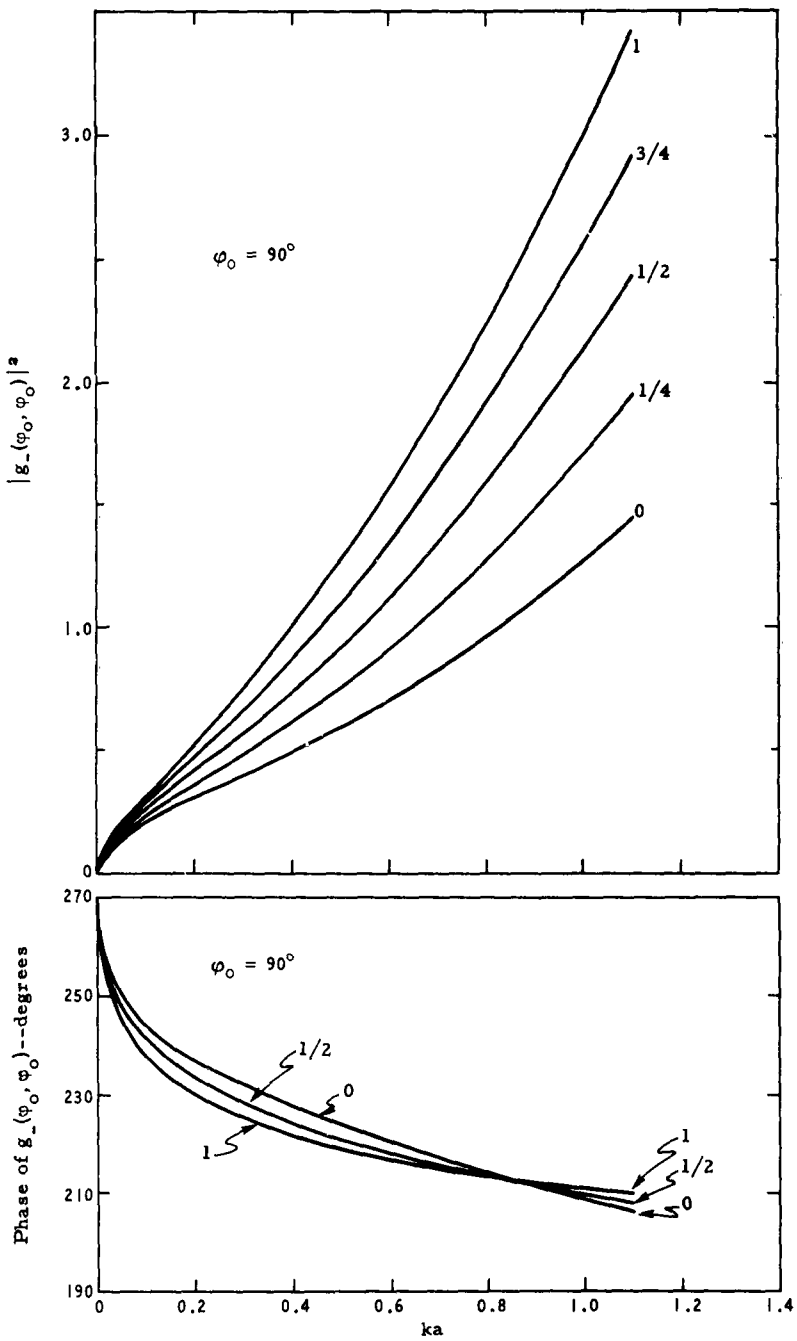
$|g_-(\varphi_o, \varphi_o)|^2$
3.0
2.0
1.0
0
$\varphi_o = 90°$
1
3/4
1/2
1/4
0
Phase of $g_-(\varphi_o, \varphi_o)$--degrees
270
250
230
210
190
$\varphi_o = 90°$
1/2
0
1
1
1/2
0
0
0.2
0.4
0.6
0.8
1.0
1.2
1.4
ka

Graph II-3(c)

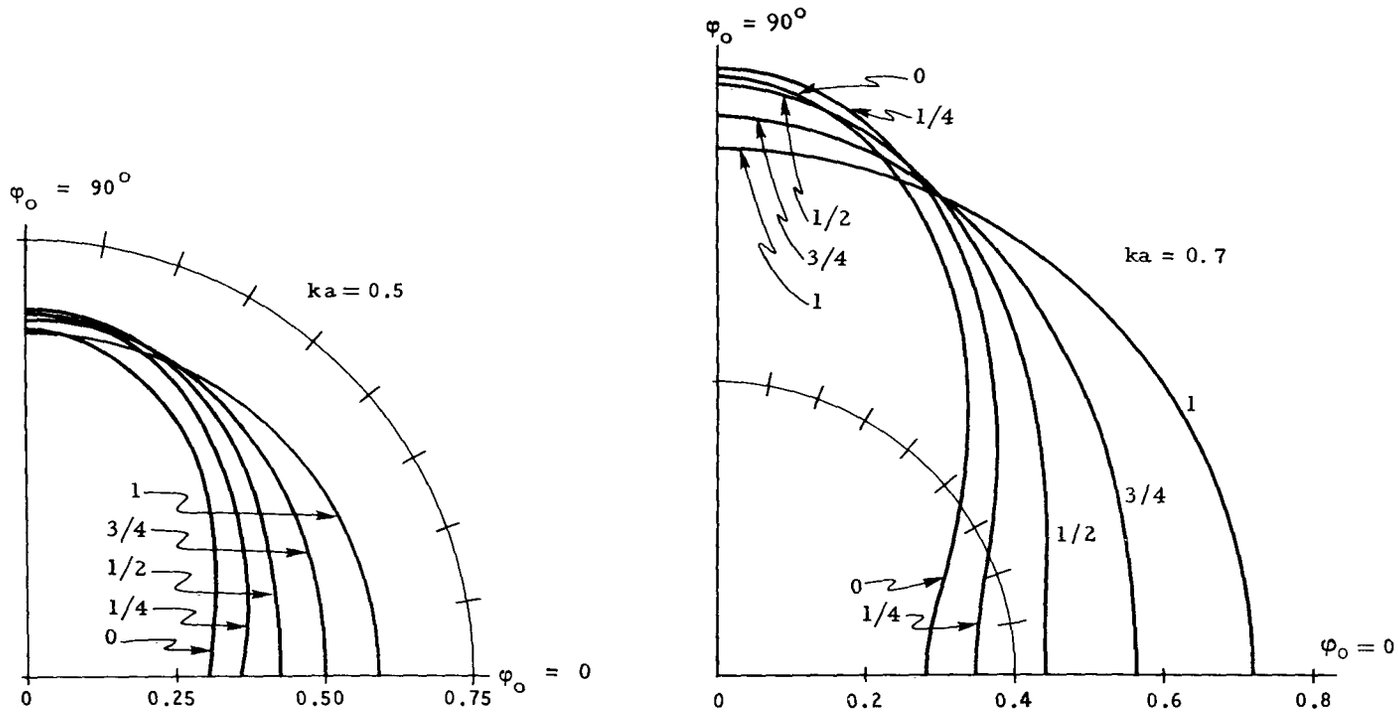

Graph II-4: $|g_{-}(\pi+\varphi_o, \varphi_o)|^2$.

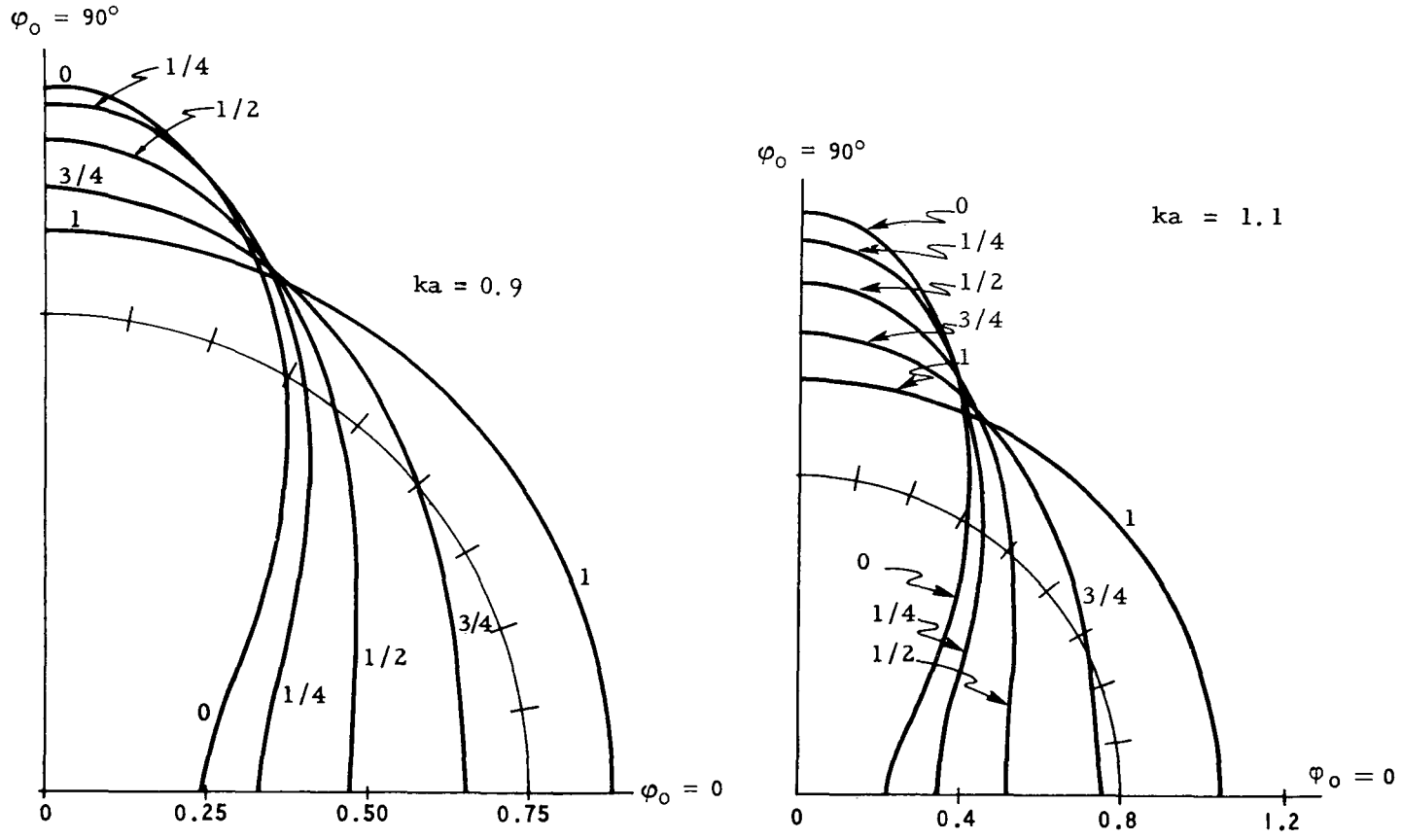

Graph II-4 (Con't): $|g_-(\pi+\varphi_o, \varphi_o)|^2$.

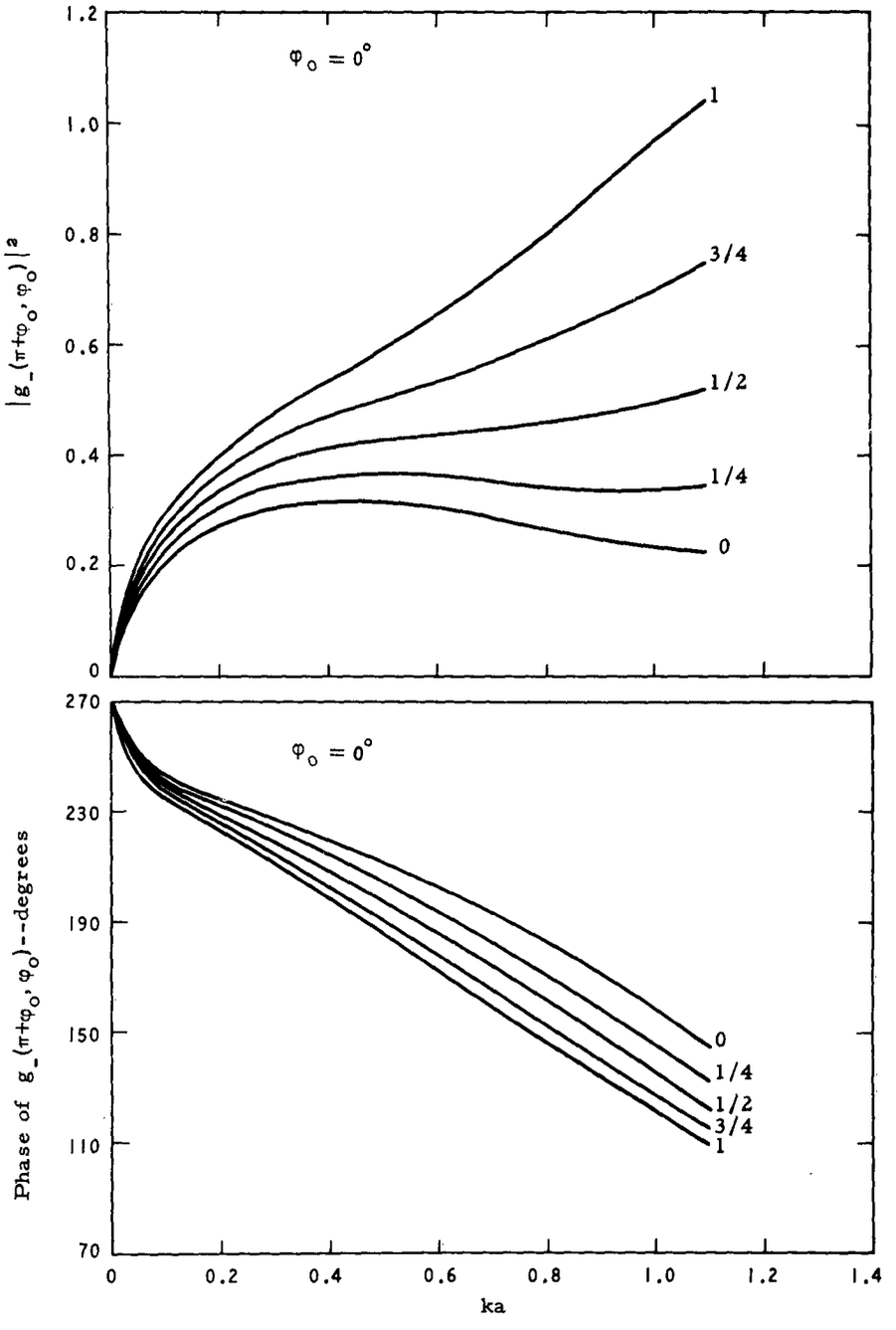
1.2
1.0
0.8
0.6
0.4
0.2
0
$\varphi_o = 0°$
1
3/4
1/2
1/4
0
$|g_-(\pi+\varphi_o, \varphi_o)|^2$
270
230
190
150
110
70
$\varphi_o = 0°$
0
1/4
1/2
3/4
1
Phase of $g_-(\pi+\varphi_o, \varphi_o)$--degrees
0
0.2
0.4
0.6
0.8
1.0
1.2
1.4
ka

Graph II-5(a).

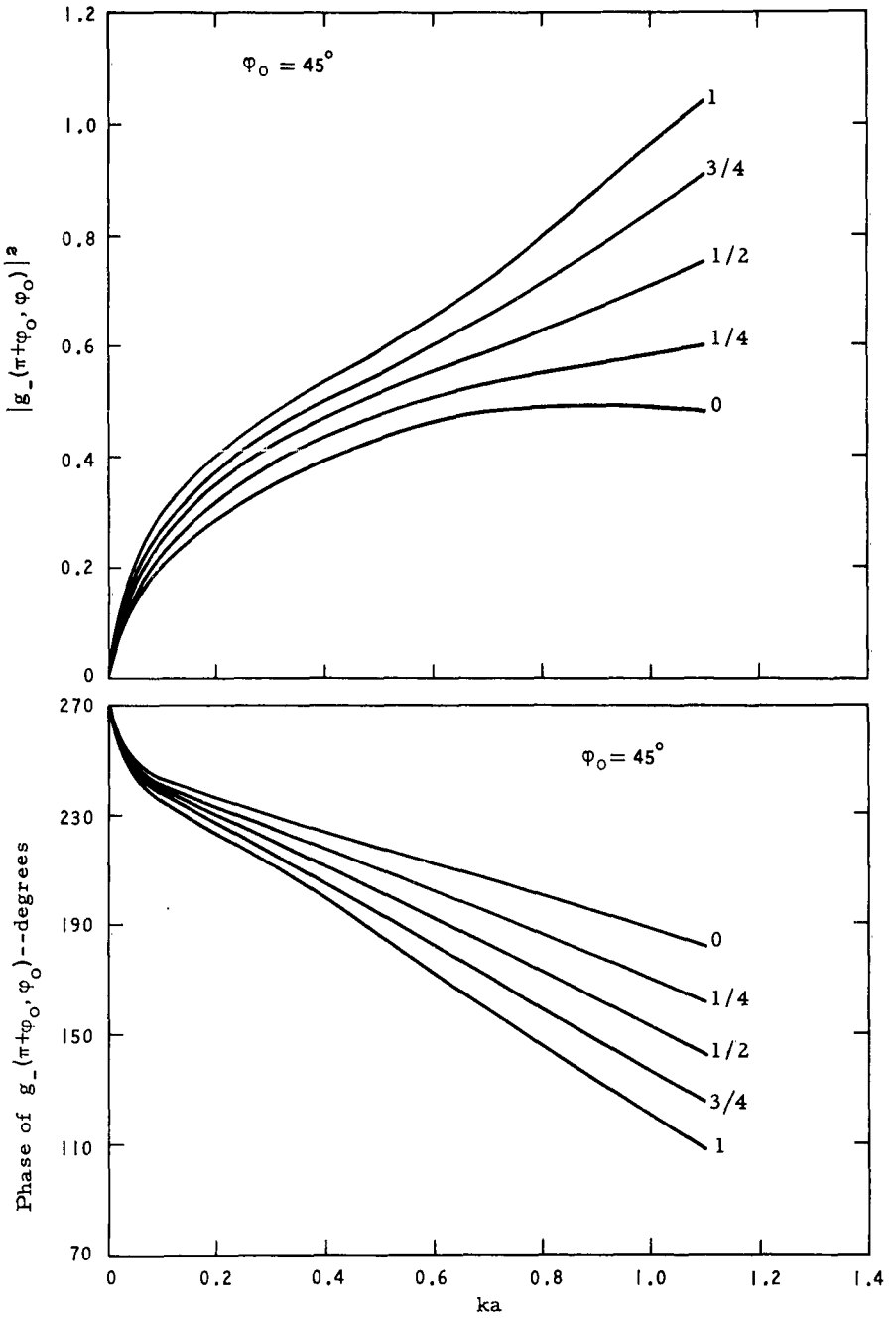
1.2
1.0
0.8
0.6
0.4
0.2
0
$\varphi_o = 45°$
1
3/4
1/2
1/4
0
$|g_-(\pi+\varphi_o, \varphi_o)|^2$
270
230
190
150
110
70
$\varphi_o = 45°$
0
1/4
1/2
3/4
1
Phase of $g_-(\pi+\varphi_o, \varphi_o)$--degrees
0
0.2
0.4
0.6
0.8
1.0
1.2
1.4
ka

Graph II-5(b).

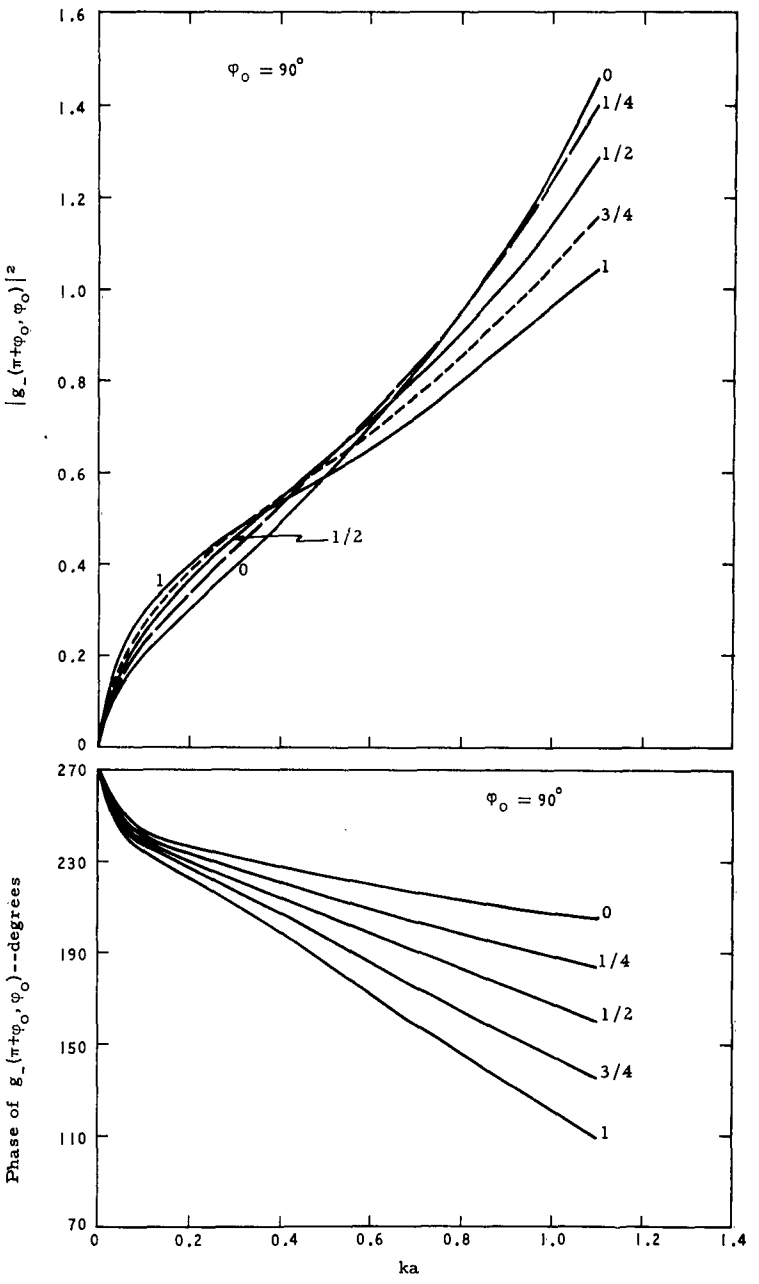
$\varphi_o = 90°$
0
1/4
1/2
3/4
1
$|g_-(\pi+\varphi_o, \varphi_o)|^2$
Phase of $g_-(\pi+\varphi_o, \varphi_o)$--degrees
ka

Graph II-5(c)

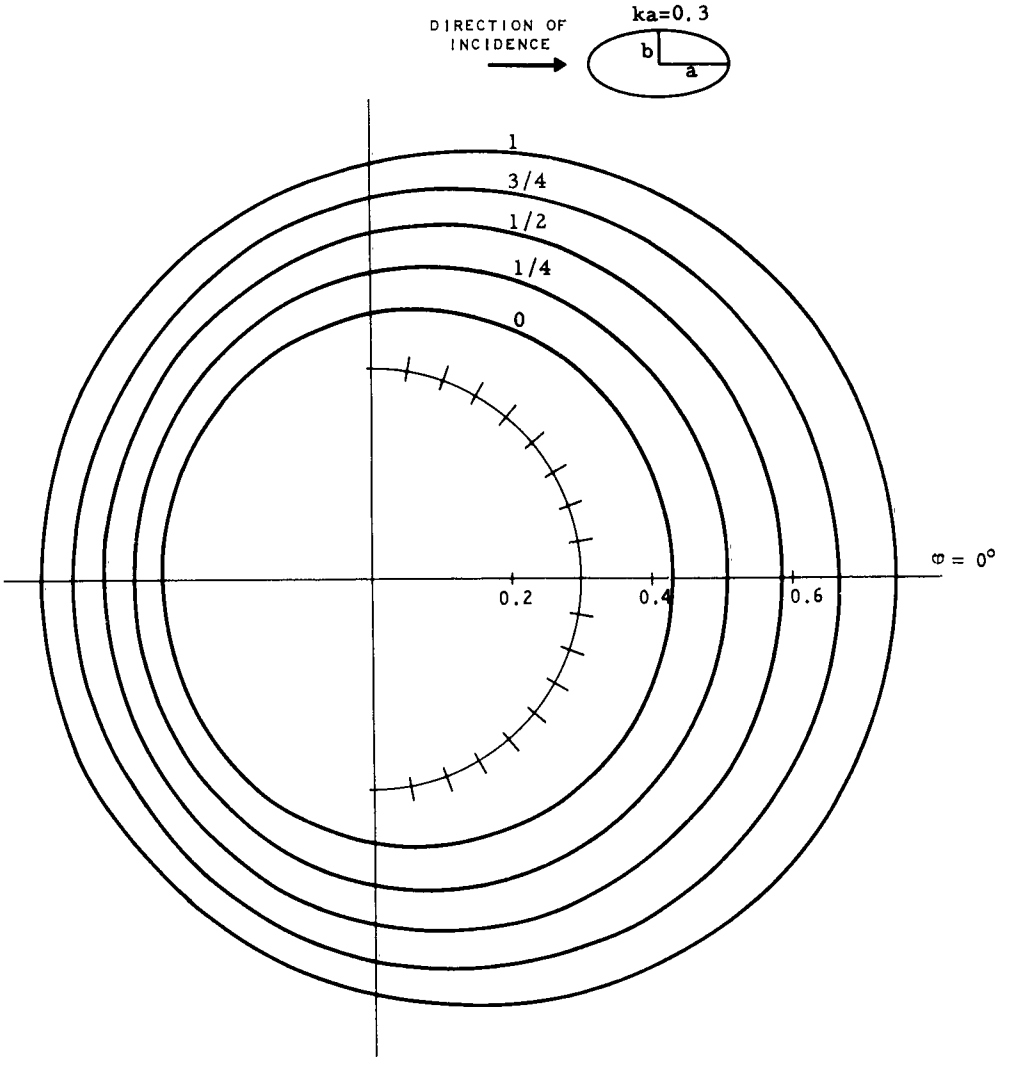

Graph II-6(a): $|g_{-}(\varphi, 0)|^2$.

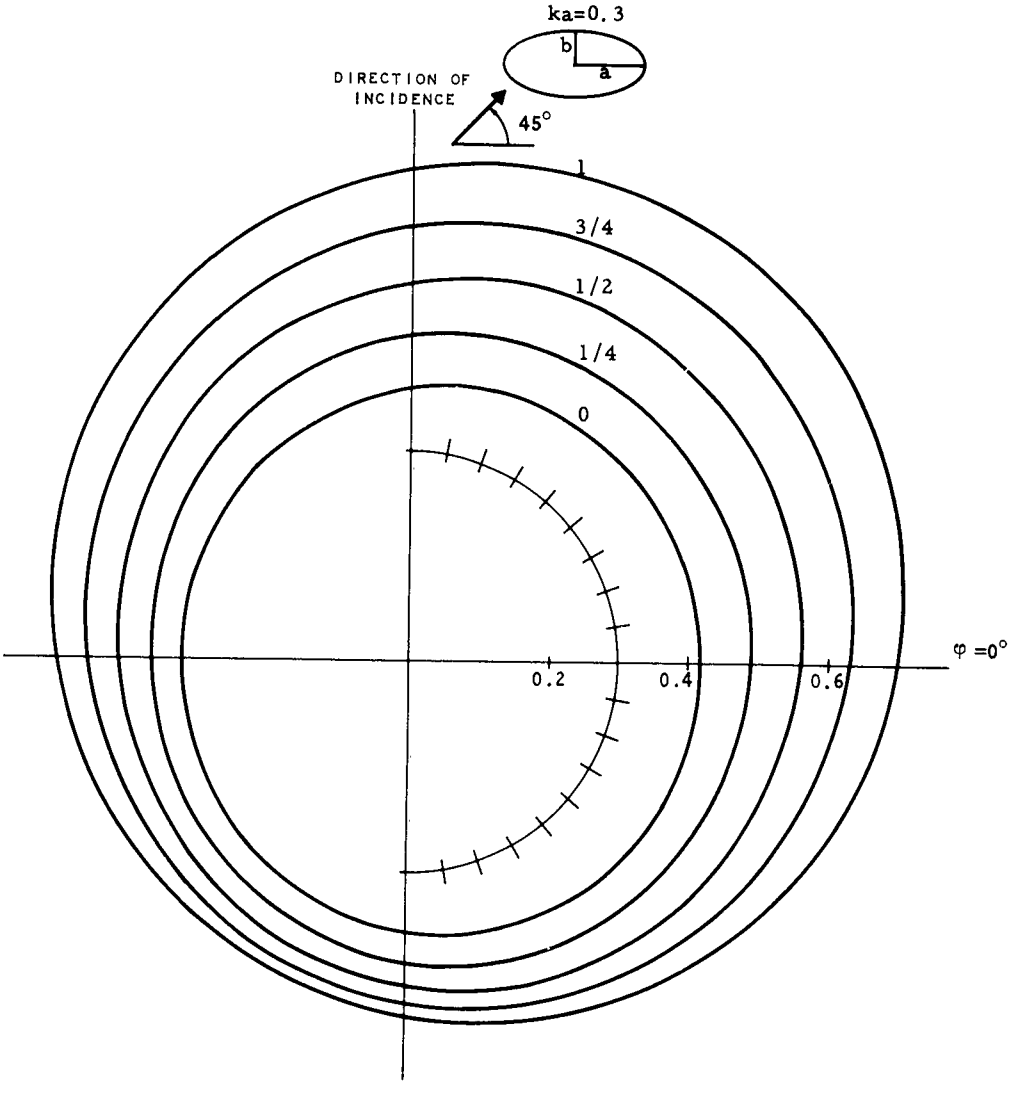

Graph II-6(b): $|g_{-}(\varphi, 45^{\circ})|^{2}$.

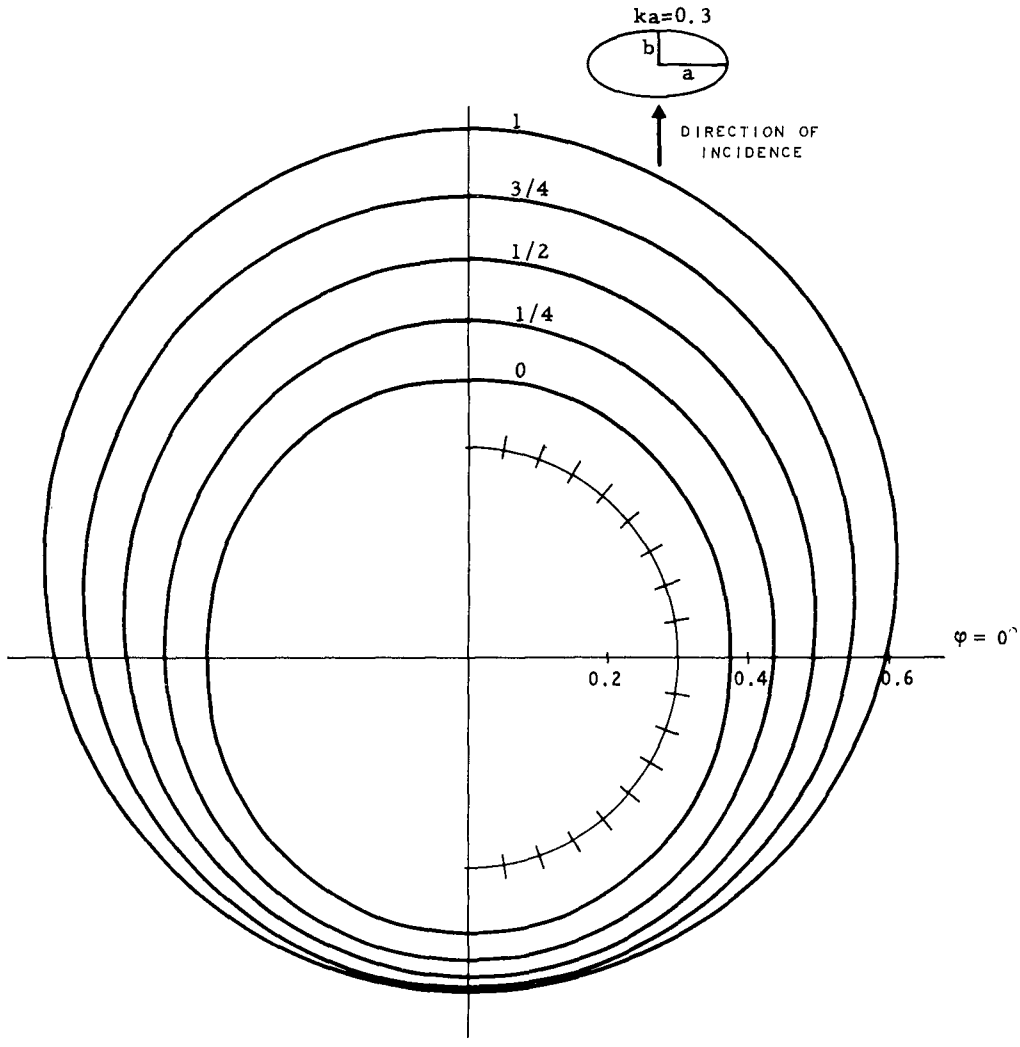

Graph II-6(c): $|g_{-}(\varphi, 90^{\circ})|^{2}$.

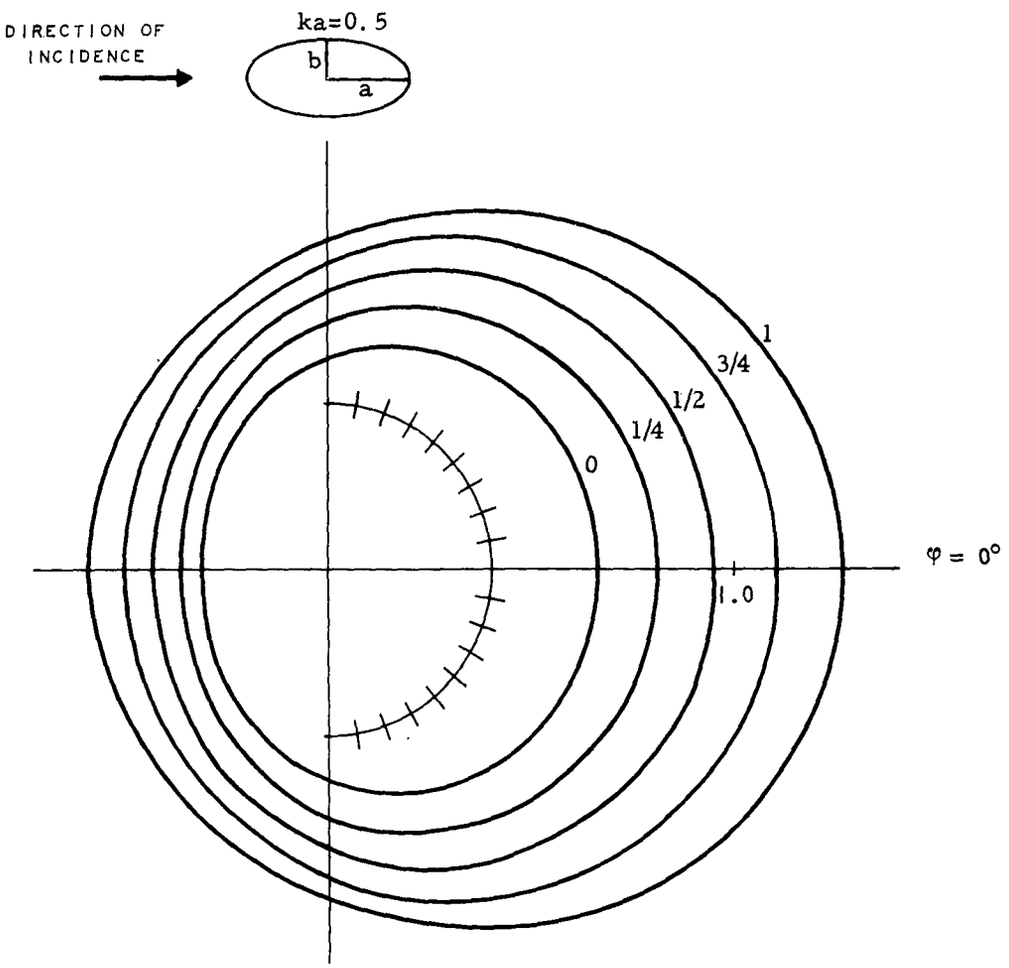

Graph II-7(a): $|g_{-}(\varphi, 0)|^2$.

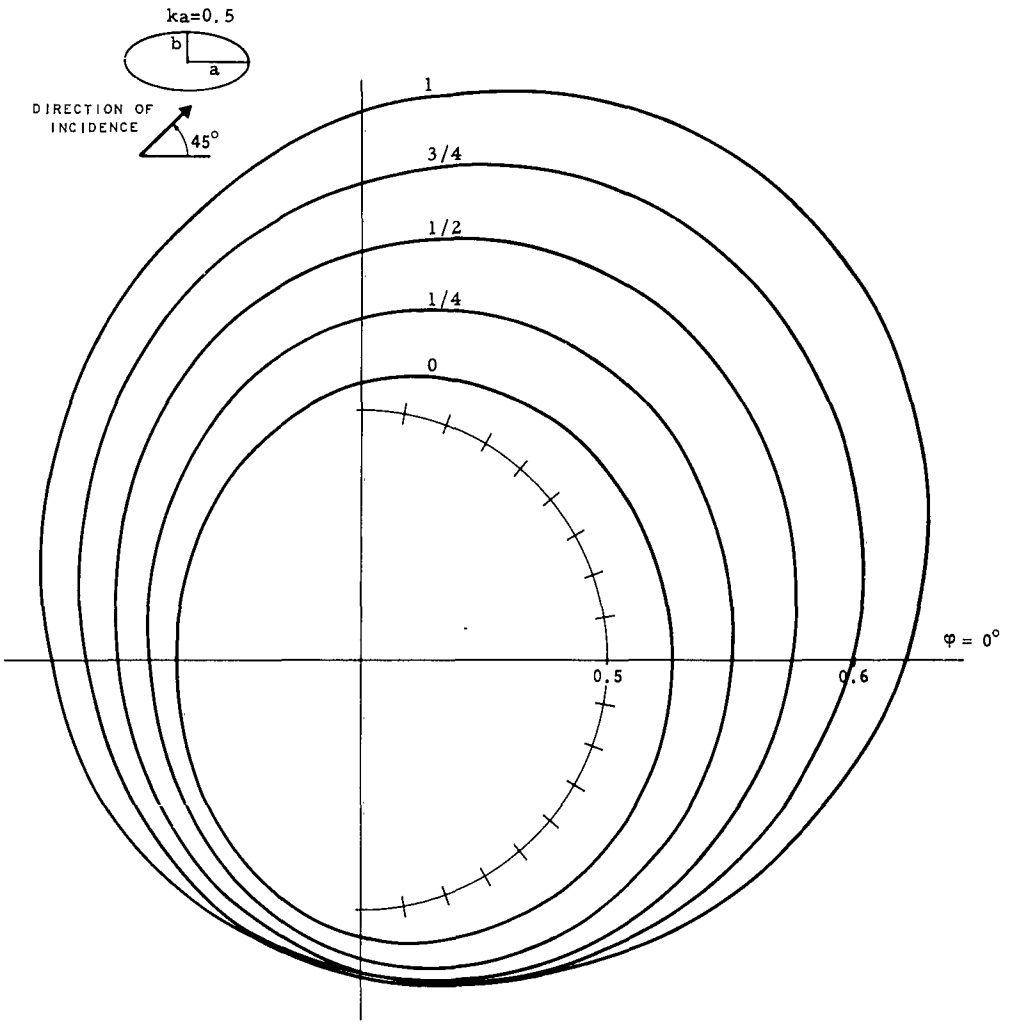

Graph II-7(b): $|g_{-}(\varphi, 45^{\circ})|^2$

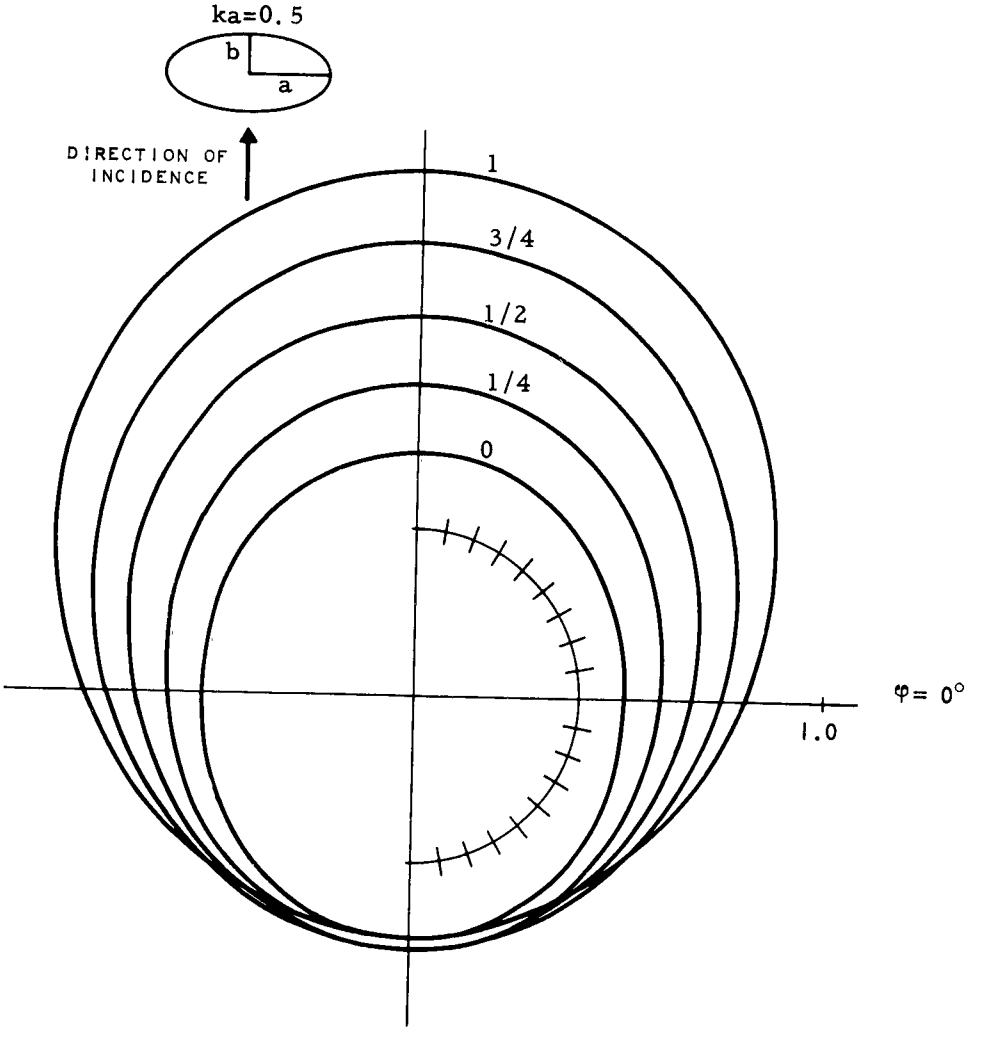

Graph II-7(c): $|g_{-}(\varphi, 90^{\circ})|^{2}$.

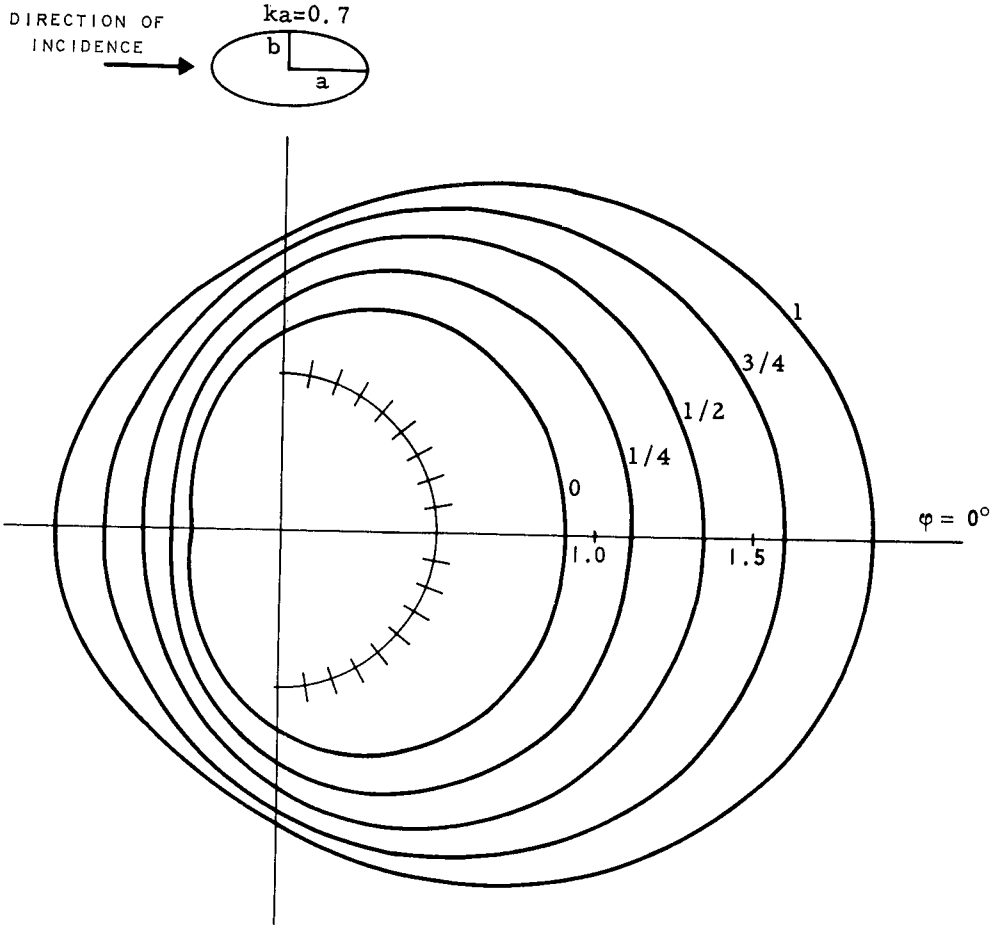

Graph II-8(a): $|g_{-}(\varphi, 0)|^2$.

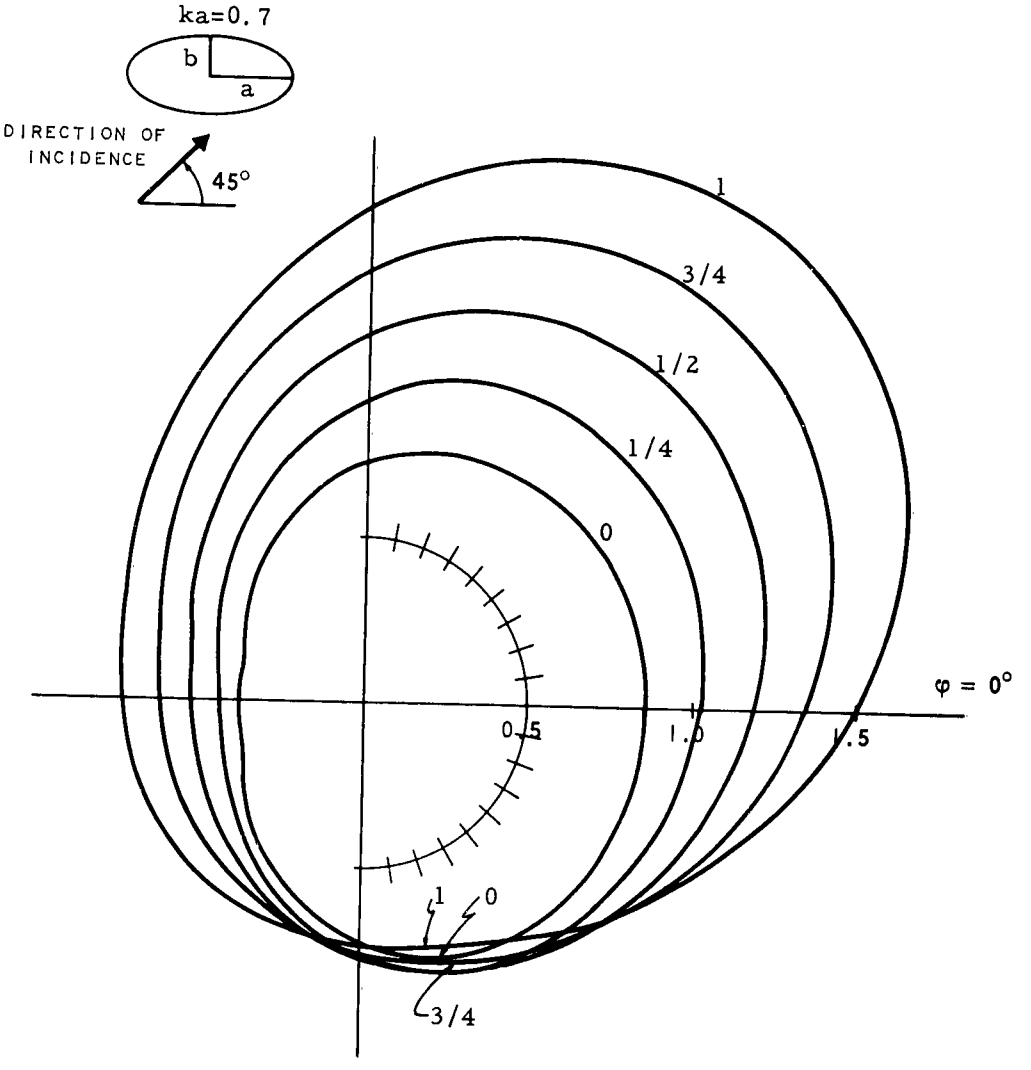

Graph II-8(b): $|g_{-}(\varphi, 45^{\circ})|^{2}$.

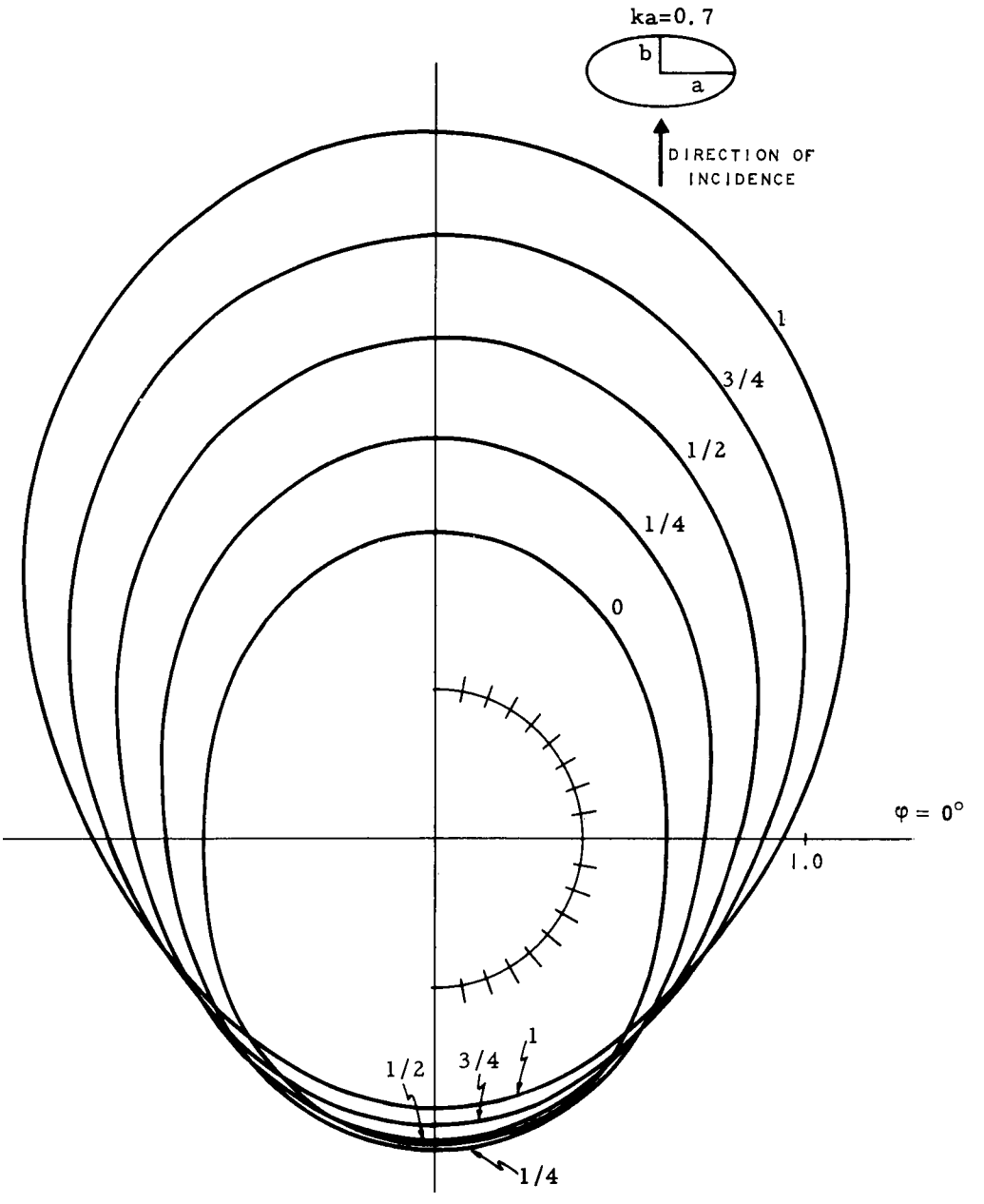

Graph II-8(c): $|g_{-}(\varphi, 90^{\circ})|^{2}$.

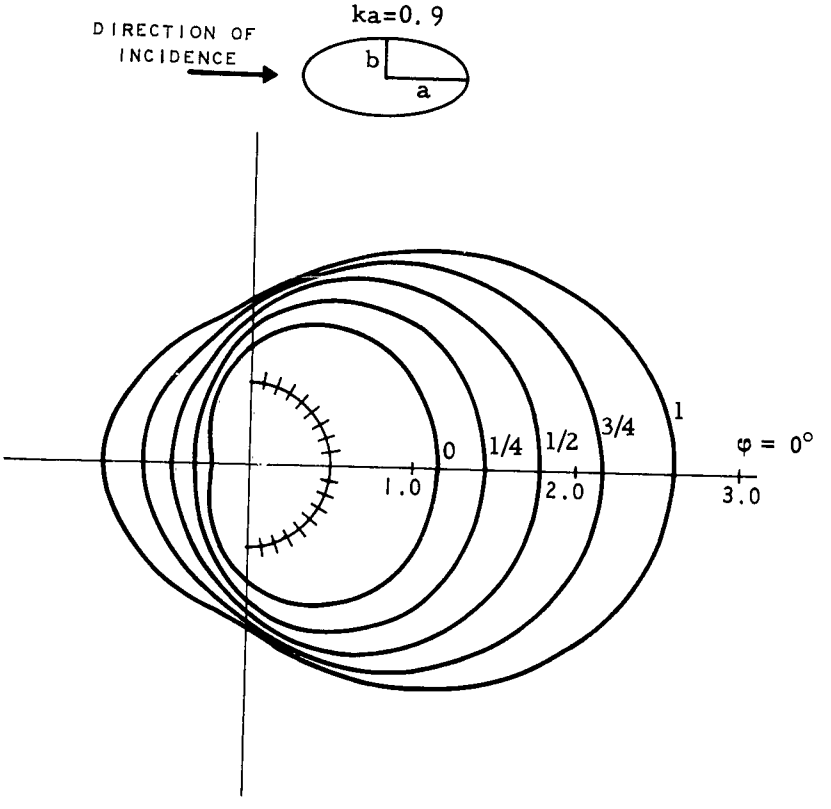

Graph II-9(a): $|g_{-}(\varphi, 0)|^2$.

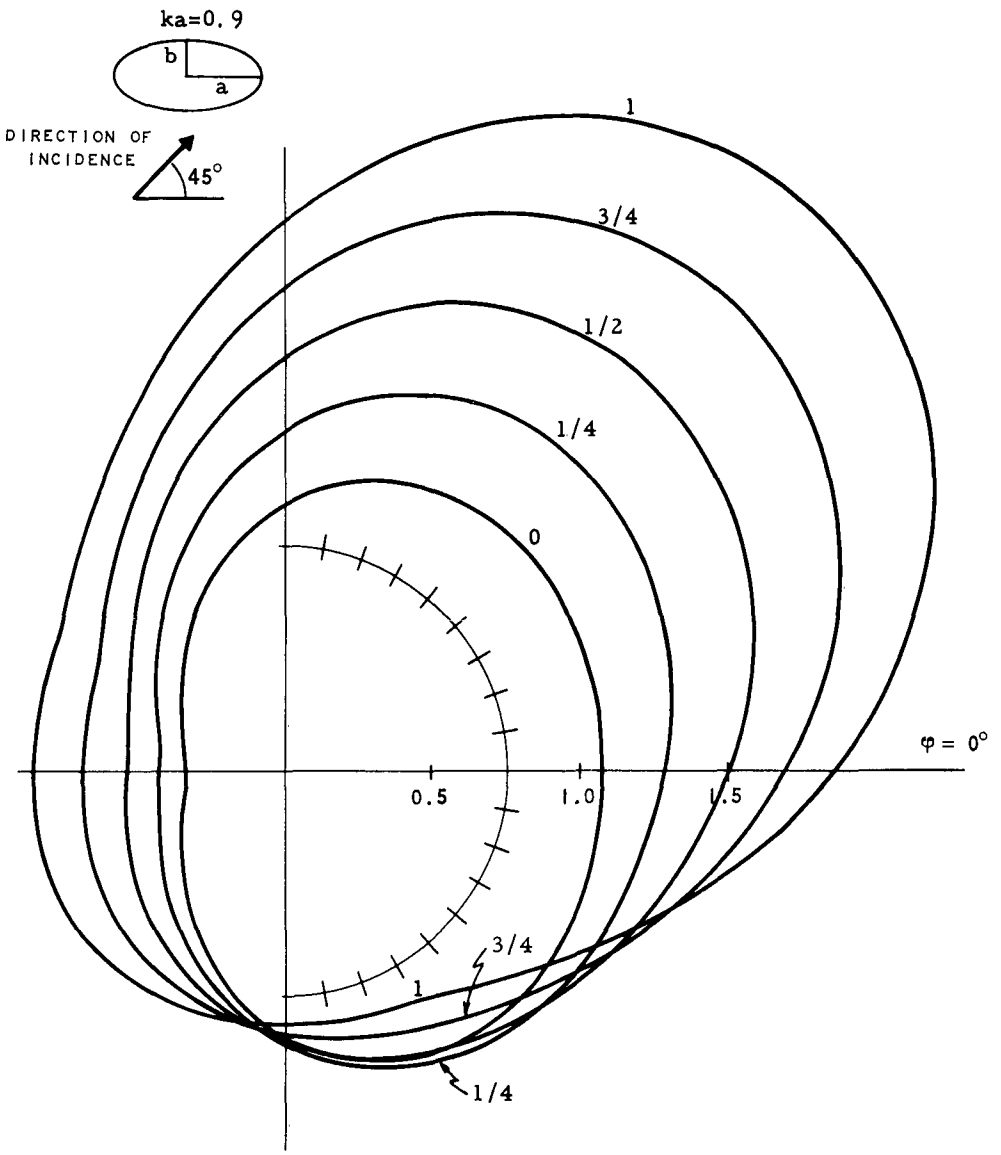

Graph II-9(b): $|g_{-}(\varphi, 45^{\circ})|^{a}$.

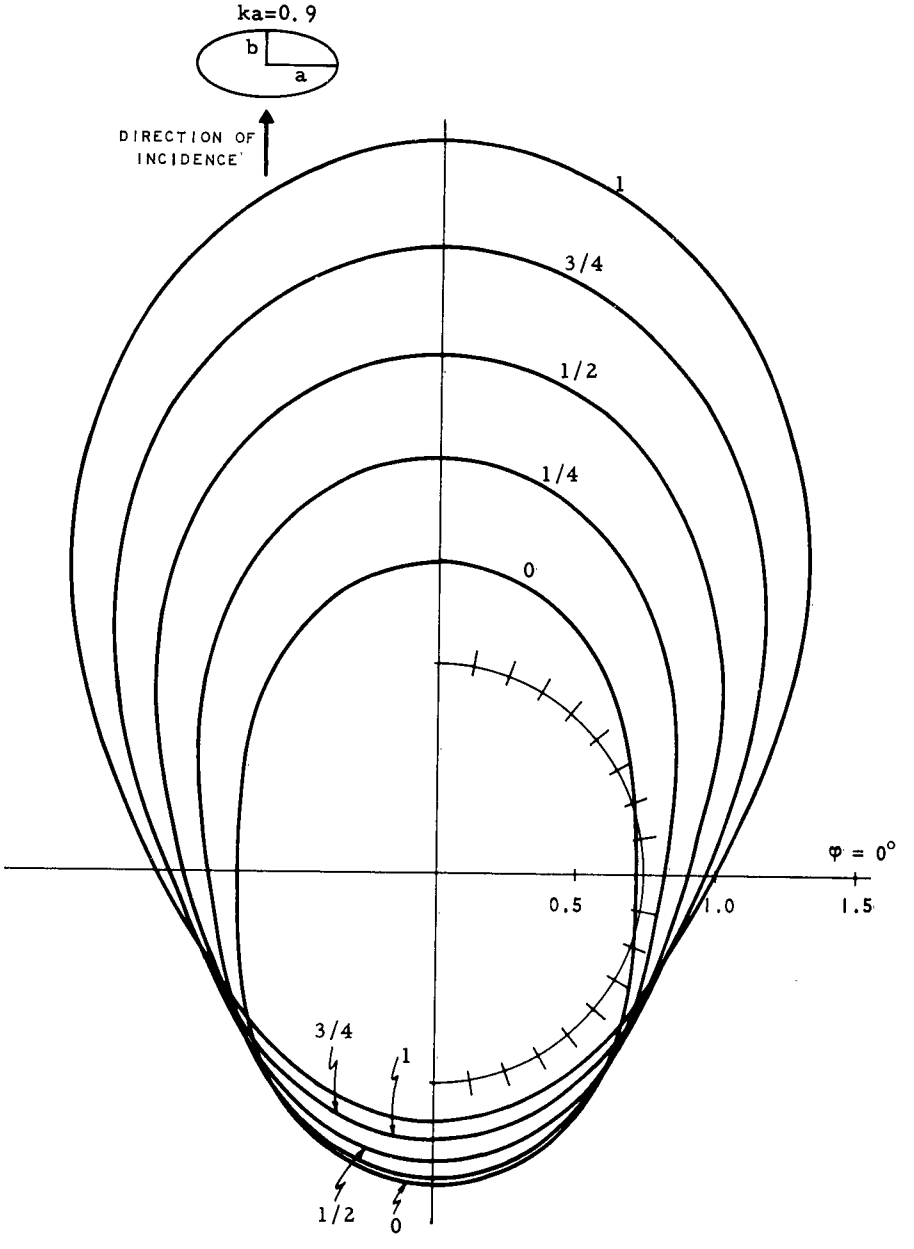

Graph II-9(c): $|g_{-}(\varphi, 90^{\circ})|^{2}$.

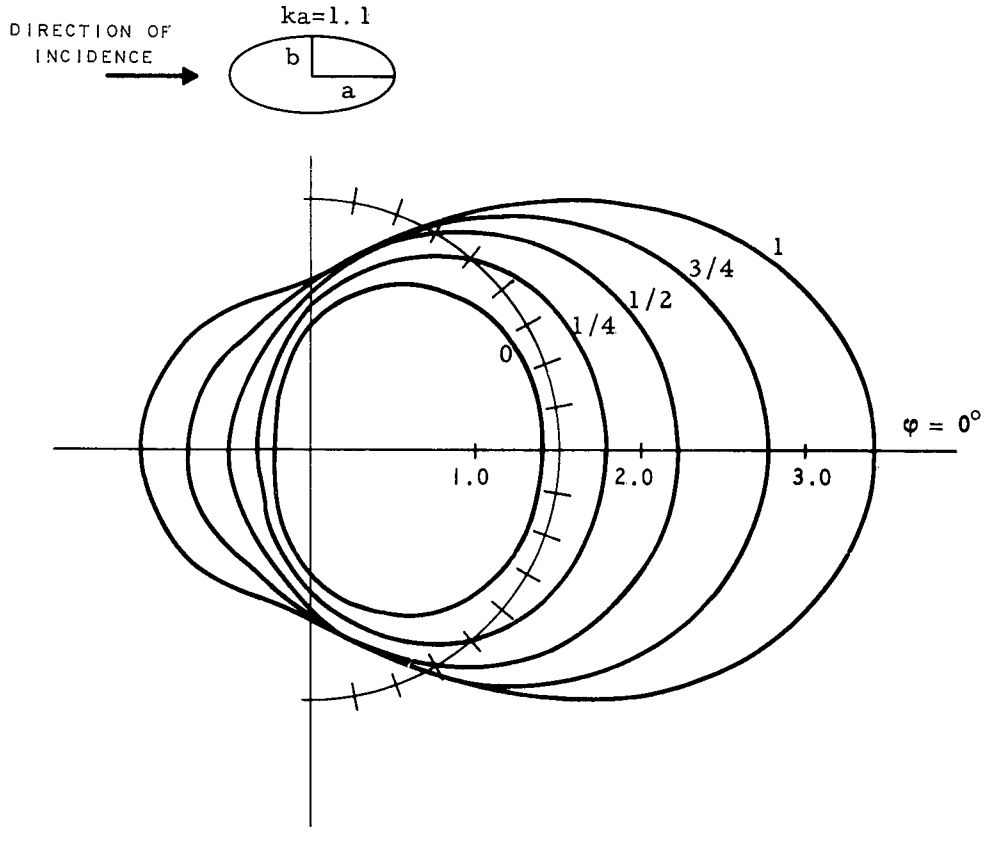

Graph II-10(a): $|g_{-}(\varphi, 0)|^2$.

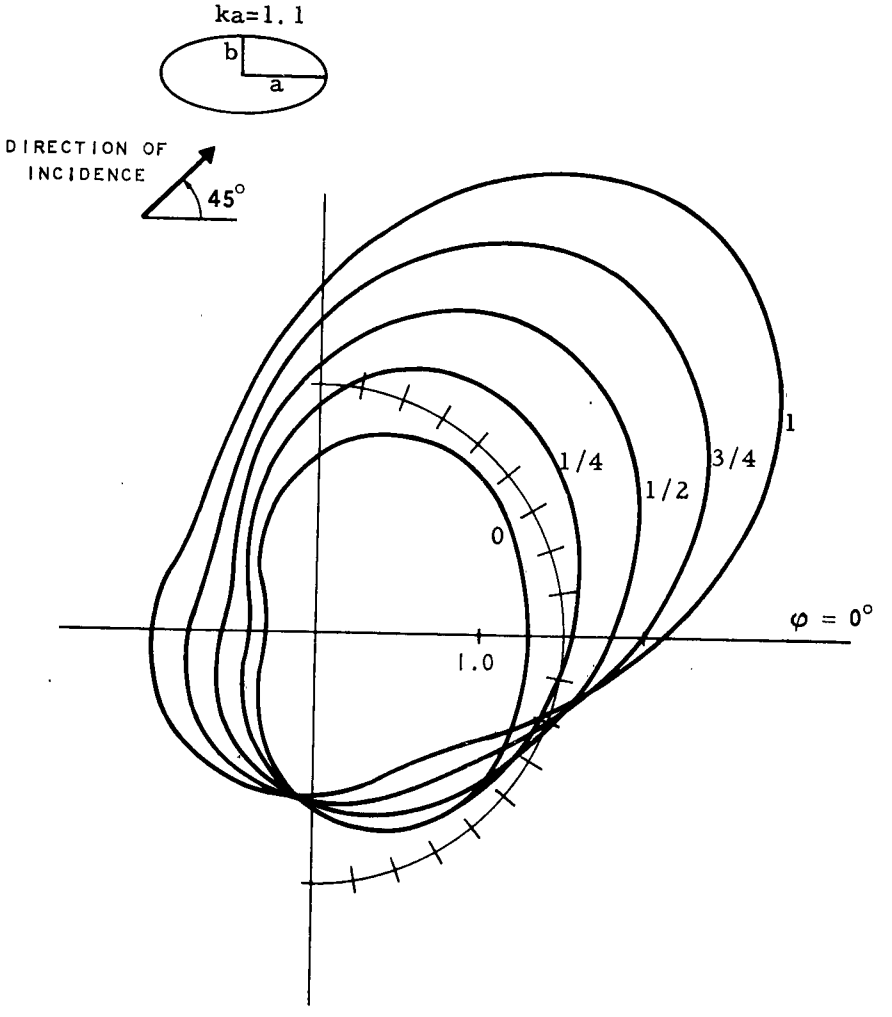

Graph II-10(b): $|g_{-}(\varphi, 45^{\circ})|^{2}$.

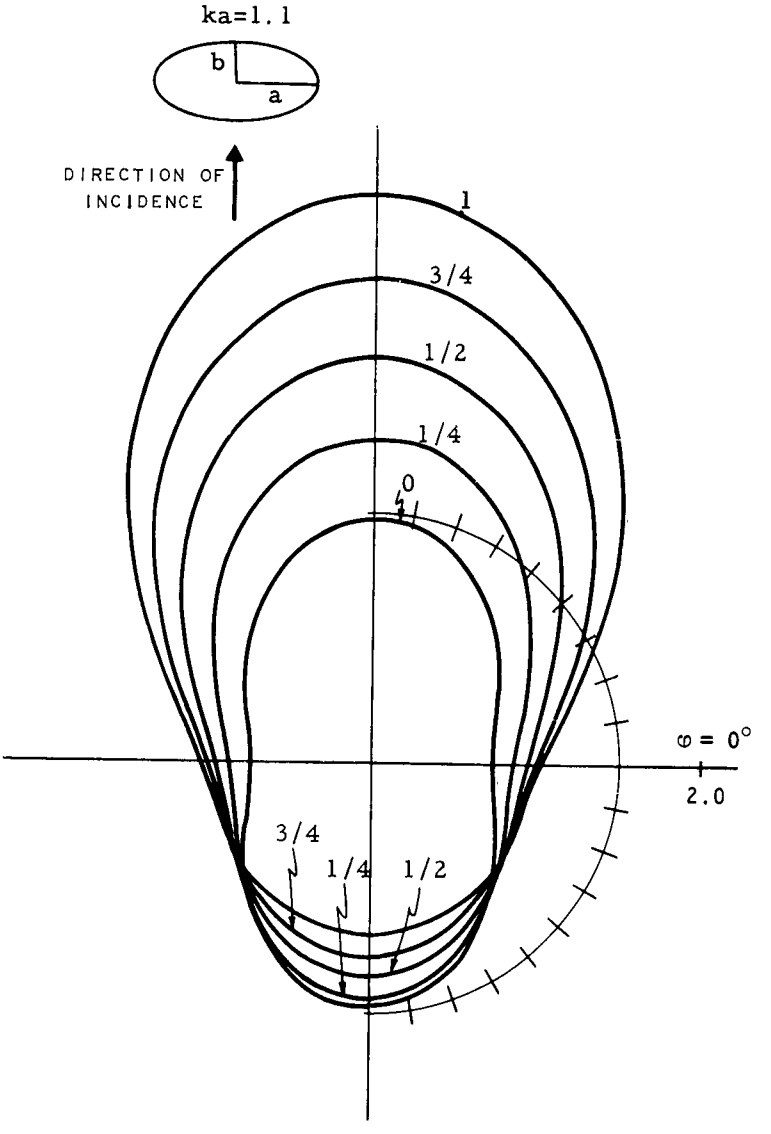

Graph II-10(c): $|g_{-}(\varphi, 90^{\circ})|^{2}$.

SET III: Graphical Results for Semi-Elliptic Protuberances and $\underset{\sim}{H}$ Parallel.

Graph III-1: $-\mathrm{Re}\, f_+(\varphi_o, \pi-\varphi_o)$ versus φ_o for ka = 0.5, 0.7, 0.9, and 1.1, and different values of δ.*

Graph III-2: $|f_+(\varphi_o, \pi-\varphi_o)|^2$ versus φ_o for ka = 0.5, 0.7, 0.9, and 1.1, and different values of δ.*

Graph III-3: $|f_+(\varphi_o, \pi-\varphi_o)|^2$ and the phase of $f_+(\varphi_o, \pi-\varphi_o)$ versus $ka \leq 1.1$, for $\varphi_o = 0^o$(a) and 45^o(b), and different values of δ.*

Graph III-4: $|f_+(-\varphi_o, \pi-\varphi_o)|^2$ versus φ_o for ka = 0.5, 0.7, 0.9, and 1.1, and different values of δ.*

Graph III-5: $|f_+(-\varphi_o, \pi-\varphi_o)|^2$ and the phase of $f_+(-\varphi_o, \pi-\varphi_o)$ versus $ka \leq 1.1$, for $\varphi_o = 45^o$, and different values of δ.*

Graph III-6: $|f_+(\varphi, \pi-\varphi_o)|^2$ versus φ for $\varphi_o = 0$, 45^o, and 80^o, ka = 0.3, and different values of δ.*

Graph III-7: $|f_+(\varphi, \pi-\varphi_o)|^2$ versus φ for $\varphi_o = 0$, 45^o, and 80^o, ka = 0.7, and different values of δ.*

Graph III-8: $|f_+(\varphi, \pi-\varphi_o)|^2$ versus φ for $\varphi_o = 0$, 45^o, and 90^o, ka = 1.1, and different values of δ.*

*The number next to a curve gives the value of $\delta = \eta/\xi$ = (axis $\parallel$ ground plane)/(axis $\perp$ ground plane); $\delta = 0$ corresponds to perpendicular strips, $\delta = 1$ to semi-circles, and $\delta = \infty$ to flat strips (see Fig. 3).

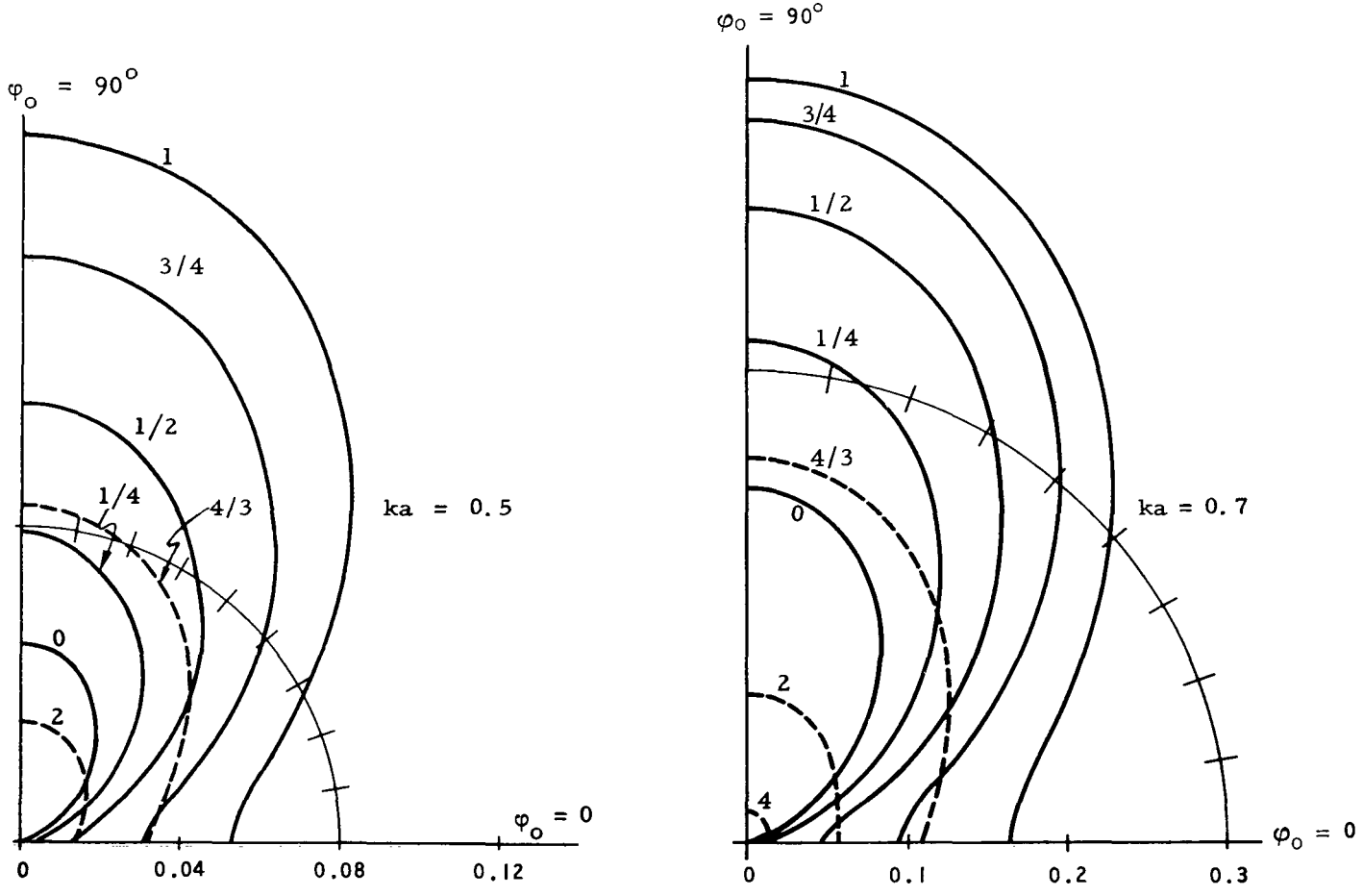

Graph III-1: -Re $f_+(\varphi_o, \pi-\varphi_o)$.

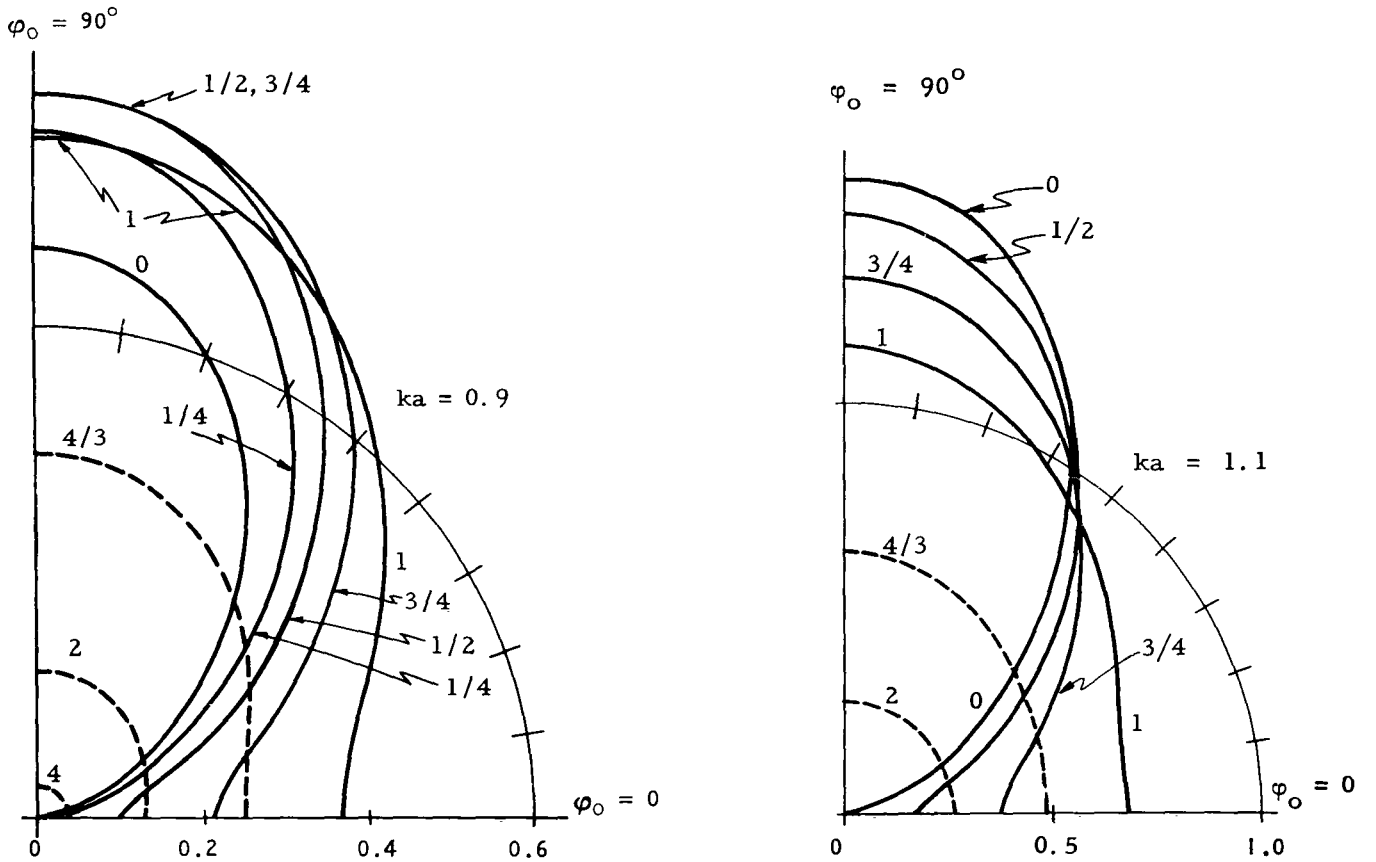

Graph III-1 (Con't): -Re $f_+(\varphi_o, \pi-\varphi_o)$.

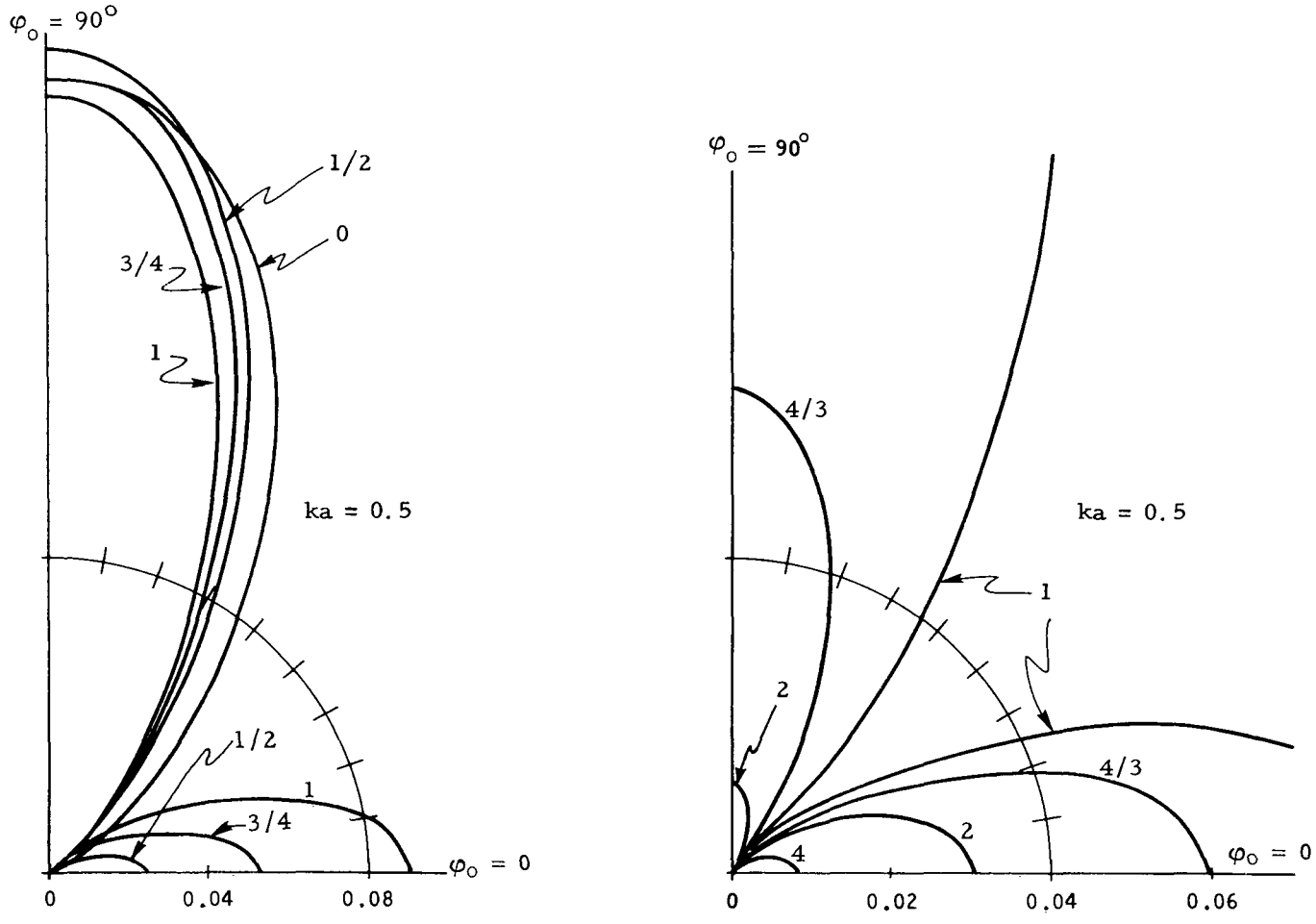

Graph III-2: $|f_+(\varphi_o, \pi-\varphi_o)|^2$.

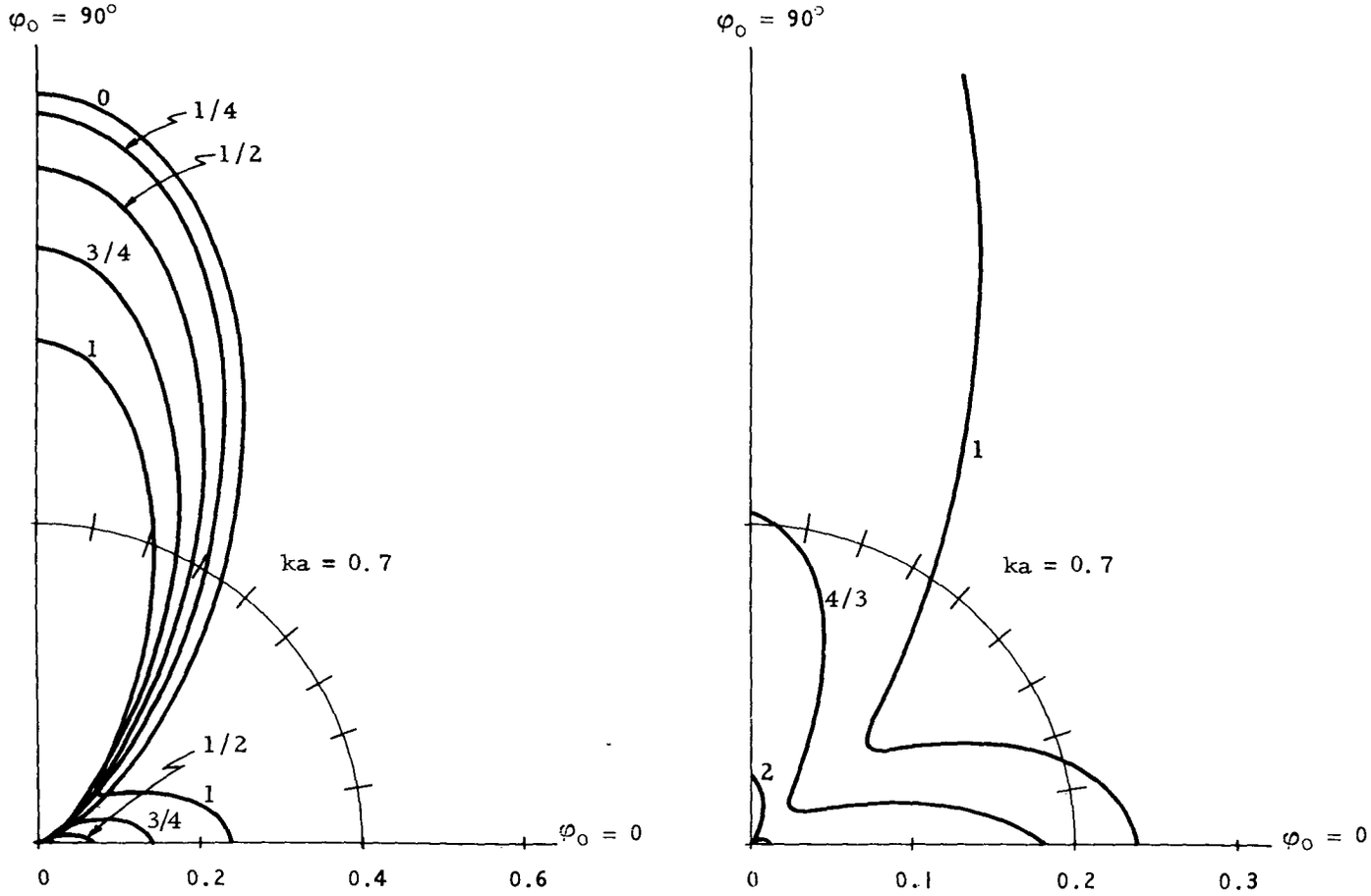

Graph III-2 (Con't): $|f_+(\varphi_o, \pi-\varphi_o)|^2$.

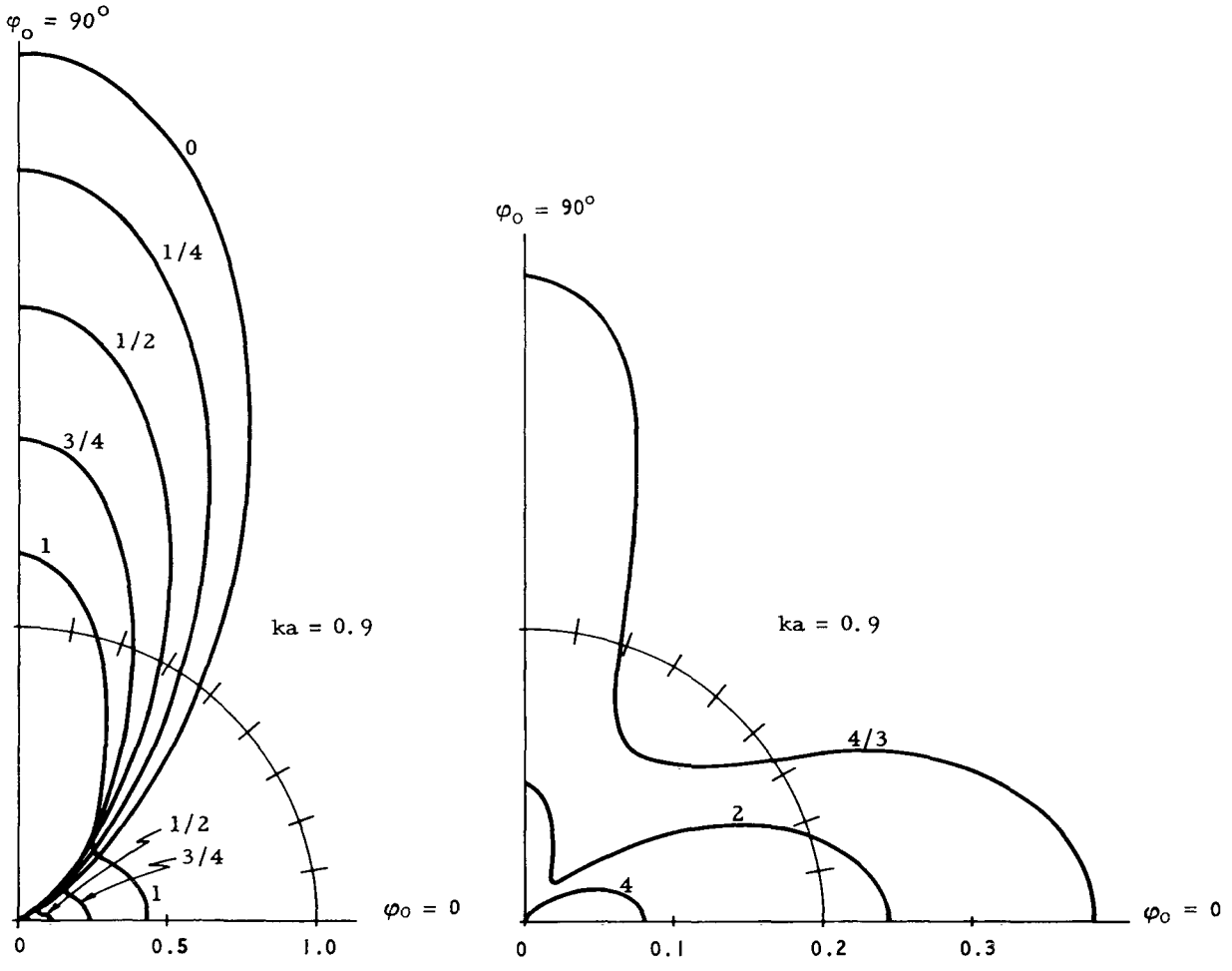

Graph III-2 (Con't): $|f_+(\varphi_o, \pi-\varphi_o)|^2$.

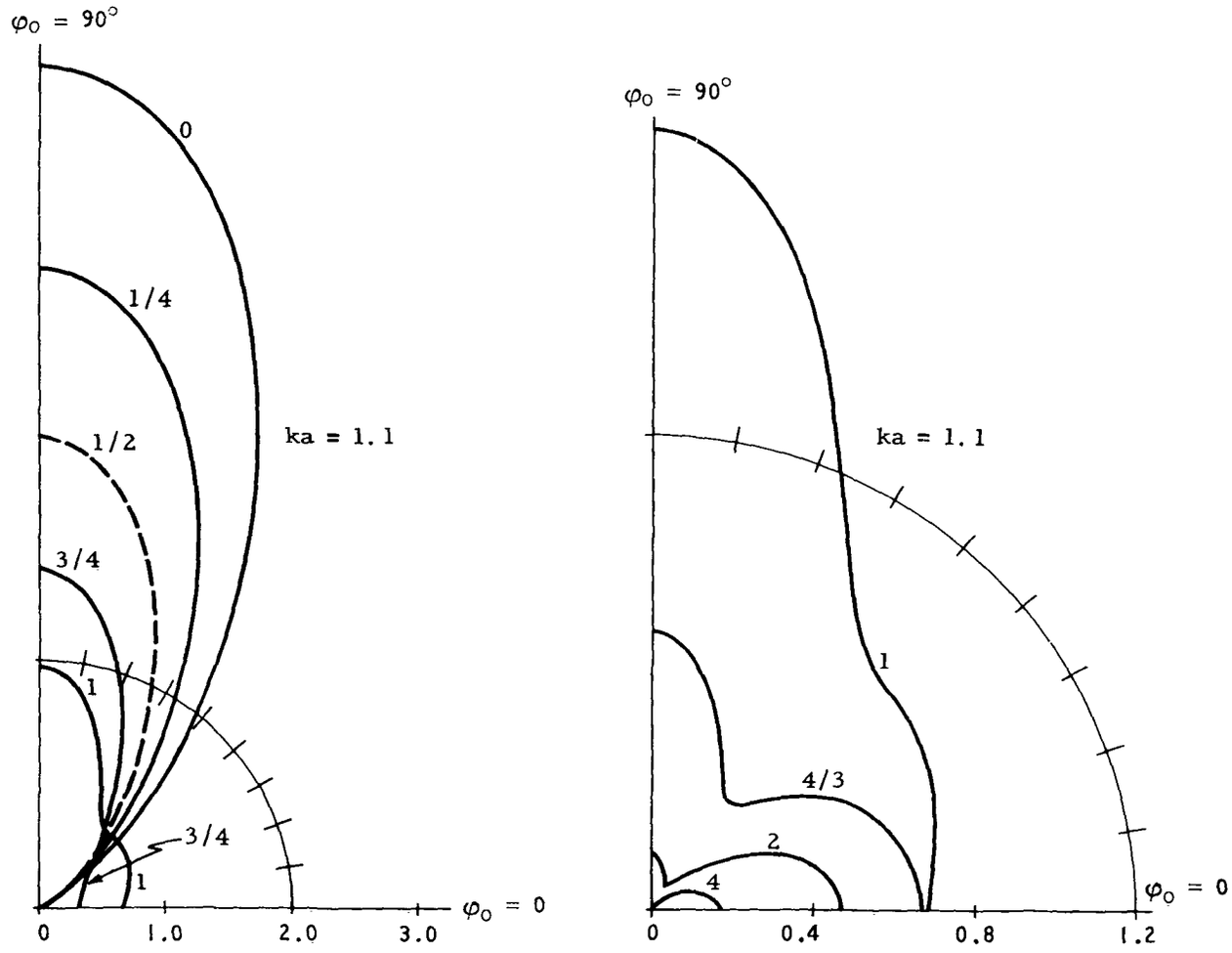

Graph III-2 (Con't): $|f_+(\varphi_o, \pi-\varphi_o)|^2$.

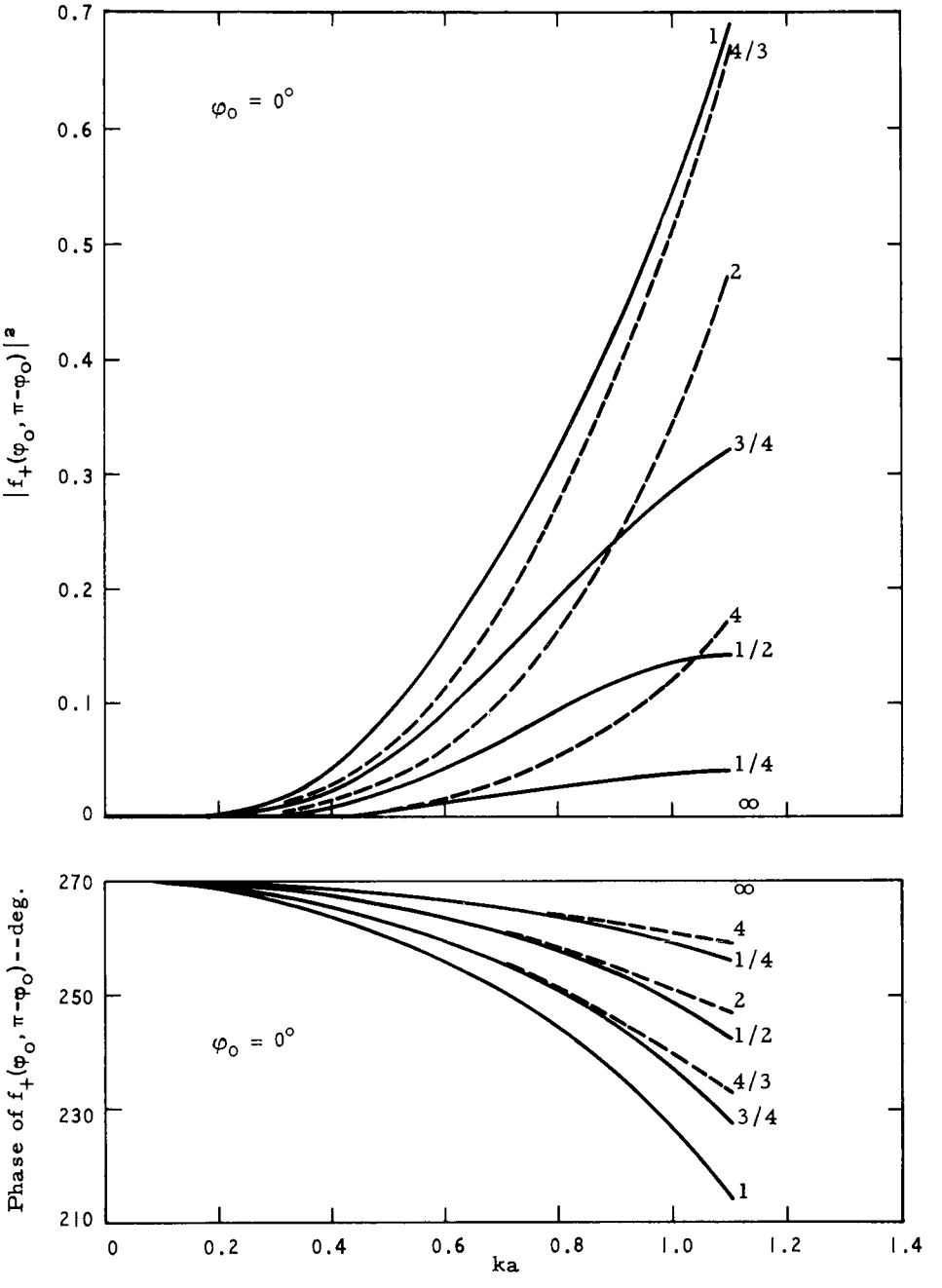
0.7
0.6
0.5
0.4
0.3
0.2
0.1
0
$|f_+(\varphi_o, \pi-\varphi_o)|^2$
$\varphi_o = 0°$
1
4/3
2
3/4
4
1/2
1/4
∞
270
250
230
210
Phase of $f_+(\varphi_o, \pi-\varphi_o)$--deg.
$\varphi_o = 0°$
∞
4
1/4
2
1/2
4/3
3/4
1
0
0.2
0.4
0.6
0.8
1.0
1.2
1.4
ka

Graph III-3(a)

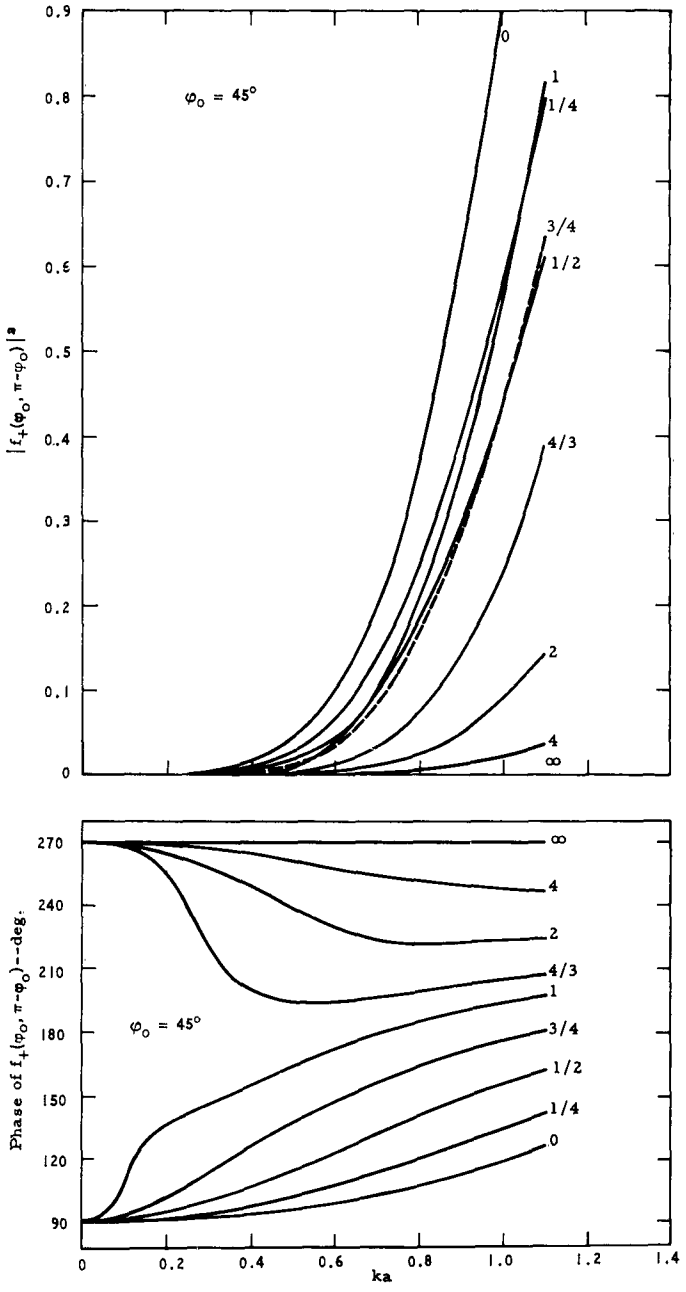
φ_o = 45°
$|f_+(\varphi_o, \pi-\varphi_o)|^2$
0
1
1/4
3/4
1/2
4/3
2
4
∞
Phase of $f_+(\varphi_o, \pi-\varphi_o)$--deg.
ka

Graph III-3(b)

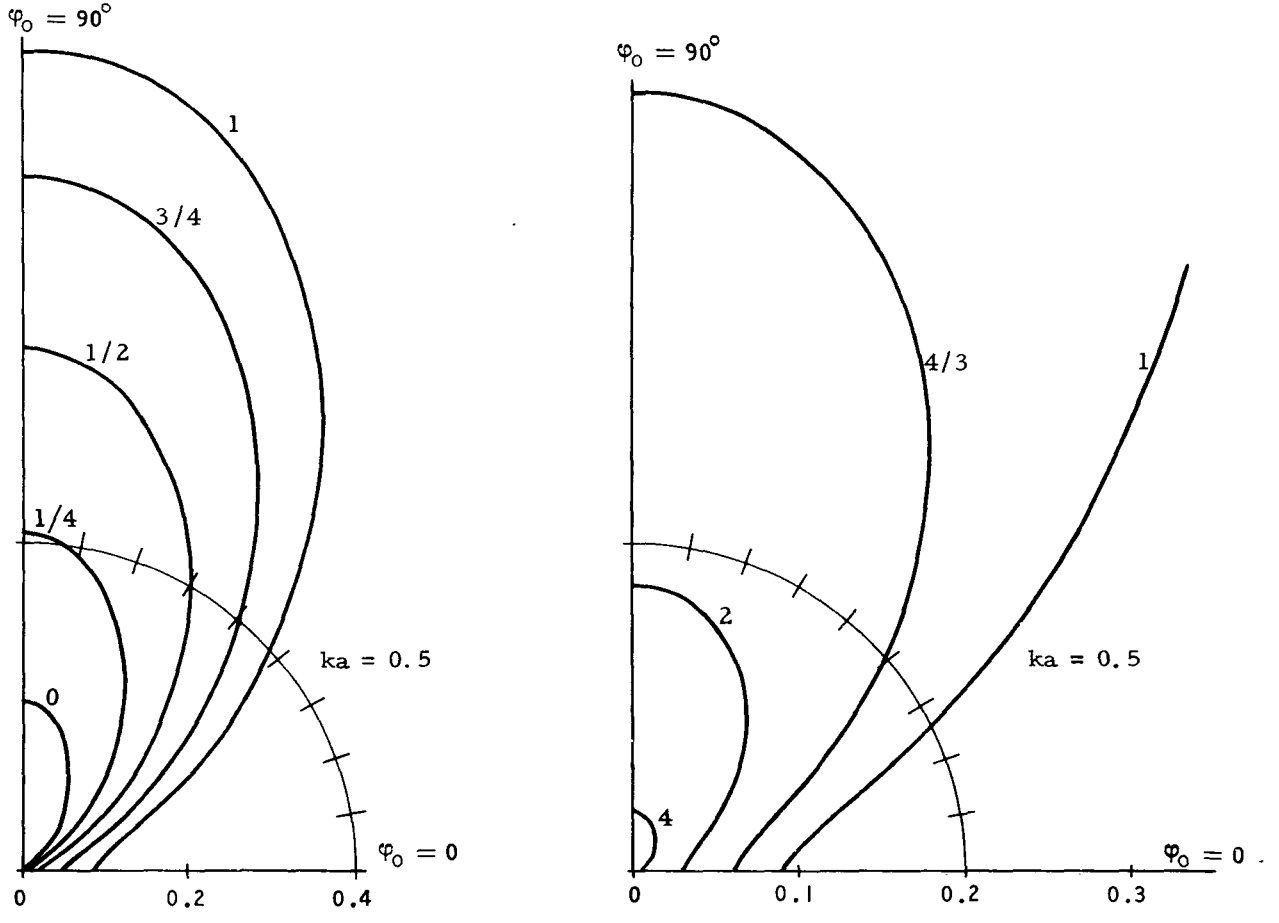

Graph III-4: $|f_+(-\varphi_o, \pi-\varphi_o)|^2$.

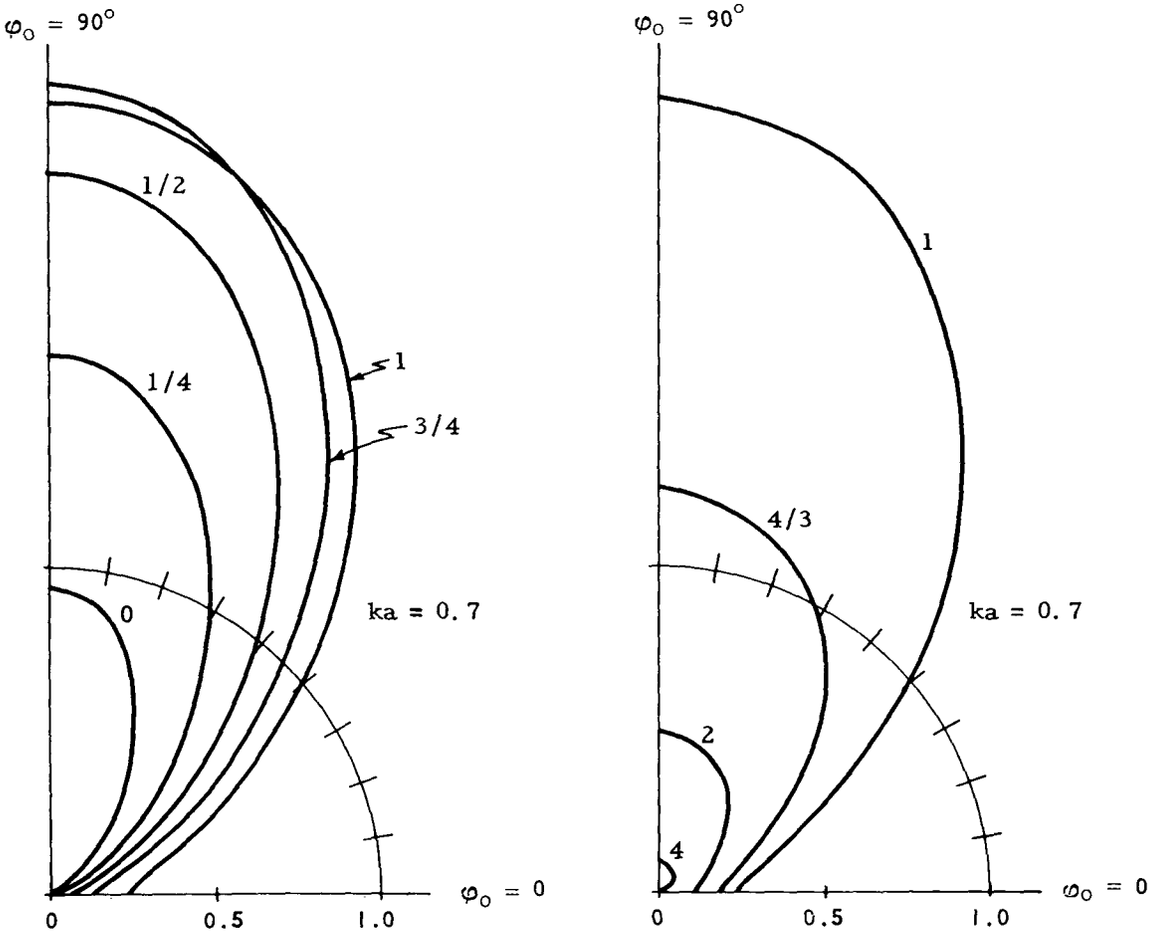

Graph III-4 (Con't): $|f_+(-\varphi_o, \pi-\varphi_o)|^2$.

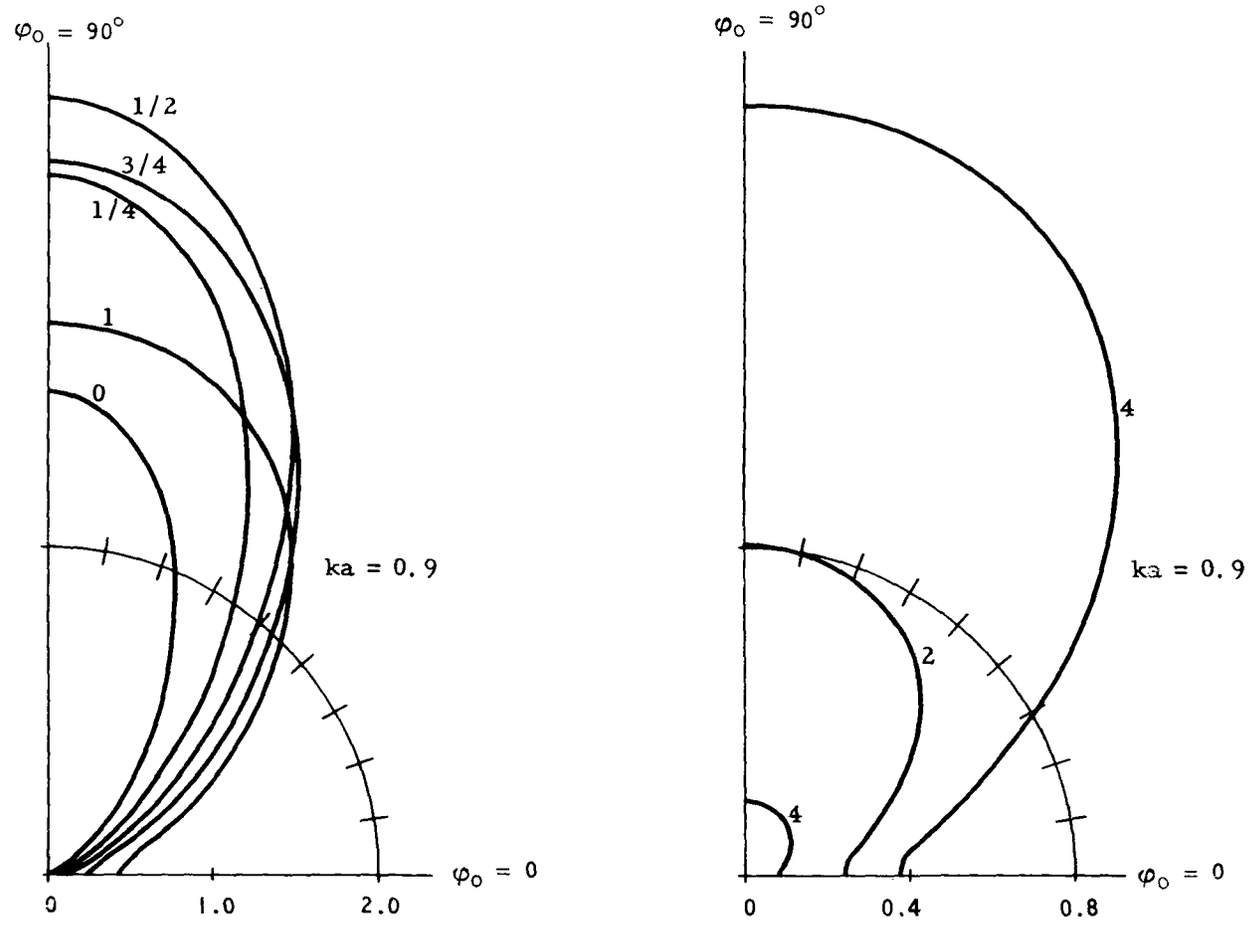

Graph III-4 (Con't): $|f_+(-\varphi_o, \pi-\varphi_o)|^2$.

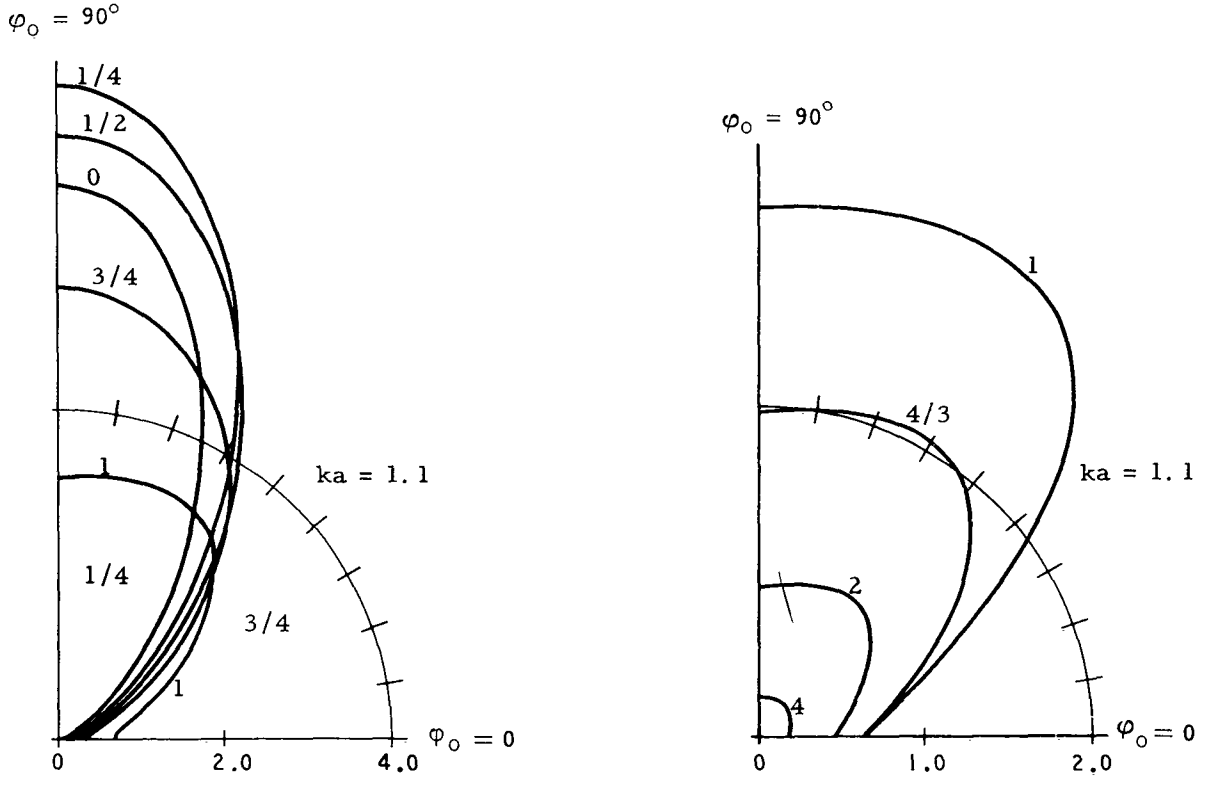

Graph III-4 (Con't): $|f_+(-\varphi_o, \pi-\varphi_o)|^2$.

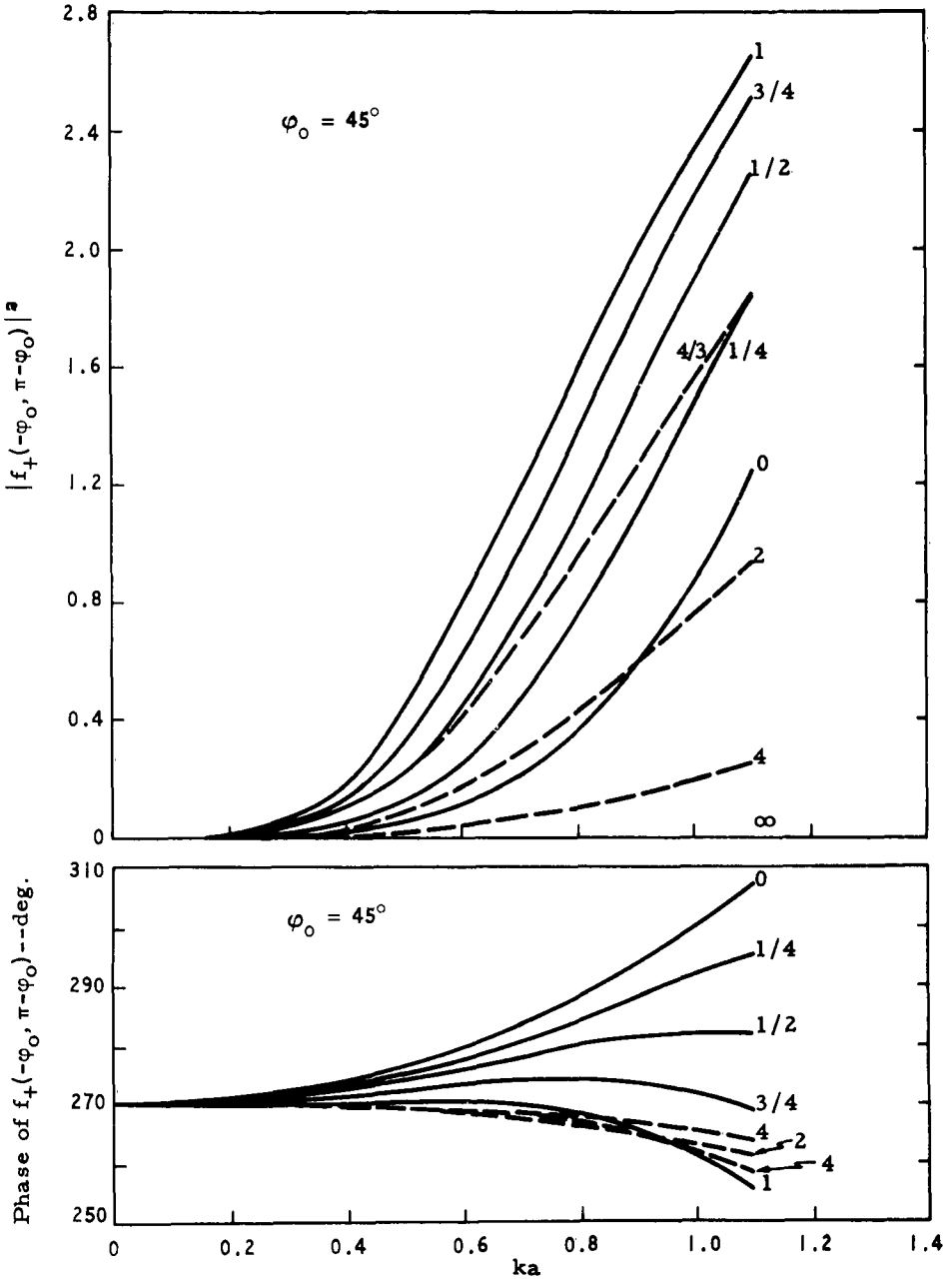
2.8
2.4
2.0
1.6
1.2
0.8
0.4
0
$|f_+(-\varphi_o, \pi-\varphi_o)|^2$
$\varphi_o = 45°$
1
3/4
1/2
4/3
1/4
0
2
4
∞
310
290
270
250
Phase of $f_+(-\varphi_o, \pi-\varphi_o)$--deg.
$\varphi_o = 45°$
0
1/4
1/2
3/4
4
2
4
1
0
0.2
0.4
0.6
0.8
1.0
1.2
1.4
ka

Graph III-5

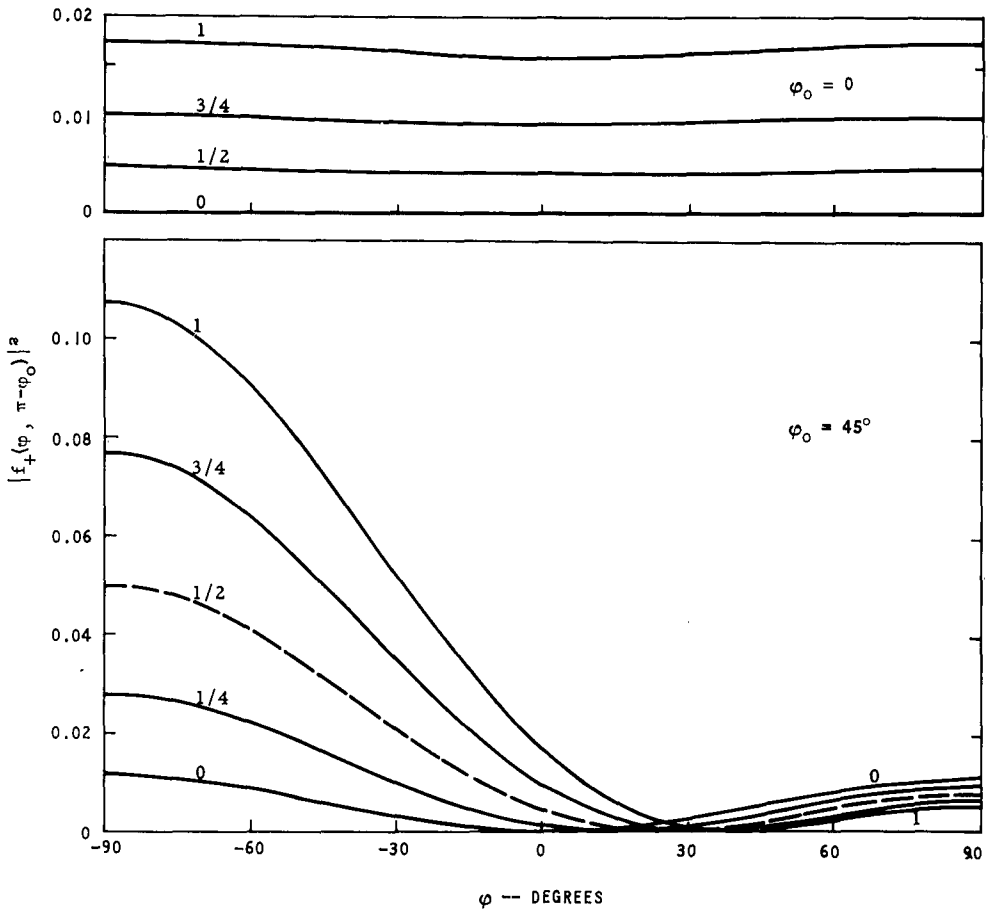

Graph III-6 : ka = 0.3

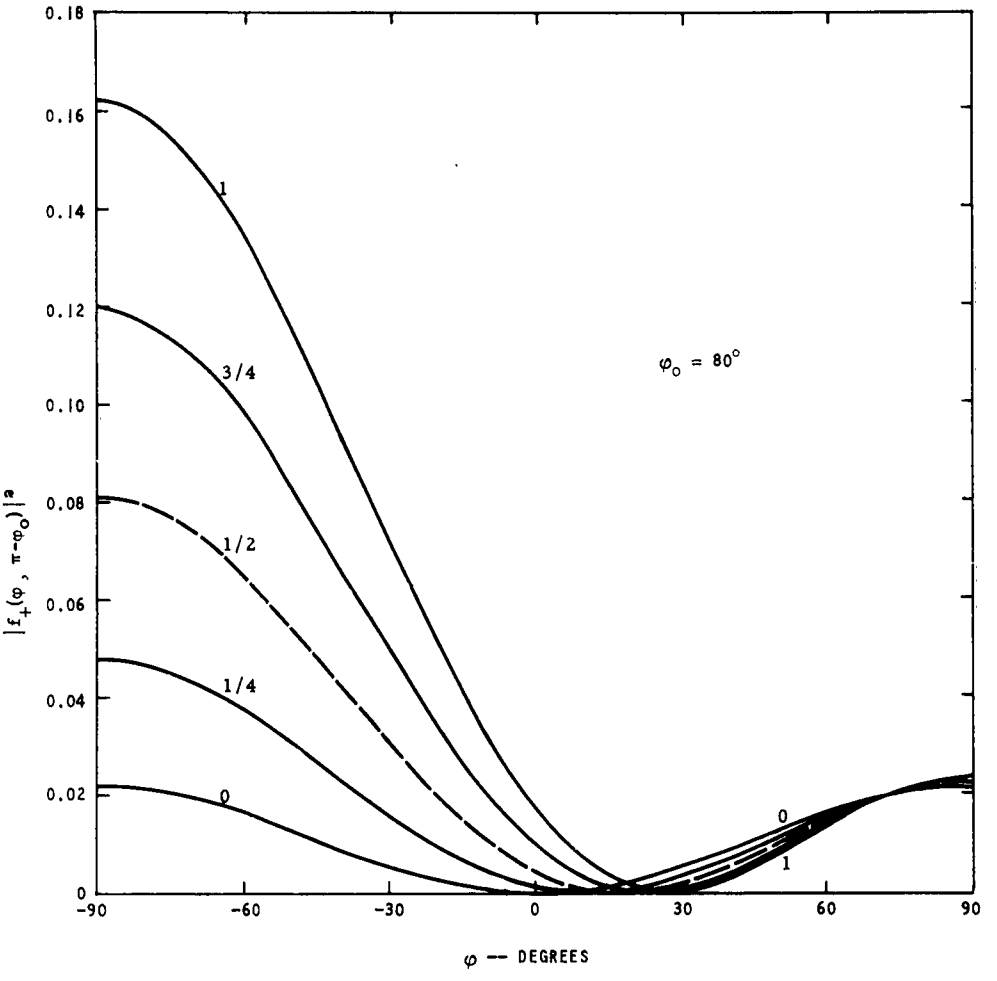

Graph III-6 (con't): ka = 0.3

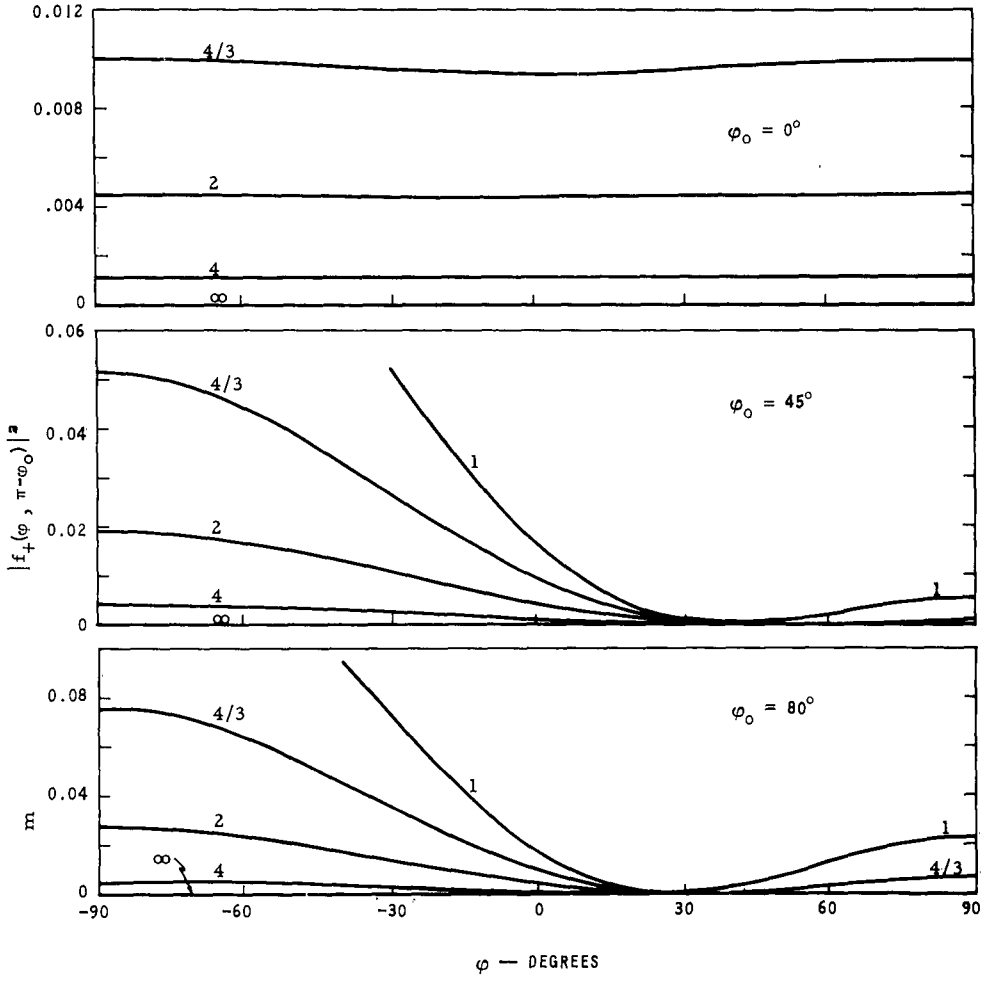

Graph III-6 (con't) : ka = 0.3

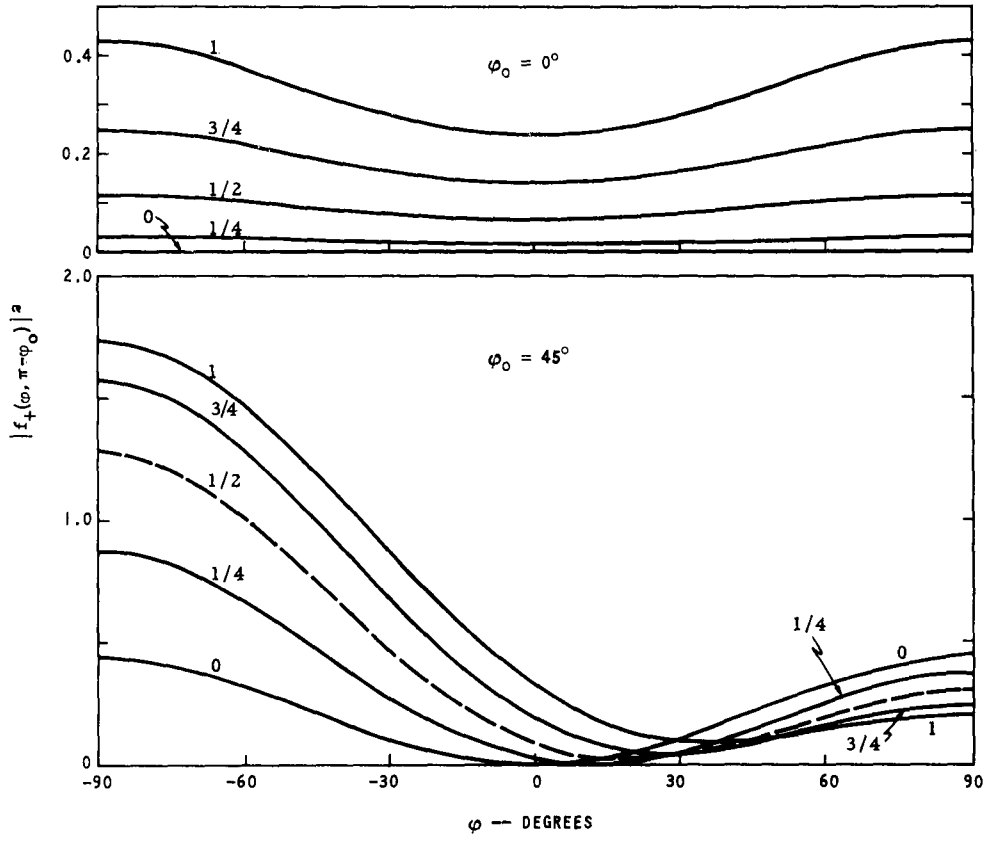

Graph III-7: ka = 0.7

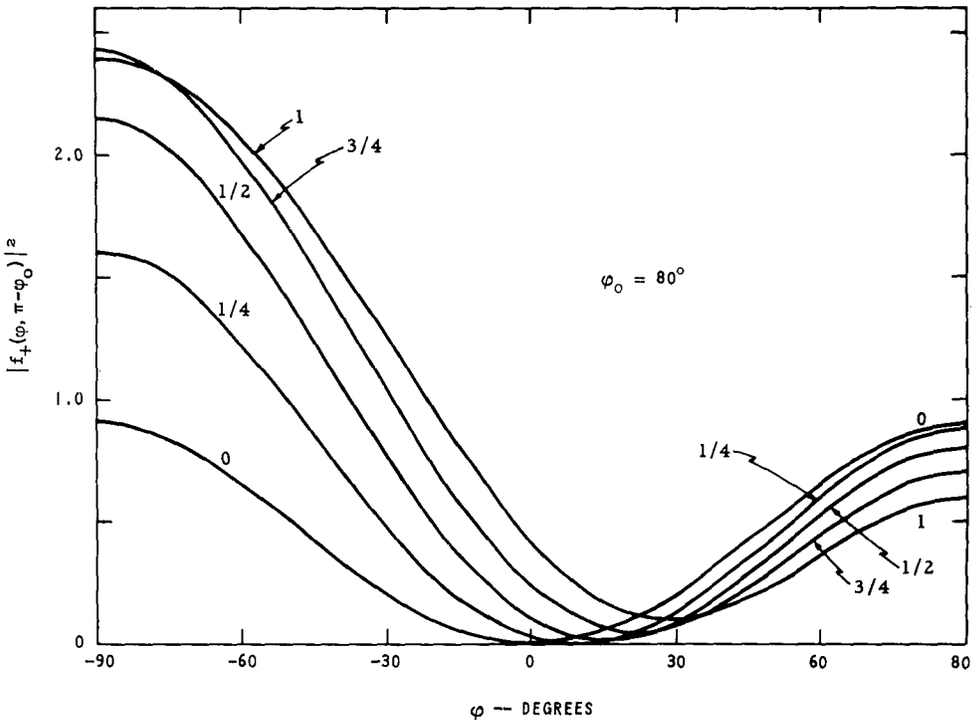

Graph III-7 (con't): ka = 0.7

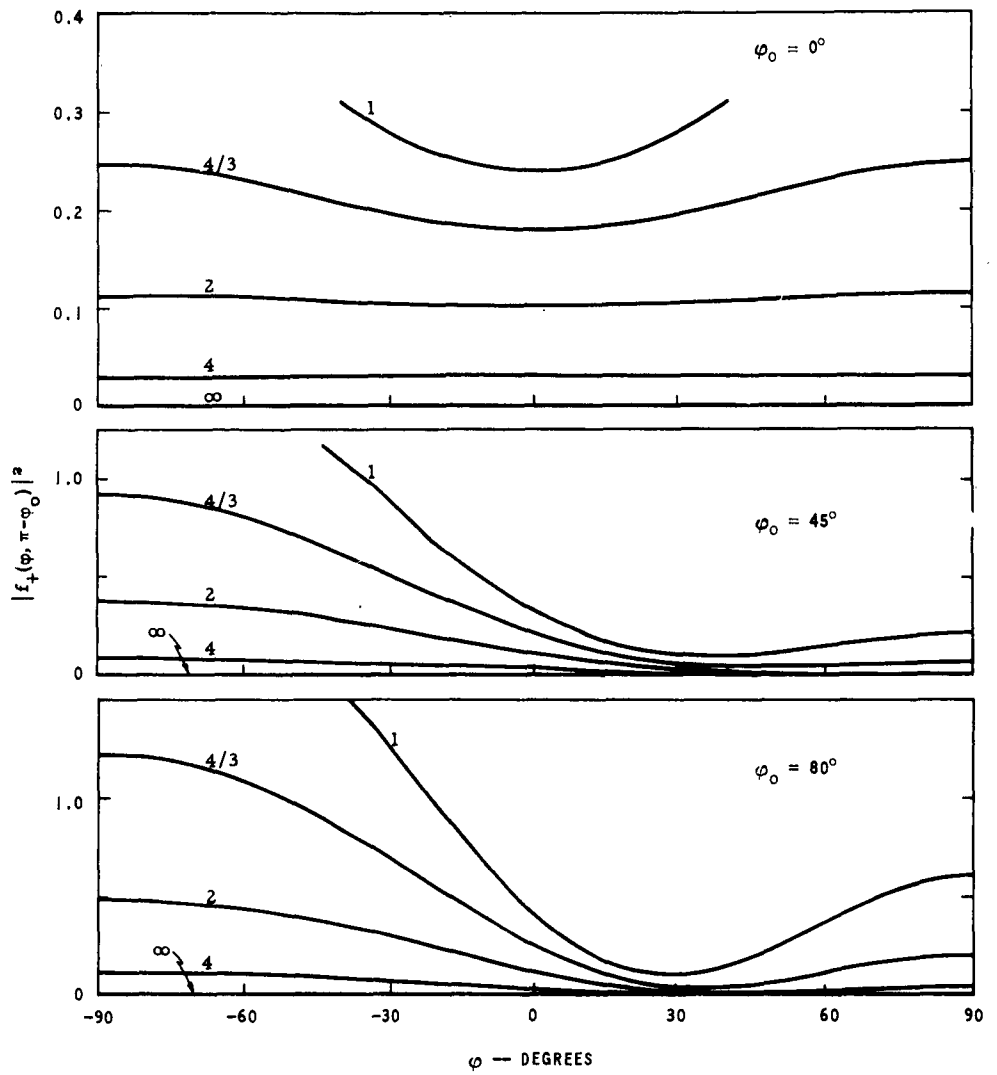

Graph III-7 (con't): ka = 0.7

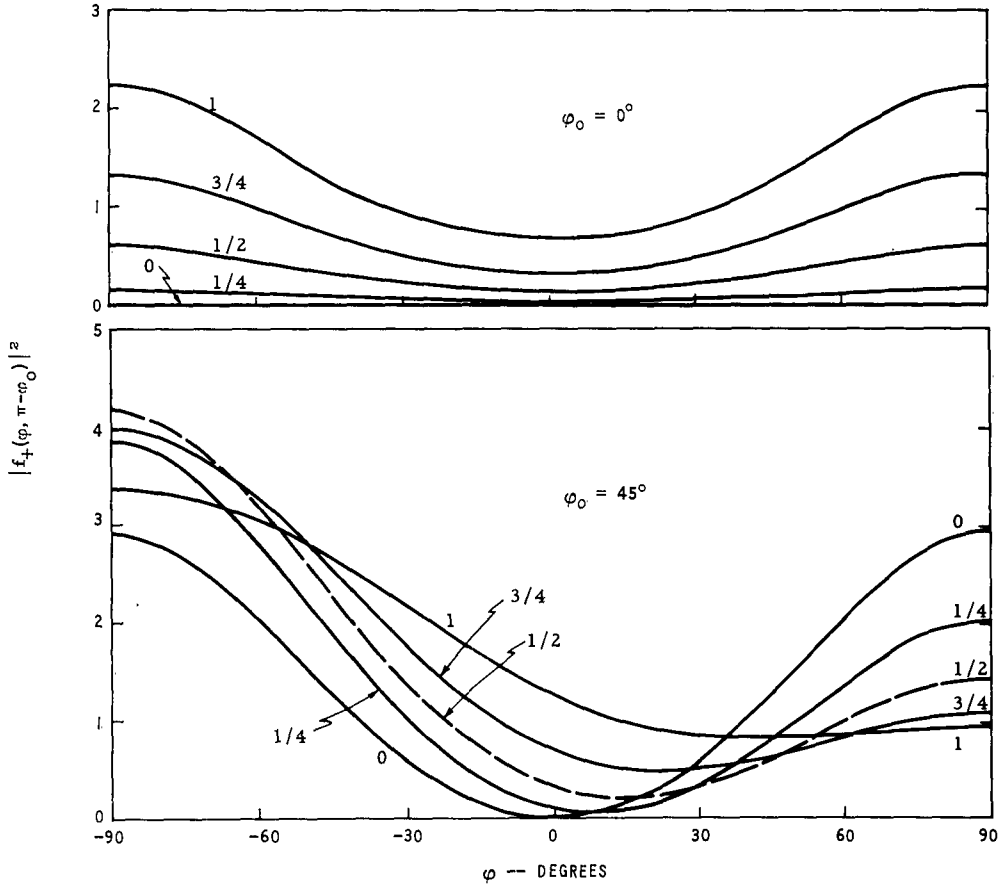

Graph III-8: ka = 1.1

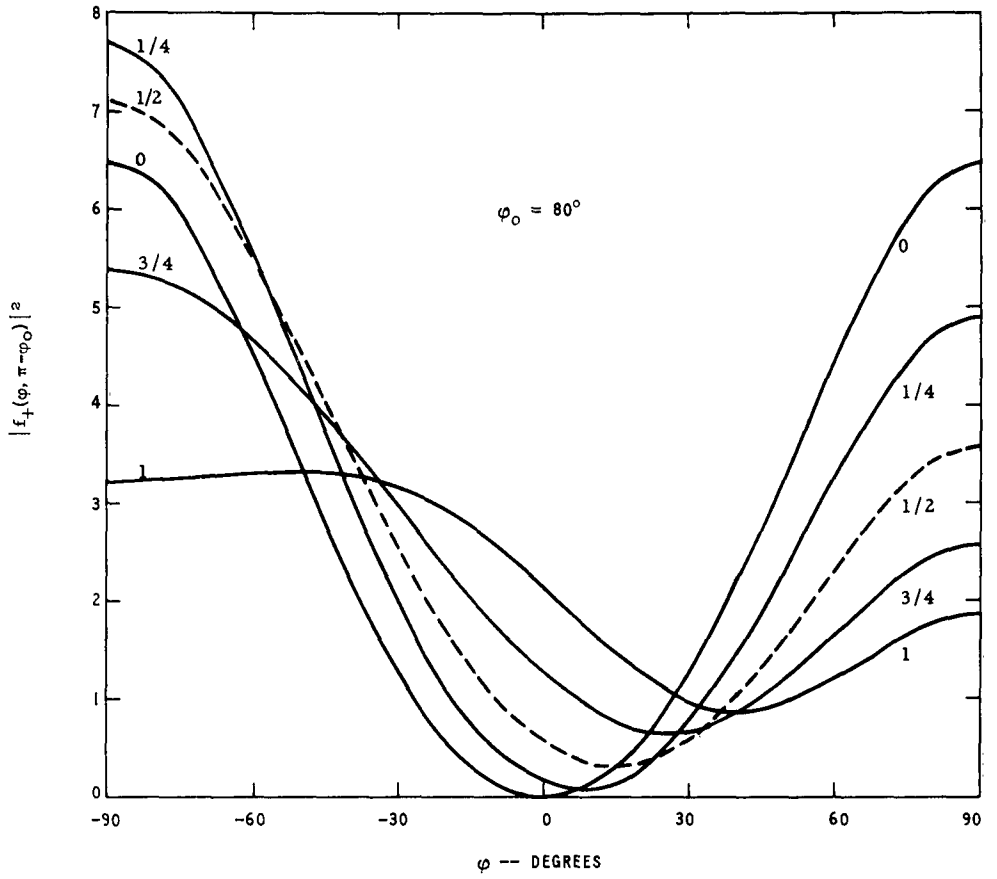

Graph III-8 (con't): ka = 1.1

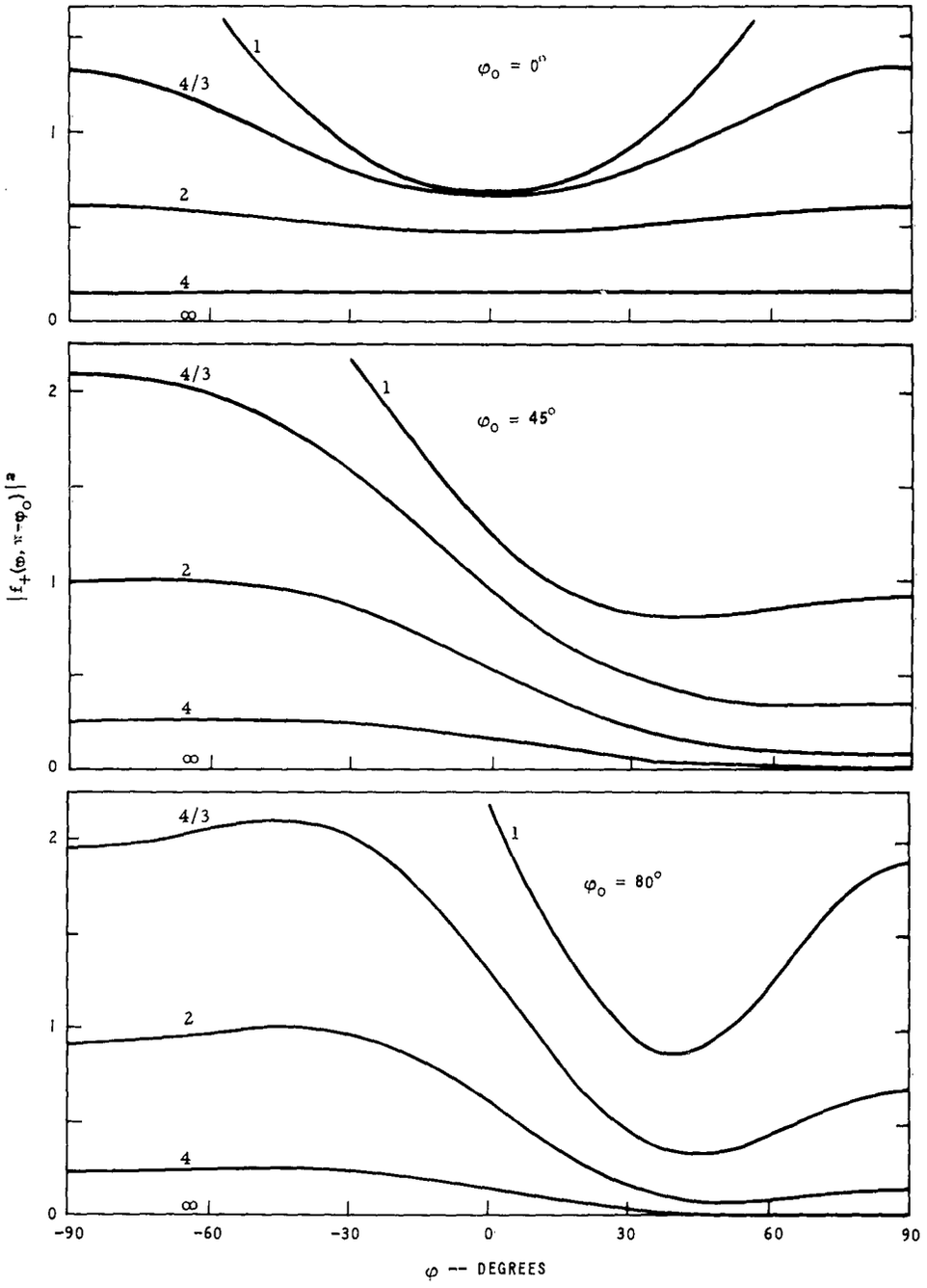

Graph III-8 (con't): ka = 1.1

SET IV: Graphical Results for Semi-Elliptic Protuberances and $\underline{E}$ Parallel.

Graph IV-1: $-\mathrm{Re}\, f_-(\varphi_o, \pi-\varphi_o)$ versus φ_o for ka = 0.5, 0.7, 0.9, and 1.1, and different values of δ.*

Graph IV-2: $|f_-(\varphi_o, \pi-\varphi_o)|^2$ versus φ_o for ka = 0.5, 0.7, 0.9, and 1.1, and different values of δ.*

Graph IV-3: $|f_-(\varphi_o, \pi-\varphi_o)|^2$ and the phase of $f_-(\varphi_o, \pi-\varphi_o)$ versus $ka \leq 1.1$, for $\varphi_o = 0^o$(a) and 45^o(b), and different values of δ.*

Graph IV-4: $|f_-(-\varphi_o, \pi-\varphi_o)|^2$ versus φ_o for ka = 0.5, 0.7, 0.9, and 1.1, and different values of δ.*

Graph IV-5: $|f_-(-\varphi_o, \pi-\varphi_o)|^2$ and the phase of $f_-(-\varphi_o, \pi-\varphi_o)$ versus $ka \leq 1.1$, for $\varphi_o = 45^o$ and different values of δ.*

Graph IV-6: $|f_-(\varphi, \pi-\varphi_o)|^2$ versus φ for $\varphi_o = 0, 45^o$, and 80^o, ka = 0.3, and different values of δ.*

Graph IV-7: $|f_-(\varphi, \pi-\varphi_o)|^2$ versus φ for $\varphi_o = 0, 45^o$, and 80^o, ka = 0.7, and different values of δ.*

Graph IV-8: $|f_-(\varphi, \pi-\varphi_o)|^2$ versus φ for $\varphi_o = 0, 45^o$, and 90^o, ka = 1.1, and different values of δ.*

*The number next to a curve gives the value of $\delta = \eta/\xi =$ (axis $\parallel$ ground plane)/(axis $\perp$ ground plane); $\delta = 0$ corresponds to perpendicular strips, $\delta = 1$ to semi-circles, and $\delta = \infty$ to flat strips (see Fig. 3).

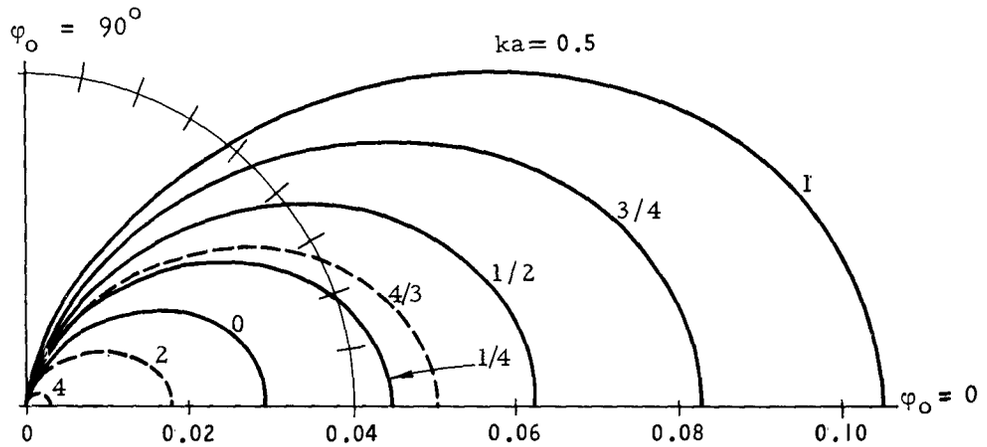

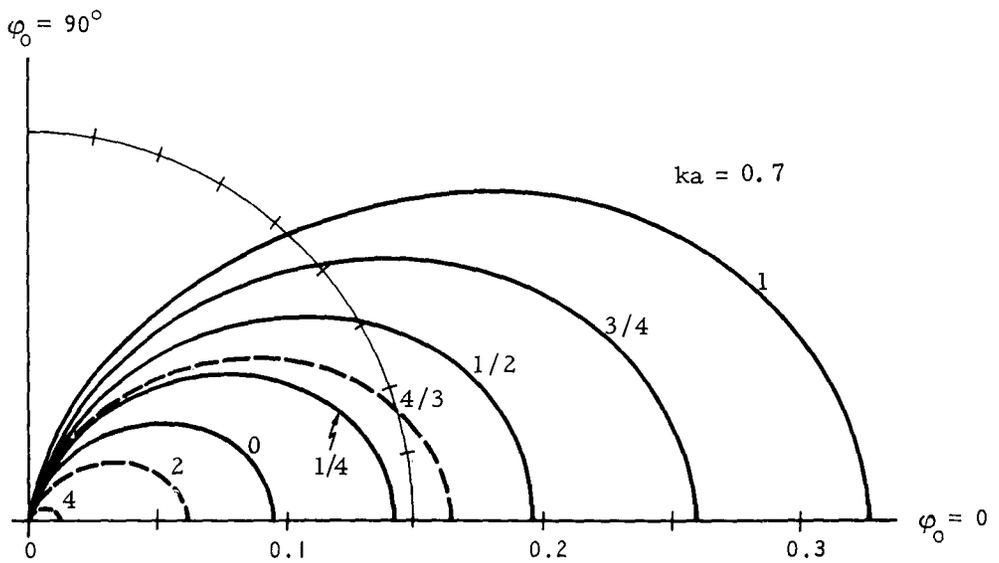

Graph IV-1: -Re $f_+(\varphi_o, \pi-\varphi_o)$.

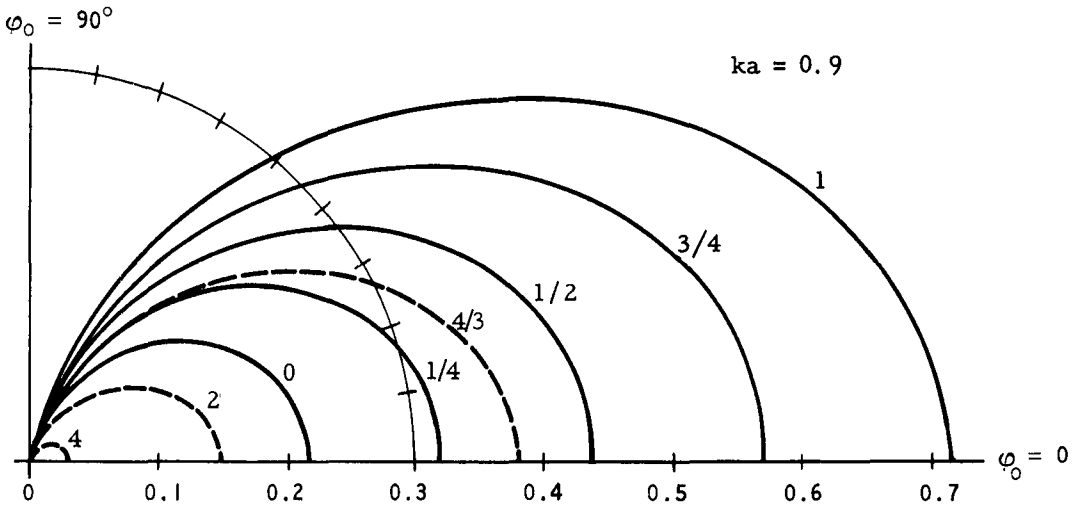

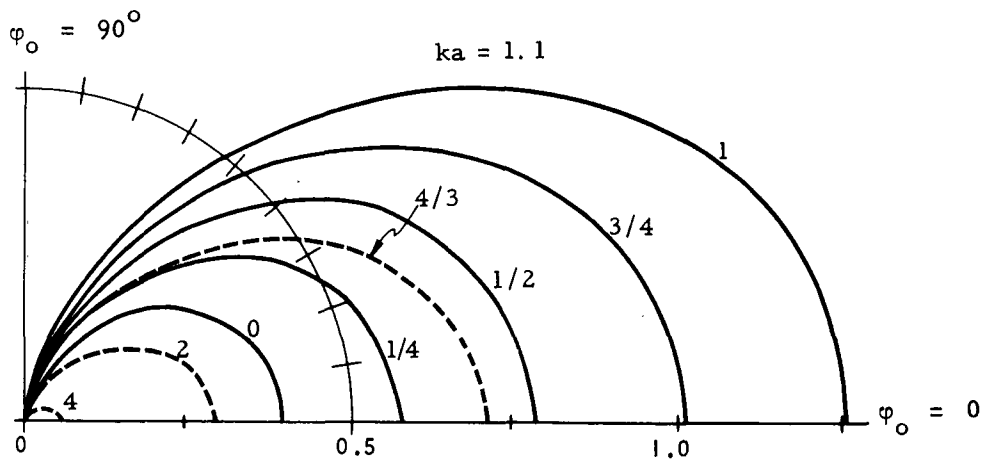

Graph IV-1 (Con't): -Re $f_+(\varphi_o, \pi-\varphi_o)$.

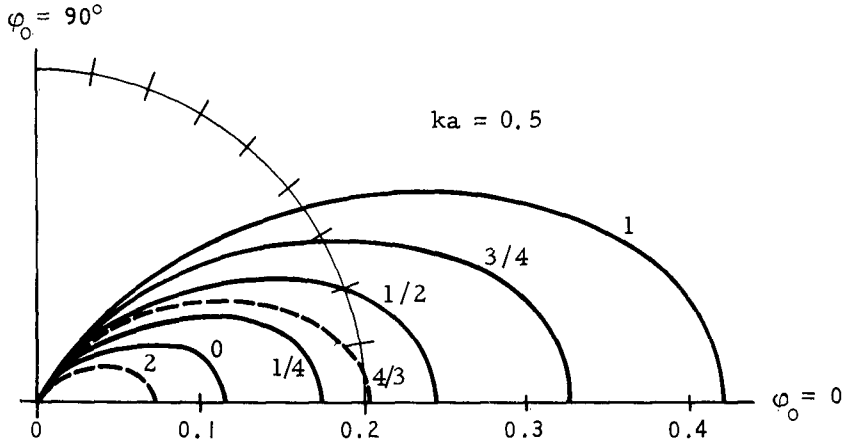

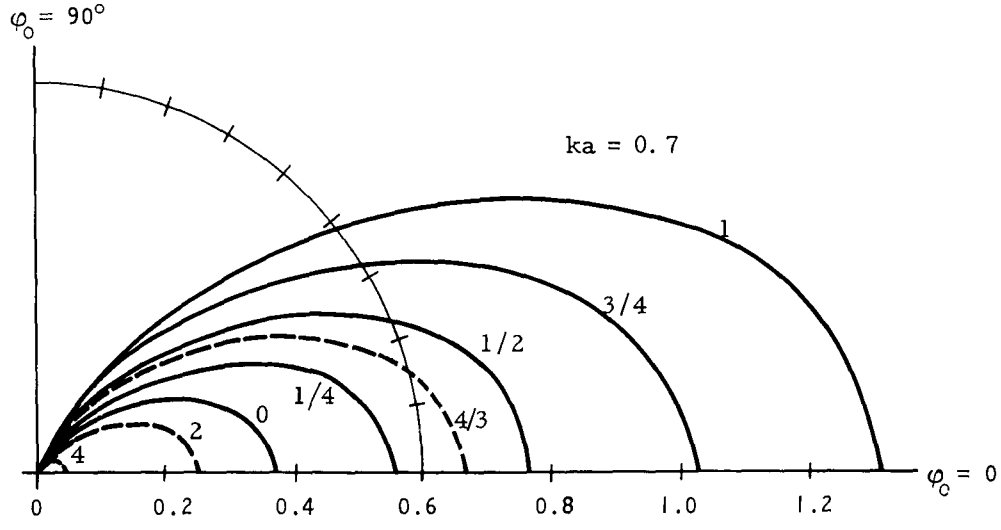

Graph IV-2: $|f_{-}(\varphi_o, \pi-\varphi_o)|^2$.

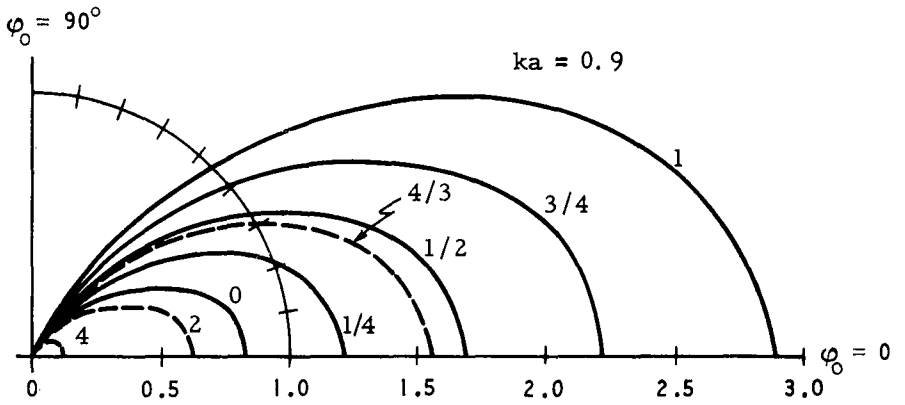

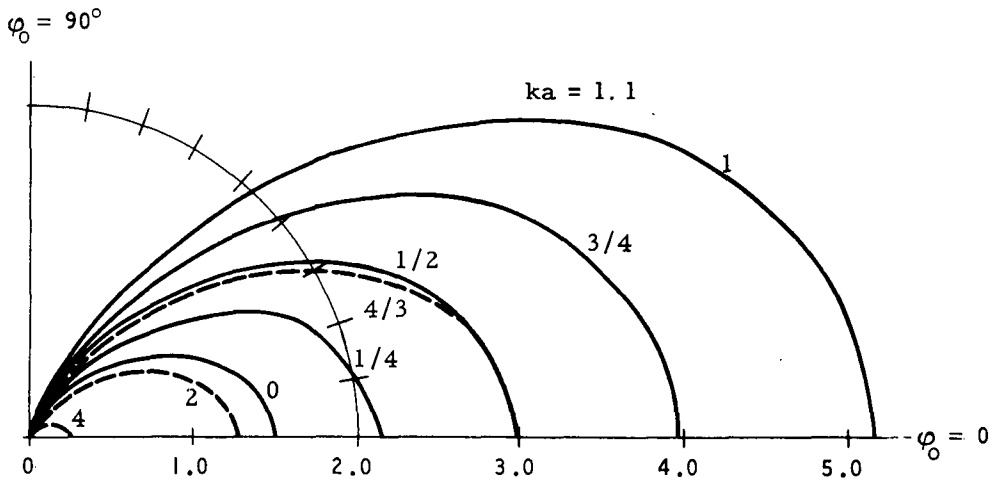

Graph IV-2 (Con't): $|f_{-}(\varphi_o, \pi-\varphi_o)|^2$.

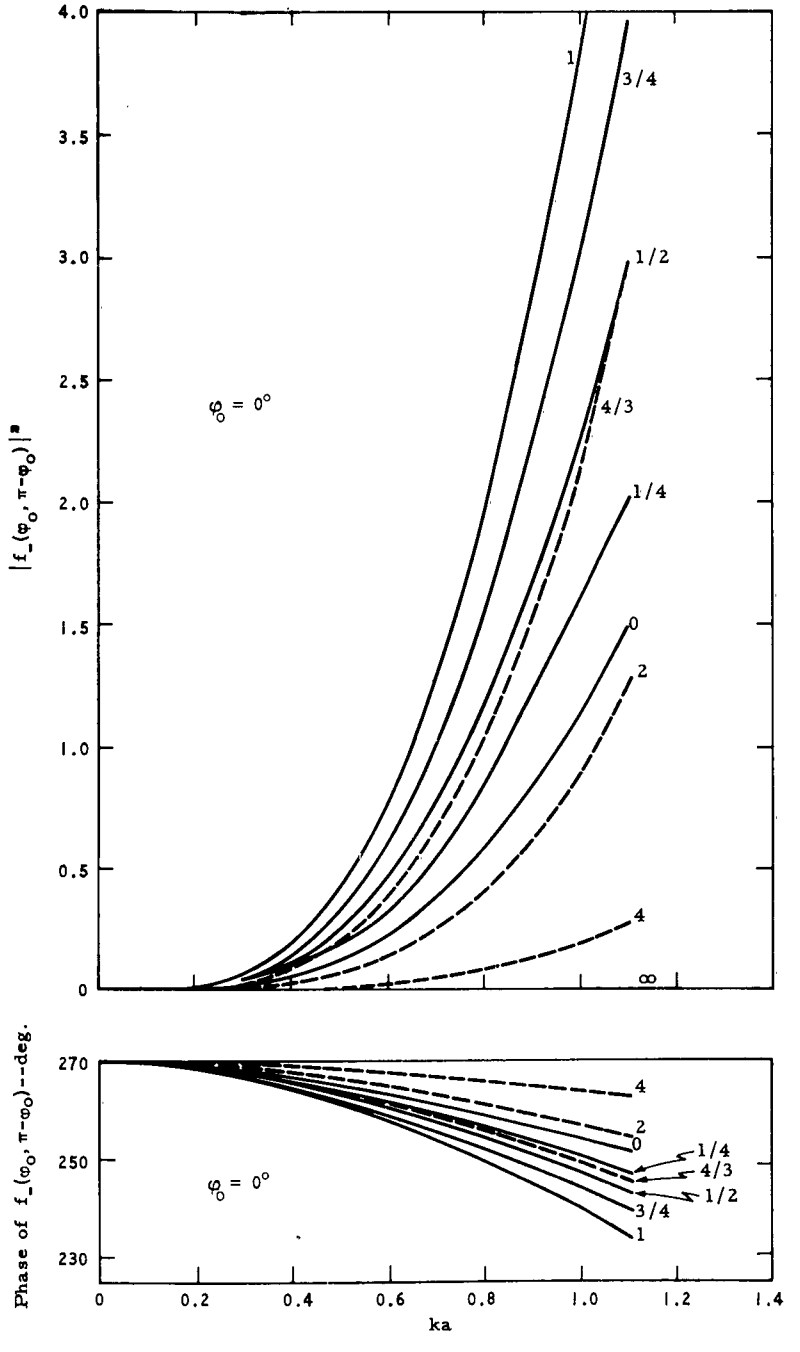
4.0
3.5
3.0
2.5
2.0
1.5
1.0
0.5
0
$|f_-(\varphi_o, \pi-\varphi_o)|^2$
$\varphi_o = 0°$
1
3/4
1/2
4/3
1/4
0
2
4
∞
270
250
230
Phase of $f_-(\varphi_o, \pi-\varphi_o)$--deg.
$\varphi_o = 0°$
4
2
0
1/4
4/3
1/2
3/4
1
0
0.2
0.4
0.6
0.8
1.0
1.2
1.4
ka

Graph IV-3(a)

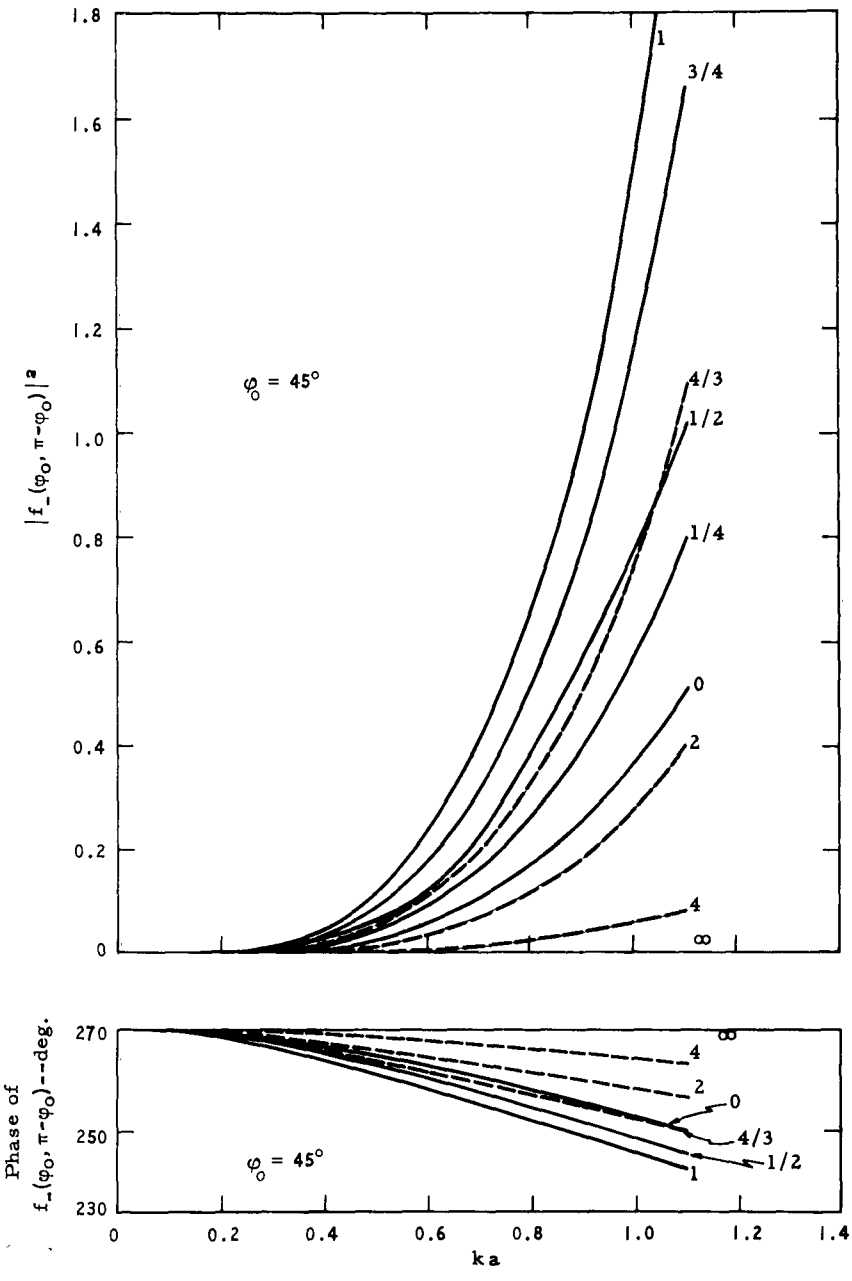
1.8
1.6
1.4
1.2
1.0
0.8
0.6
0.4
0.2
0
$|f_-(\varphi_o, \pi-\varphi_o)|^2$
$\varphi_o = 45°$
1
3/4
4/3
1/2
1/4
0
2
4
∞
270
250
230
Phase of $f_-(\varphi_o, \pi-\varphi_o)$--deg.
$\varphi_o = 45°$
0
0.2
0.4
0.6
0.8
1.0
1.2
1.4
ka

Graph IV-3(b)

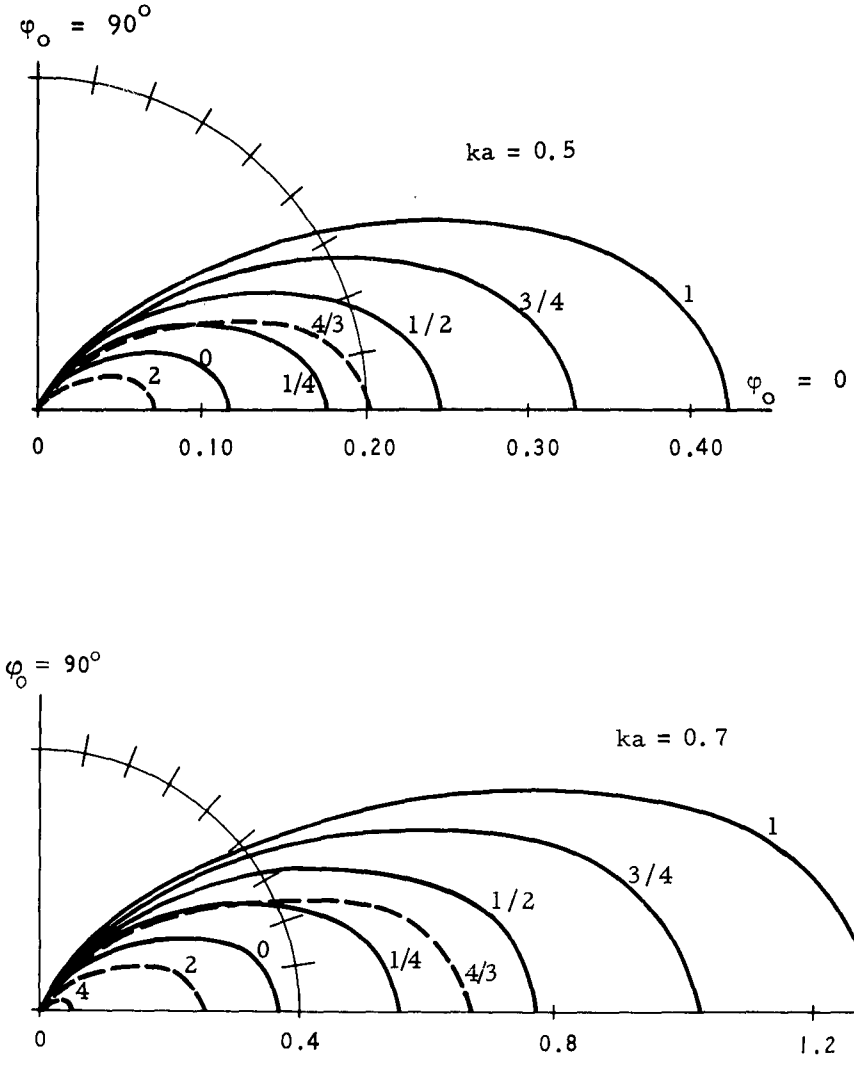

Graph IV-4: $|f_-(-\varphi_o, \pi-\varphi_o)|^2$.

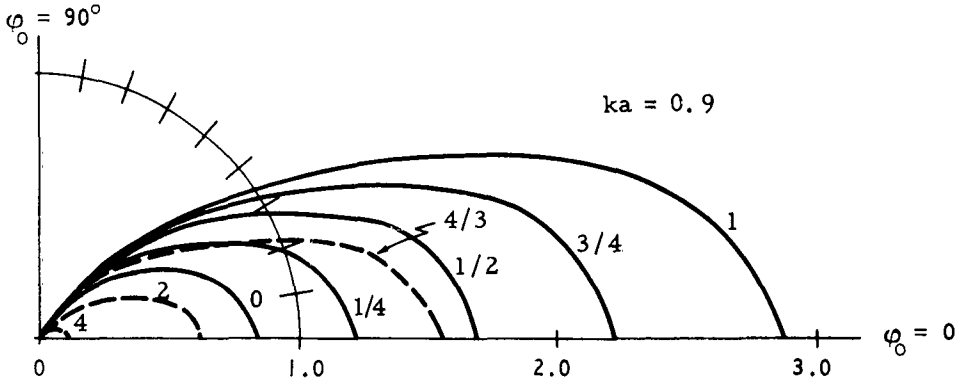

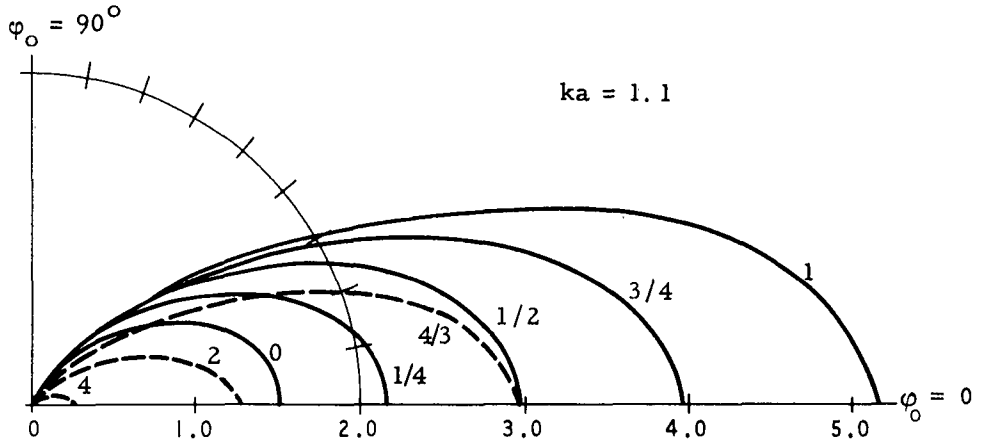

Graph IV-4 (Con't): $|f_-(-\varphi_o, \pi-\varphi_o)|^2$.

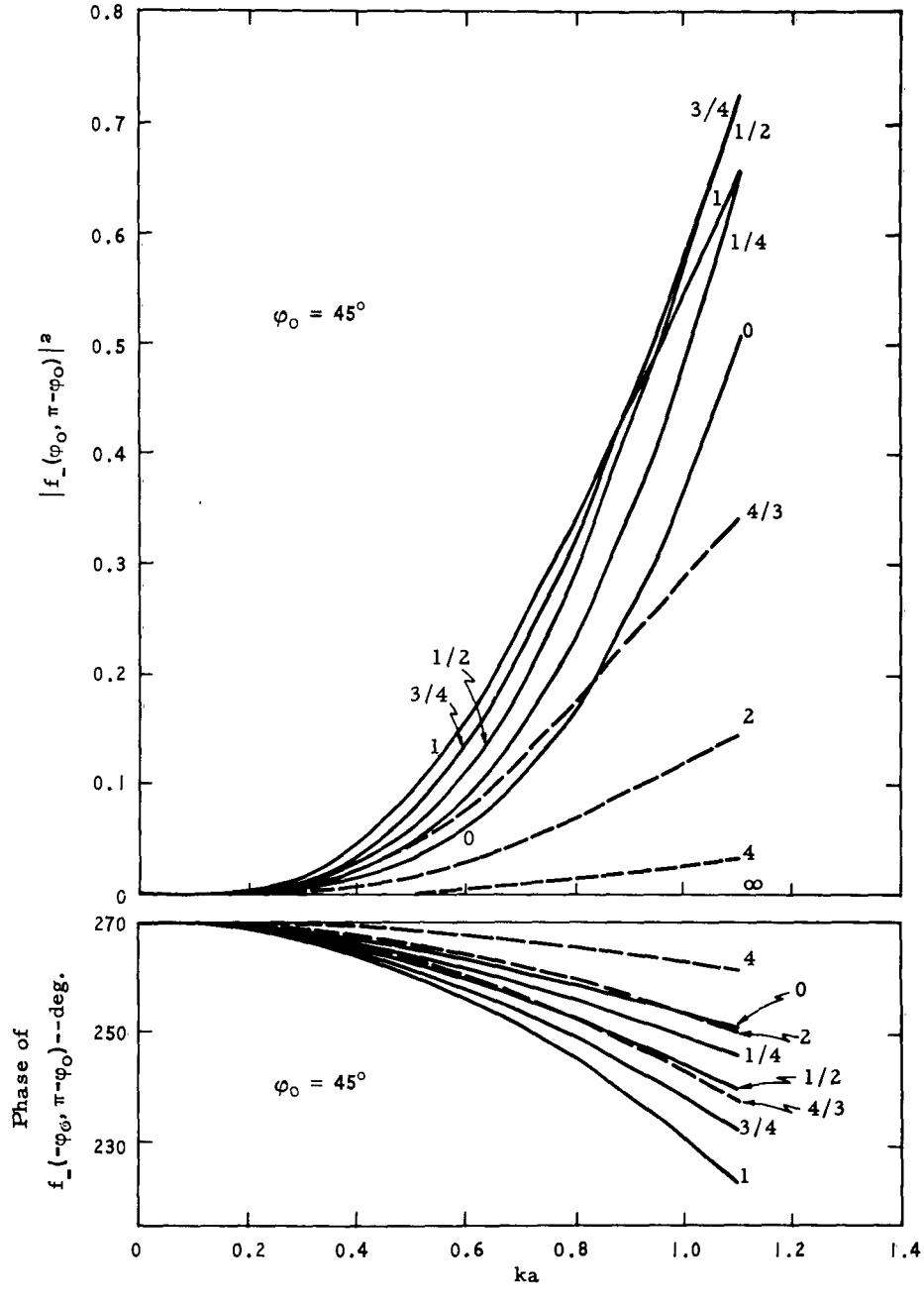
0.8
0.7
0.6
0.5
0.4
0.3
0.2
0.1
0
$|f_-(\varphi_o, \pi-\varphi_o)|^2$
$\varphi_o = 45°$
3/4
1/2
1
1/4
0
4/3
2
4
∞
270
250
230
Phase of
$f_-(-\varphi_o, \pi-\varphi_o)$--deg.
$\varphi_o = 45°$
4
0
-2
1/4
1/2
4/3
3/4
1
0
0.2
0.4
0.6
0.8
1.0
1.2
1.4
ka

Graph IV-5

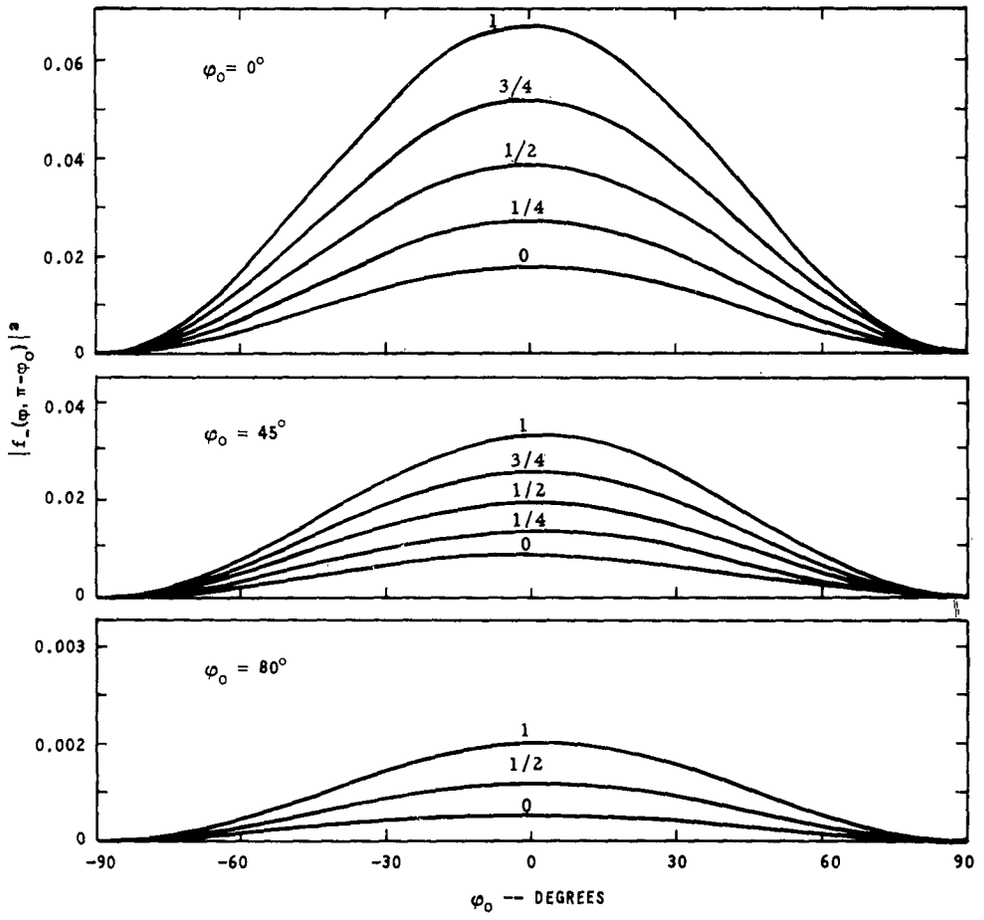

Graph IV-6 : ka = 0.3

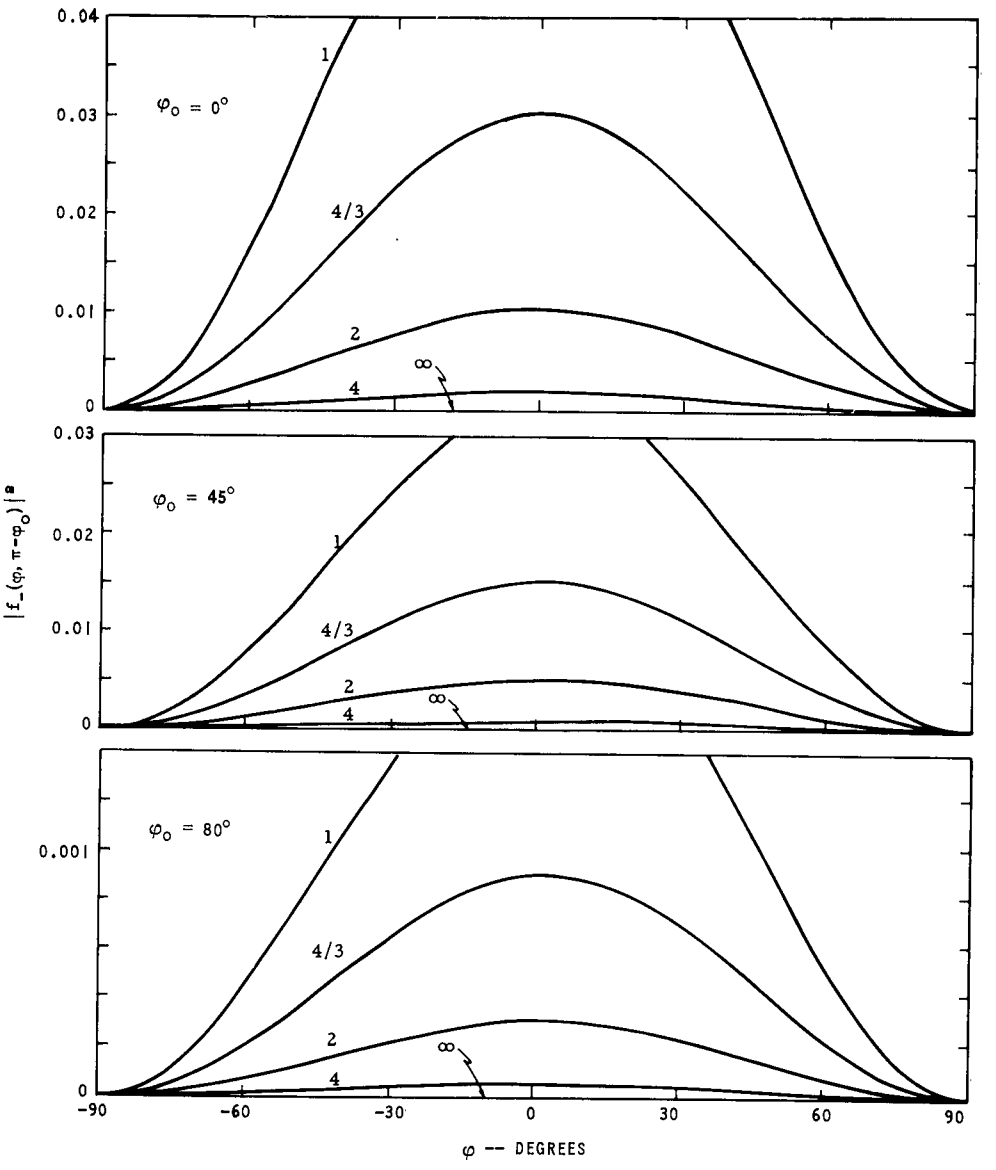

Graph IV-6 (con't): ka = 0.3

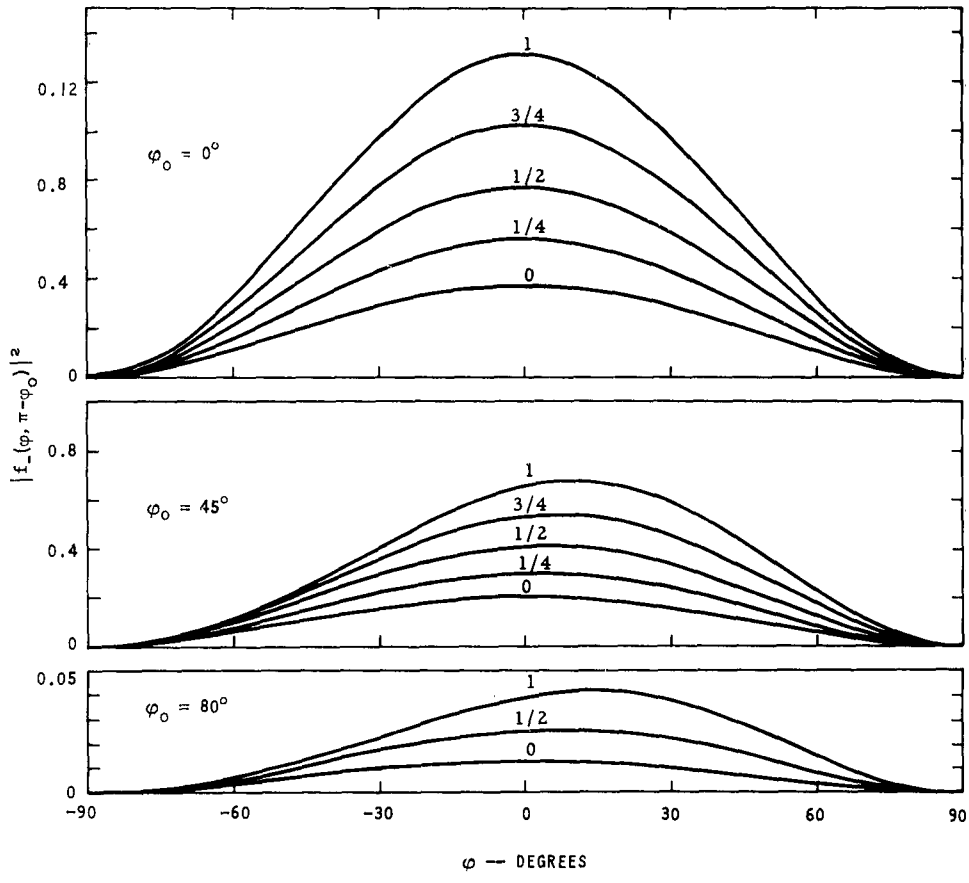

Graph IV-7: ka = 0.7

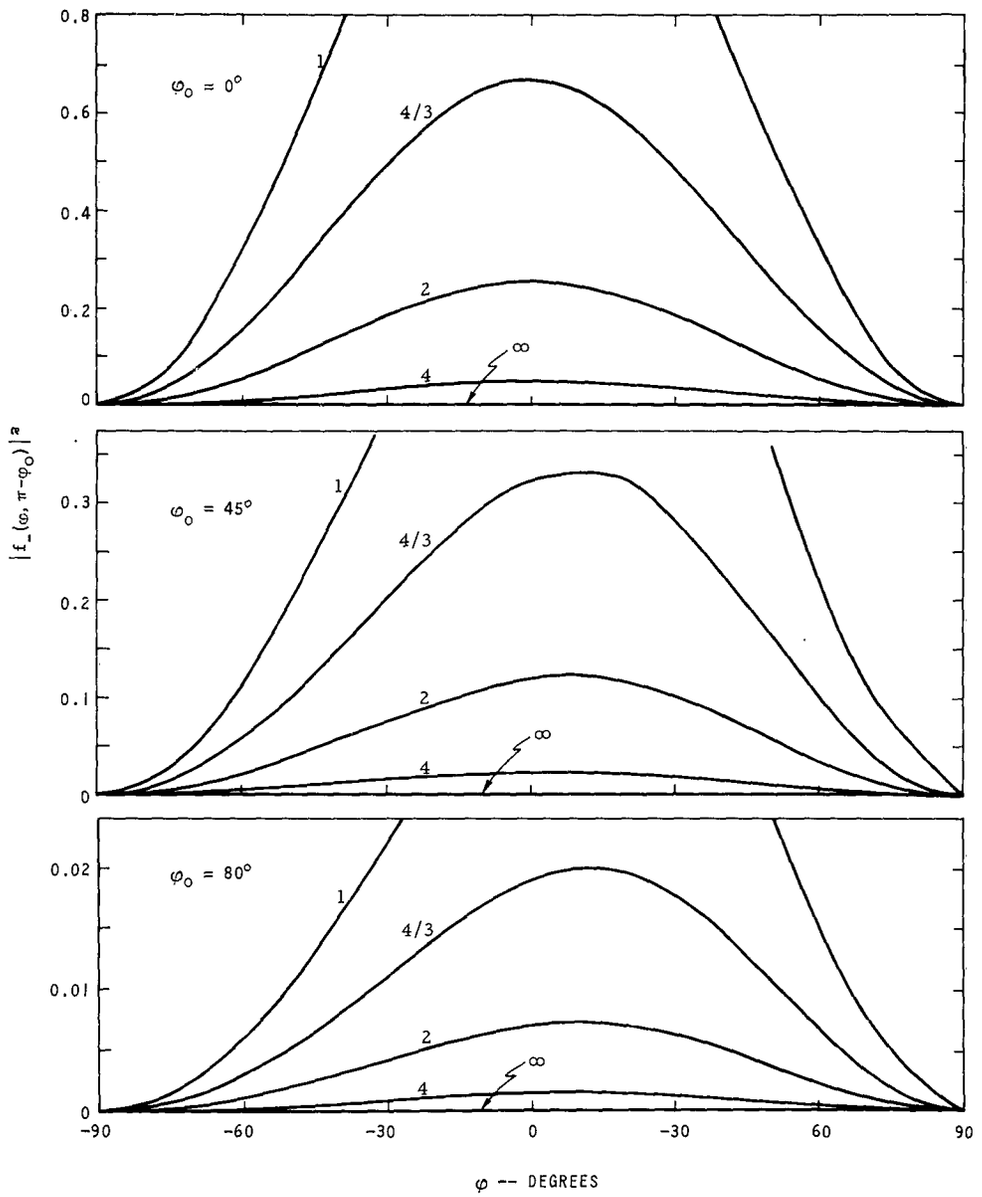

Graph IV-7 (con't): ka = 0.7

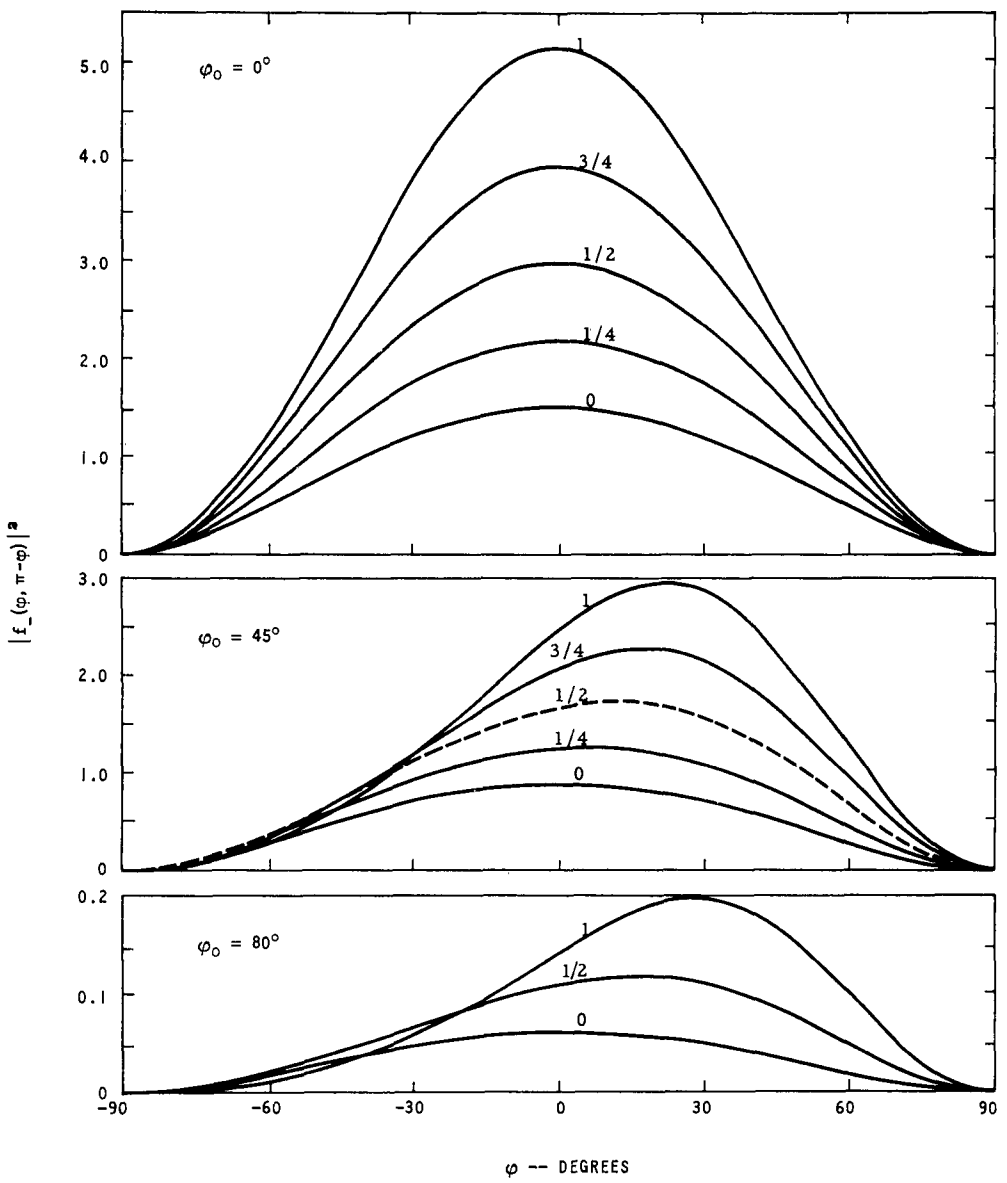

Graph IV-8: ka = 1.1

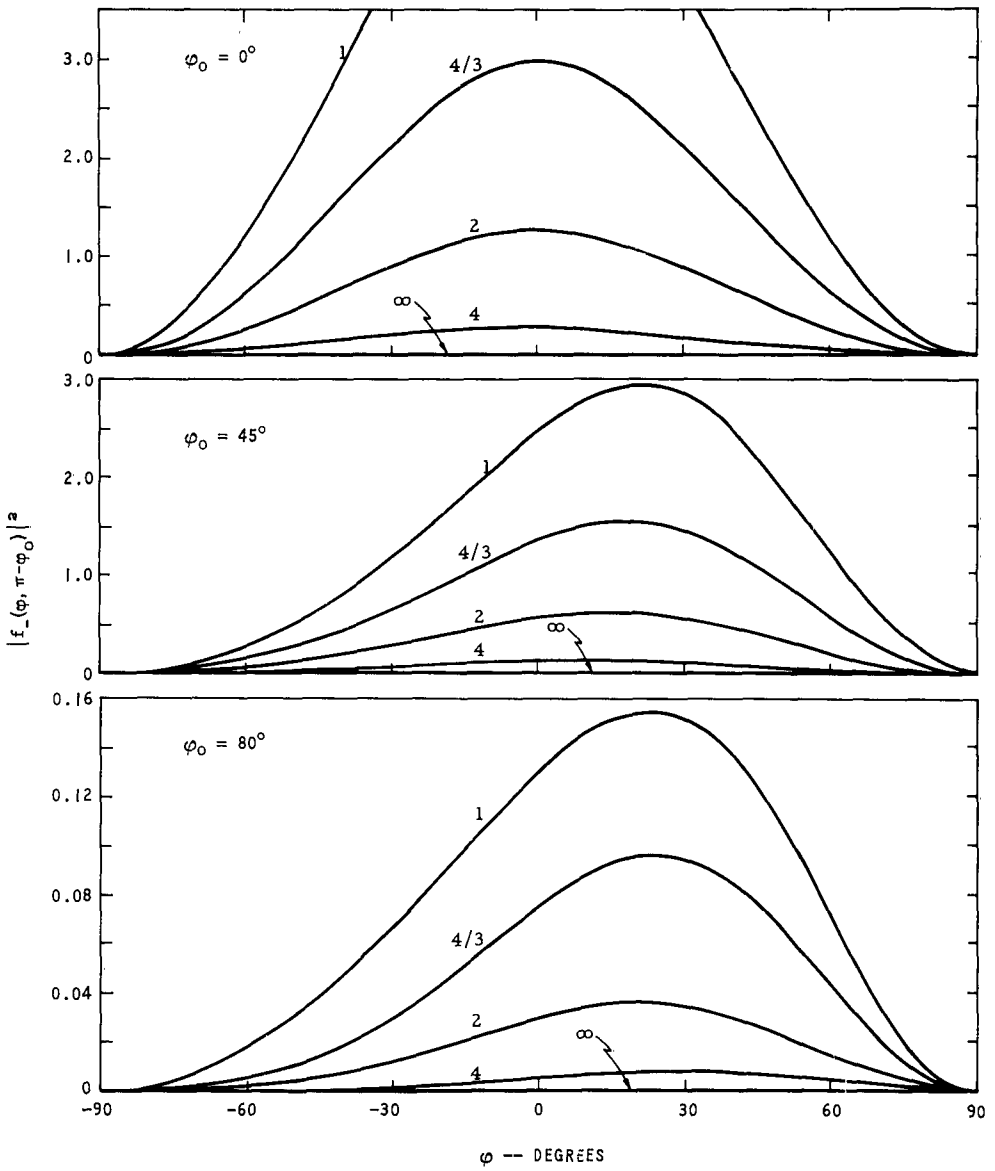

Graph IV-8 (con't): ka = 1.1

REFERENCES

1. B. Sieger, "Die Beungung einen ehenen Elektrischen Wellen an einen Schirm von Elliptischen Querschnitt", Annalen der Physik 27, 626, 1908.

2. N. W. McLachlan, "Theory and Application of Mathieu Functions" (Clarendon Press, Oxford, 1951), Ch. 19.

3. J. A. Stratton, "Electromagnetic Theory" (McGraw-Hill Book Co., Inc., New York, 1941), Ch. 6.

4. P. M. Morse and P. J. Rubenstein, Phys. Rev. 54, 895 (1938).

5. J. C. Wiltse and M. J. King, "Values of the Mathieu Functions", The Johns Hopkins University Radiation Laboratory, Report AF-53, August, 1958.

6. J. C. Wiltse and M. J. King, "Derivatives, Zeros, and Other Data Pertaining to Mathieu Functions", The Johns Hopkins University Radiation Laboratory, Report AF-57, December, 1958.

7. J. E. Burke and V. Twersky, "On Scattering of Waves by an Elliptic Cylinder and by a Semi-Elliptic Protuberance on a Ground Plane", Report EDL-M266, Sylvania Electronic Defense Laboratories, 1960.

8. J. E. Burke and V. Twersky, "On Scattering of Waves by the Infinite Grating of Elliptic Cylinders", Report EDL-E44, Sylvania Electronic Defense Laboratories, 1959.

9. J. E. Burke and V. Twersky, "On Scattering and Reflection of Waves by Elliptically Striated Surfaces", Report EDL-E66, Sylvania Electronic Defense Laboratories, 1962.

10. J. Meixner and F. W. Schafke, "Matheiusche Funktionen Und Spharoidfunktionen" (Springer, Berlin, 1954).

11. P. M. Morse and H. Feshbach, "Methods of Theoretical Physics" (McGraw-Hill Book Co., Inc., New York, 1946), Ch. 11.

12. Rayleigh, Phil. Mag. 14, 350 (1907).

13. N. D. Kazarinoff and R. K. Ritt, "Scalar Diffraction by an Elliptic Cylinder", IRE Trans. AP-7, S21 (1959).

14. B. Levy, "Diffraction by an Elliptic Cylinder", Report EM-121, Courant Institute of Mathematical Sciences, New York University, 1958.

15. J.A. Stratton, P.M. Morse, L.J. Chu, J.P. Little, and R.A. Hutner, "Elliptic Cylinders and Spheroidal Wave Functions" (Wiley, New York, 1951).

16. National Bureau of Standards, "Tables Relating to Mathieu Functions" (Columbia University Press, New York, 1951).

17. Rayleigh, Phil. Mag. 44, 28 (1897); see also H. Lamb, "Hydrodynamics" (Dover, New York, 1945), p 519 ff.

18. G.N. Watson, "A Treatise of the Theory of Bessel Functions" (second edition, McMillan, New York, 1944).

AD_____Accession No._____

Electronic Defense Labs., Mountain View, Calif. NUMERICAL RESULTS FOR LOW FREQUENCY SCATTERING BY ELLIPTIC CYLINDERS AND BY ISOLATED SEMI-ELLIPTIC PROTUBERANCES - J. E. Burke, E. J. Christensen and S. B. Lyttle. Technical Memorandum EDL-M455, 1 August 1962 (Contract DA 36-039 SC-87499) UNCLASSIFIED report.

The low frequency approximations ("closed form" and series) derived previously for the fields scattered by elliptic cylinders, and by semi-elliptic protuberances, are applied numerically. For the two cases, $\underline{E}$ or $\underline{H}$ paralled to the generators, the results presented include total scattering cross sections, forward and back scattered intensity and phase curves and far-field scattering patterns; for various angles of incidence, various eccentricities, and for various values of $ka \leq 1.1$ (where $k = 2\pi/\lambda$ and 2a is the major axis of the scatters). Attention is restricted to the low frequency range not covered by published tables of Mathieu functions.

Copy No.

1. Numerical
2. *Low-Frequency
3. *Scattering
4. Electromagnetic
5. Waves
6. *Elliptic
7. *Cylinders
8. *Isolated
9. *Semi-Elliptic
10. *Protuberances
11. Mathieu
12. Functions
13. Amplitude
14. Closed
15. Form
16. Series

I. Burke, J. E.
II. Christensen, E. J.
III. Lyttle, S. B.
IV. Contract DA 36-039 SC-87499

8.6/15.2/25.3

AD_____Accession No._____

Electronic Defense Labs., Mountain View, Calif. NUMERICAL RESULTS FOR LOW FREQUENCY SCATTERING BY ELLIPTIC CYLINDERS AND BY ISOLATED SEMI-ELLIPTIC PROTUBERANCES - J. E. Burke, E. J. Christensen and S. B. Lyttle. Technical Memorandum EDL-M455, 1 August 1962 (Contract DA 36-039 SC-87499) UNCLASSIFIED report.

The low frequency approximations ("closed form" and series) derived previously for the fields scattered by elliptic cylinders, and by semi-elliptic protuberances, are applied numerically. For the two cases, $\underline{E}$ or $\underline{H}$ paralled to the generators, the results presented include total scattering cross sections, forward and back scattered intensity and phase curves and far-field scattering patterns; for various angles of incidence, various eccentricities, and for various values of $ka \leq 1.1$ (where $k = 2\pi/\lambda$ and 2a is the major axis of the scatters). Attention is restricted to the low frequency range not covered by published tables of Mathieu functions.

Copy No.

1. Numerical
2. *Low-Frequency
3. *Scattering
4. Electromagnetic
5. Waves
6. *Elliptic
7. *Cylinders
8. *Isolated
9. *Semi-Elliptic
10. *Protuberances
11. Mathieu
12. Functions
13. Amplitude
14. Closed
15. Form
16. Series

I. Burke, J. E.
II. Christensen, E. J.
III. Lyttle, S. B.
IV. Contract DA 36-039 SC-87499

8.6/15.2/25.3

AD_____Accession No._____

Electronic Defense Labs., Mountain View, Calif. NUMERICAL RESULTS FOR LOW FREQUENCY SCATTERING BY ELLIPTIC CYLINDERS AND BY ISOLATED SEMI-ELLIPTIC PROTUBERANCES - J. E. Burke, E. J. Christensen and S. B. Lyttle. Technical Memorandum EDL-M455, 1 August 1962 (Contract DA 36-039 SC-87499) UNCLASSIFIED report.

The low frequency approximations ("closed form" and series) derived previously for the fields scattered by elliptic cylinders, and by semi-elliptic protuberances, are applied numerically. For the two cases, $\underline{E}$ or $\underline{H}$ paralled to the generators, the results presented include total scattering cross sections, forward and back scattered intensity and phase curves and far-field scattering patterns; for various angles of incidence, various eccentricities, and for various values of $ka \leq 1.1$ (where $k = 2\pi/\lambda$ and 2a is the major axis of the scatters). Attention is restricted to the low frequency range not covered by published tables of Mathieu functions.

Copy No.

1. Numerical
2. *Low-Frequency
3. *Scattering
4. Electromagnetic
5. Waves
6. *Elliptic
7. *Cylinders
8. *Isolated
9. *Semi-Elliptic
10. *Protuberances
11. Mathieu
12. Functions
13. Amplitude
14. Closed
15. Form
16. Series

I. Burke, J. E.
II. Christensen, E. J.
III. Lyttle, S. B.
IV. Contract DA 36-039 SC-87499

8.6/15.2/25.3

AD_____Accession No._____

Electronic Defense Labs., Mountain View, Calif. NUMERICAL RESULTS FOR LOW FREQUENCY SCATTERING BY ELLIPTIC CYLINDERS AND BY ISOLATED SEMI-ELLIPTIC PROTUBERANCES - J. E. Burke, E. J. Christensen and S. B. Lyttle. Technical Memorandum EDL-M455, 1 August 1962 (Contract DA 36-039 SC-87499) UNCLASSIFIED report.

The low frequency approximations ("closed form" and series) derived previously for the fields scattered by elliptic cylinders, and by semi-elliptic protuberances, are applied numerically. For the two cases, $\underline{E}$ or $\underline{H}$ paralled to the generators, the results presented include total scattering cross sections, forward and back scattered intensity and phase curves and far-field scattering patterns; for various angles of incidence, various eccentricities, and for various values of $ka \leq 1.1$ (where $k = 2\pi/\lambda$ and 2a is the major axis of the scatters). Attention is restricted to the low frequency range not covered by published tables of Mathieu functions.

Copy No.

1. Numerical
2. *Low-Frequency
3. *Scattering
4. Electromagnetic
5. Waves
6. *Elliptic
7. *Cylinders
8. *Isolated
9. *Semi-Elliptic
10. *Protuberances
11. Mathieu
12. Functions
13. Amplitude
14. Closed
15. Form
16. Series

I. Burke, J. E.
II. Christensen, E. J.
III. Lyttle, S. B.
IV. Contract DA 36-039 SC-87499

8.6/15.2/35.3